AD-A275 893

NSWCDD/TR-93/249

SOLID-STATE, ACTIVE-PHASED ARRAYS–
SOME ASPECTS OF RECEIVER DESIGN

BY JOSEPH D. HARROP
SHIP DEFENSE SYSTEMS DEPARTMENT

FEBRUARY 1994

DTIC
ELECTE
FEB 17 1994
S B D

DTIC QUALITY INSPECTED

NAVAL SURFACE WARFARE CENTER
DAHLGREN DIVISION
Dahlgren, Virginia 22448-5000

94 2 16 018

94-05149

SOLID-STATE, ACTIVE-PHASED ARRAYS– SOME ASPECTS OF RECEIVER DESIGN

BY JOSEPH D. HARROP
SHIP DEFENSE SYSTEMS DEPARTMENT

FEBRUARY 1994

NAVAL SURFACE WARFARE CENTER
DAHLGREN DIVISION
Dahlgren, Virginia 22448-5000

FOREWORD

Although solid-state receiver technology has been used for many years, much of the Navy's use of solid-state transmitter technology has been limited to communication equipment or other uses requiring relatively low power, low frequency, or both. The uses have expanded to the point that it has now become necessary to address some of the issues and trade offs involved in the design of transmit/receive modules so that active phased-array characteristics can be fully understood.

The analytical work performed here investigates the general relationship among the system-noise figure, third-order intercept, and dynamic range of active antenna array receivers. That relationship can be used to analyze the performance of, and understand the requirements for, active phased-array radar receivers.

This report analyzes the dynamic range and third-order intercept requirements of phased-array receivers and the effect on noise figure of adding receiver attenuation to implement weighting (taper) of the array elements. However, additional analysis is needed to develop a reliable and accurate design tool.

This report has been reviewed by Stuart A. Koch, James I. Miller, Richard Giorgis, Charles E. Spooner, John Cavanaugh, and Tom Hitt.

Approved by:

THOMAS C. PENDERGRAFT, Head
Ship Defense Systems Department

ABSTRACT

The Navy's use of solid-state transmitter technology has been limited to communication equipment or other uses requiring relatively low power, low frequency, or both. It has now become necessary to address some of the issues and trade offs involved in the design of transmit/receive modules so that active phased-array characteristics can be fully understood.

The analytical work performed here determines the general relationship among the system-noise figure, third-order intercept, and dynamic range of active antenna array receivers. This report analyzes the dynamic range and third-order intercept requirements of phased-array receivers and the effect on noise figure of adding receiver attenuation to implement weighting (taper) of the array elements.

CONTENTS

ILLUSTRATIONS

INTRODUCTION

Although solid-state receiver technology has been used for many years, much of the military's, specifically the Navy's, use of solid-state transmitter technology has been limited to communication equipment or other uses requiring relatively power, low frequency, or both. With improvements in device power versus frequency, solid-state devices have entered the traditionally held realms of tube technologies; i.e., radar transmitters; e.g., AN/SPS-40 solid-state transmitter replacement, AN/TPS-59 transmitter, and others. Along with these new devices, new approaches to old problems have emerged, specifically, the implementation of active element phased-array radars. In addition to moving the transmitting device to the array face, came locating the receiver front ends at the array face, reducing receive losses, and making the receiver an integral part of the transmit/receive (TR) modules. These receivers' outputs are then combined in subarray groupings or individually to form the composite receiver output. Some of the issues and trade offs involved in the design of these TR modules must be addressed so active phased-array characteristics can be fully understood.

The analytical work performed here determines the general relationship among the system-noise figure, third-order intercept, and dynamic range of active antenna-array receivers. That relationship can then be used to analyze the performance of, and to understand and develop the requirements for, active phased-array radar receivers. These parameters are particularly useful for their ability to provide insight into a radar's potential performance in clutter environments.

The system-noise figure is a measure of a receiver's sensitivity or minimum detectable signal level. In its simplest form, it represents the noise level in the receiver that a signal must exceed to become detectable. The third-order intercept point is used as a receiver/amplifier figure of merit that represents the level of intermodulation distortion created by two interfering signals at the input to the receiver/amplifier. Under certain in-band signal interference conditions, intermodulation products appear in the passbands of the receiver's clutter rejection filters. The third-order intercept point affects the ability of the radar to reject that clutter. In general, good noise-figure and third-order intercept point performance presents conflicting requirements to the radar system designer. When noise figure is improved, the third-order intercept point is degraded and vice versa. The dynamic range of a receiver is a measure of its ability to achieve a high third-order intercept point and at the same time achieve a low noise figure.

Many others[1,2,3] have done similar work that contributed to an understanding of the subject. This work originally began as confirmation and extension of work by J.B. Hoffman of Technology Service Corporation.[1] However, what makes this work unique is the inclusion of receiver attenuator losses combined with beamformer network (array manifold) characteristics to determine their effect on array performance. As discussed in Appendix A, the gain of the

beamformer is different for signal and noise. The gain for the signal is 1 per channel, while the gain for noise is $1/G_B$, where G_B is the beamformer gain (see Appendix A), because the signal voltages are added coherently (in phase) while the noise voltages are added noncoherently (random phase). It is concluded that, under certain circumstances, these parameters can effect the system-noise figure in such a way as to have a determinable effect on third-order intercept, dynamic range, and overall array-noise figure. As a check of this work, the equations developed here were used to reevaluate the test case designs offered in Mr. Hoffman's study.[1] The noise figure analysis of Appendix A is a direct result of using that study's module configuration and was used to check the match between this and that study.

This report is presented in four parts with four appendixes. Part 1 is the introduction and Part 2 is the analysis of the dynamic range and third-order intercept requirements of phased-array receivers. Part 3 is an analysis of the effect on noise figure of adding receiver attenuation to implement weighting (taper) of the array elements. Part 4 attempts to tie Parts 2 and 3 together in a general sense. It is essentially the *results* of the effort, but it is clear that additional analyses must be done to develop a reliable and accurate design tool. It is hoped that this work can be useful in pointing the way to future needs and efforts. Appendixes A and B develop the noise-figure and third-order intercept expressions, respectively, used to generate the results of Appendix C. The results of Parts 1 and 2 was also applied to the test designs mentioned above and shown in Appendix C. Appendix D demonstrates the effect on noise figure of adding either linear or cosine-squared-on-a-pedestal taper to an array antenna.

DYNAMIC RANGE AND THIRD-ORDER INTERCEPT

The third-order intercept characteristics of an amplifier are shown in Figure 1. The signal and third-order gain curves are clearly labeled. Their intersection is the third-order intercept point—the point that the third-order intermodulation products of two equal and closely spaced (in frequency) input signals would intersect the signal-gain curve if no gain compression occurred. The graph axes are labeled *Output Power (dBm)* and *Output Signal Power (dBm)*. Because of this, the signal gain curve has a gain of 1 and the third-order intercept gain curve has a slope of 3. All inputs are given in terms of the output power resulting from them. On this graph, the dynamic range would be the difference between $P_{0,max}$ and $P_{0,dst}$. This assumes that it is desirable to keep the distortion output ($P_{0,dst}$) equal to the noise-output level of the system at that point—a fact that will be a key factor later in the discussion.

FIGURE 1. SIGNAL AND THIRD-ORDER INTERCEPT CURVES

We will now develop an expression for the input-intercept point, $P_{i,ip}$, the output-intercept point referenced to the input of amplifier chain. The first step is to write an expression for the slope of each curve.

$$m_1 = \frac{B}{C}$$

$$= \frac{P_{o,ip} - P_{o,\max}}{P_{i,ip} + G_S - (P_{i,\max} + G_S)}$$

$$= 1$$

3

and:

$$m_2 = \frac{A}{C}$$

$$= \frac{P_{o,ip} - P_{o,dst}}{P_{i,ip} + G_S - (P_{i,max} + G_S)}$$

$$= 3$$

where:

G_S = *system gain*

$P_{i,max}$ = *maximum input power producing distortion*

$(P_{o,dst})$ *equal with noise level*

$P_{i,ip}$ = *input intercept point*

$P_{o,ip}$ = *output intercept point*

$P_{o,max}$ = *maximum signal output, corresponding with $P_{i,max}$*

occurs when $P_{o,dst}$ equals noise level

$P_{o,dst}$ = *distortion (third order) output signal*

These combine to yield:

$$\frac{m_1}{m_2} = \frac{P_{o,ip} - P_{o,max}}{P_{o,ip} - P_{o,dst}} = \frac{1}{3}$$

which reduces to yield:

$$P_{o,dst} = 3 * P_{o,max} - 2 * P_{o,ip}$$

But:

$$P_{o,max} = (P_{i,max} + G_S) * m_1$$

$$= (P_{i,max} + G_S) * 1$$

and finally:

$$P_{o,dst} = 3 * P_{i,max} + 3 * G_s - 2 * P_{o,ip} \tag{1}$$

Since we want the maximum output distortion not to exceed the output noise level to obtain maximum dynamic range, then:

$$P_{o,dst} = NL_o = NL_i + G_n$$

where:

NL_o = *system output noise level*

NL_i = *system input noise level*

G_n = *system noise gain*

= $G_s - G_B$

= *system signal gain-beamformer gain*

G_B = *beamformer gain*

= $G_S - G_n$

Similarly:

$$P_{o,ip} = (P_{i,ip} + G_s) * 1$$

Substituting these into Equation (1) gives:

$$NL_i + G_n = 3*P_{i,max} + 3*G_s - 2*P_{i,ip} - 2*G_s$$

which finally reduces to:

$$P_{i,ip} = \frac{3*P_{i,max} - NL_i + G_B}{2} \tag{2}$$

Next, we need to determine the relationship between $P_{i,max}$ and dynamic range so it can be substituted into Equation (2). Looking at dynamic range at the output of the beamformer, $DR_{o,b}$, from Figure 1:

$$DR_{o,b} = P_{o,max} - P_{o,dst} \tag{3}$$

Earlier we stated that to have maximum dynamic range requires the output distortion be no greater than the output noise level, we can write:

$$P_{o,dst} = NL_o$$

where:

$$NL_o = NL_i + G_n$$

Combining yields:

$$P_{o,dst} = NL_i + G_n \tag{4}$$

Also from Figure 1:

$$P_{o,max} = P_{i,max} + G_s \tag{5}$$

Combining Equations (4) and (5), and noting that:

$$G_n = G_s - G_B$$

yields:

$$DR_{o,b} = P_{i,\max} + G_s - (NL_i + G_r)$$

$$= P_{i,\max} + G_s - NL_i - G_s + G_B \qquad (6)$$

$$DR_{o,b} = P_{i,\max} - NL_i + G_B$$

and we can rearrange Equation 6 to show:

$$P_{i,\max} = DR_{o,b} + NL_i - G_B \qquad (7)$$

The final steps are as follows: First we substitute $P_{i,\max}$, in the form of Equation 7, into Equation 2 and solve for $DR_{o,b}$:

$$P_{i,ip} = \frac{3*DR_{o,b} + 3*NL_i - 3*G_B - NL_i + G_B}{2}$$

which reduces to:

$$DR_{o,b} = \frac{2}{3} * (P_{i,ip} - NL_i + G_B) \qquad (8)$$

This s the dynamic range out of the beamformer network. To determine the dynamic range of each individual module, the beamformer gain is subtracted from $DR_{o,b}$.

$$DR_m = \frac{2}{3}*(P_{i,ip}-NL_i)-\frac{1}{3}*G_B \tag{9}$$

This equation allows one to determine the dynamic range and third-order intercept requirements for the array modules. Note also that this expression relates dynamic range to noise figure through NL_i.

Since:

$$NL_i = 10*\log(K*T_0*B*F_{SA})$$

then:

$$DR_m = \frac{2}{3}*(P_{i,ip}-10*\log(K*T_0*B*F_{SA})-\frac{G_B}{2}) \tag{10}$$

and:

$$DR_{o,b} = \frac{2}{3}*(P_{i,ip}-10*\log(K*T_0*B*F_{SA})+G_B) \tag{11}$$

also:

$$G_B = DR_{o,b}-DR_m$$

These equations demonstrate that the dynamic range, noise figure, third-order intercept point, and the beamformer gain are all tied together and need to be considered mutually. By manipulating the terms of these equations, proposed designs can be evaluated and modified to optimize the various parameters.

Consider, for example, the need for a system dynamic range of 85 dB, a noise figure of 2 dB, and a bandwidth of 40 MHz. Then Equation 11 would indicate that an input third-order intercept of -5.45 dBm is needed if the array has 5,000 elements ($G_B = 37$ dB). Equation 10 shows that the array module needs only 48 dBm of dynamic range to satisfy these requirements. A further reduction in required module dynamic range could be achieved by increasing the number of array modules. By going to a narrower bandwidth system (i.e., 4MHz) the intercept point is correspondingly reduced to -15.45 dBm.

Therefore, array and waveform designs need to be closely matched to the receiver design to obtain optimum performance. Soft parameters (i.e., noise figure and third-order intercept point) can and should be traded off to help meet overall system requirements. Harder parameters (i.e., number of array elements and bandwidth) are more difficult to trade off when considering overall radar design.

ARRAY-NOISE FIGURE CONSIDERATIONS

It was mentioned earlier that array attenuation, used to adjust taper on receive, can have an effect on overall array noise figure. See the equations in Appendix A. Usually when taper is applied, a taper loss is suffered. This is a loss in signal-to-noise ratio because of the attenuation of the signal and is considered an acceptable trade off to achieve improved antenna beam-shape performance. There is, however, an additional phenomenon that can occur that has the effect of raising the noise figure of the receiver elements that have the taper attenuation applied to them. These are concentrated on the periphery of the array. This raises the overall array noise figure of the array which, in effect, lowers the signal-to-noise ratio even further.

This effect can be demonstrated by considering two basic types of taper, linear and cosine-squared-on-a-pedestal. The reasons for considering these tapers are that they are relatively simple to analyze and the cosine-squared-on-a-pedestal taper can be related to other, more complex tapers.[4] To begin with, we need to develop an expression for the noise figure as a function of module attenuation. To do this, go to Appendix A and retrieve the expression for noise figure for that example. Other examples will be slightly different, depending on receiver design. From Appendix A:

$$F_{SA} = F_A + L_R*[F_1 + \frac{(F_2-1)}{G_1} + \frac{(F_3-1)}{G_1*G_2} + \frac{L_m*L_B*(\frac{1-G_B}{G_B})+(L_m*L_B*F_R-1)}{G_1*G_2*G_3}]$$

This can be reduced to:

$$F_{SA} = F_A + L_R * F_1 + \frac{L_R * (F_2 - 1)}{G_1} + \frac{L_R * (F_3 - 1)}{G_1 * G_2} - \frac{L_R}{G_1 * G_2 * G_3}$$

$$+ L_m * [\frac{L_R * L_B * (\frac{1 - G_B}{G_B}) + L_R * L_B * F_R}{G_1 * G_2 * G_3}]$$

It is evident that the first part of this equation is independent of module loss and the second part is a term multiplied by module loss. If we now assume that module loss is a function of position on the array, and assuming a circular array, this equation can be reduced and rewritten in the form of a simple first-order equation:

$$F_{SA} = F_{AA} + L_m(r, \Theta) * F_{BB}$$

and this will be integrated over the surface of the array to get a *total noise figure*. The integral has to be multiplied by the density (modules per unit area) and then divided by the number of elements to get back to the average effective noise figure for the modules. This is:

$$F^1_{SA} = \frac{G_B}{\pi * R^2 * G_B} * \int_0^{2\pi} \int_0^R (F_{AA} + L_m(r, \Theta) * F_{BB}) * r * dr d\Theta$$

$$= \frac{F_{AA}}{\pi * R^2} * \int_0^{2\pi} \int_0^R r * dr d\Theta + \frac{F_{BB}}{\pi * R^2} * \int_0^{2\pi} \int_0^R r * L_m(r, \Theta) dr d\Theta$$

10

The number of modules is equal to the beamformer gain (G_B). At this point, it is convenient to note that the taper will be applied only in the radial direction so that L_m is a function of only r and not Θ. Solving the first double integration and making the appropriate substitutions result in the following simplification:

$$F^1{}_{SA} = F_{AA} + \frac{2*F_{BB}}{R^2} * \int_0^R r*L_m(r)dr \qquad (12)$$

Equation 12 provides the basis for the analyses that follows. As stated earlier, both linear and cosine-squared-on-a-pedestal tapers will be considered in the analysis. The term (L_m) will be developed for each case and applied to Equation 12 to develop an appropriate expression for each taper.

LINEAR TAPER

Linear taper is represented in Figure 2. Remembering that the module loss is a function only of radial distance, Equation 13 can be written directly from Figure 2 as:

$$L_m(r) = (\frac{L_{m,max} - 1}{R}) * r + 1 \qquad (13)$$
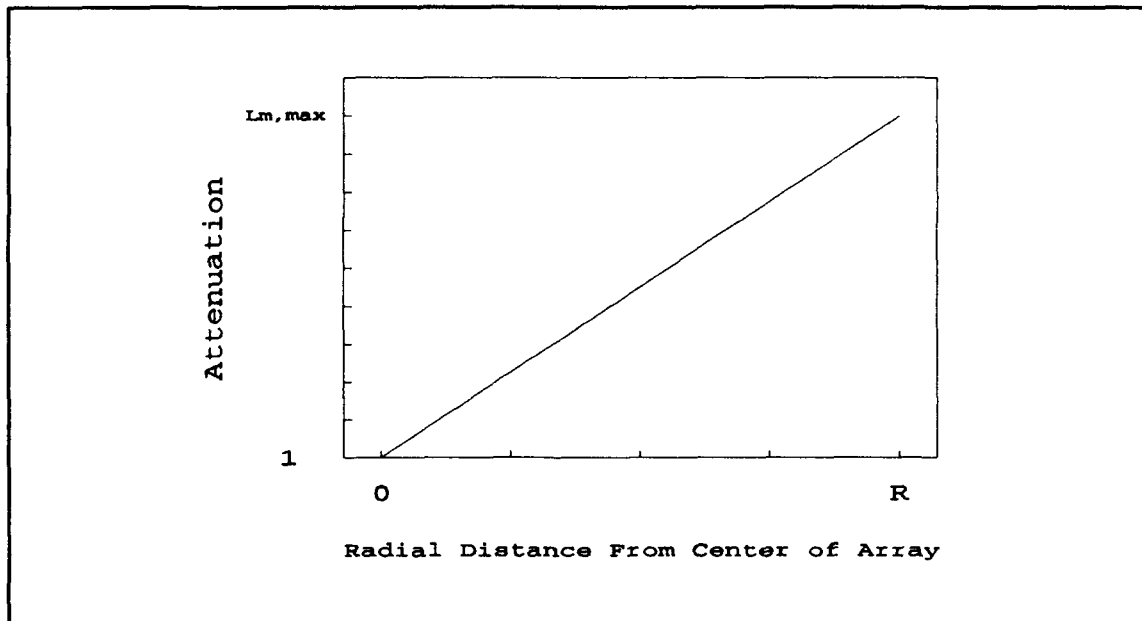
FIGURE 2. LINEAR TAPER

This assumes that the attenuation at the center of the array is zero (i.e., $L_m(0)=1$) and that it increases linearly to a maximum at the array edge. Putting Equation 13 into Equation 12 gives:

$$F^1{}_{SA} = F_{AA} + \frac{F_{BB}}{\pi * R^2} * \int_0^{2\pi} \int_0^R [(\frac{L_{m,max}-1}{R}) * r^2 + r] dr d\Theta$$

and solving the "rdrdΘ" term results in:

$$F^1{}_{SA} = F_{AA} + F_{BB} + \frac{F_{BB}}{\pi * R^2} * \int_0^{2\pi} \int_0^R (\frac{L_{m,max}-1}{R}) * r^2 \ dr d\Theta$$

Solving this last equation is relatively simple and results in Equation 14:

$$F^1{}_{SA} = F_{AA} + F_{BB} * (\frac{2 * L_{m,max} + 1}{3}) \tag{14}$$

This result is very simple, but it should be remembered that F_{AA} and F_{BB} are somewhat more complicated. Appendix D provides examples using receiver design data from Reference 1.

A result of this analysis is that, for good receiver design, unless the taper is very severe (i.e., greater than 20 dB or so), the term F_{AA} dominates, and there is little effect on overall noise figure. This stems from the fact that the noise figure is primarily determined by the first stages of amplification in a good design. If, however, there is less isolation in the amplifier chain, this effect could become noticeable and cause difficulties for lower weighting values as demonstrated in the third example of Appendix D. Also linear taper is not a normal taper to use. It does serve as a useful example however.

COSINE-SQUARED-ON-A-PEDESTAL TAPER

Cosine-squared-on-a-pedestal taper is represented in Figure 3. Equation 15 can be written directly from Figure 3 as:

$$L_m(r) = 1 + (L_{m,max} - 1) * \cos^2(\frac{\pi}{2} * (1 - \frac{r}{R})) \tag{15}$$
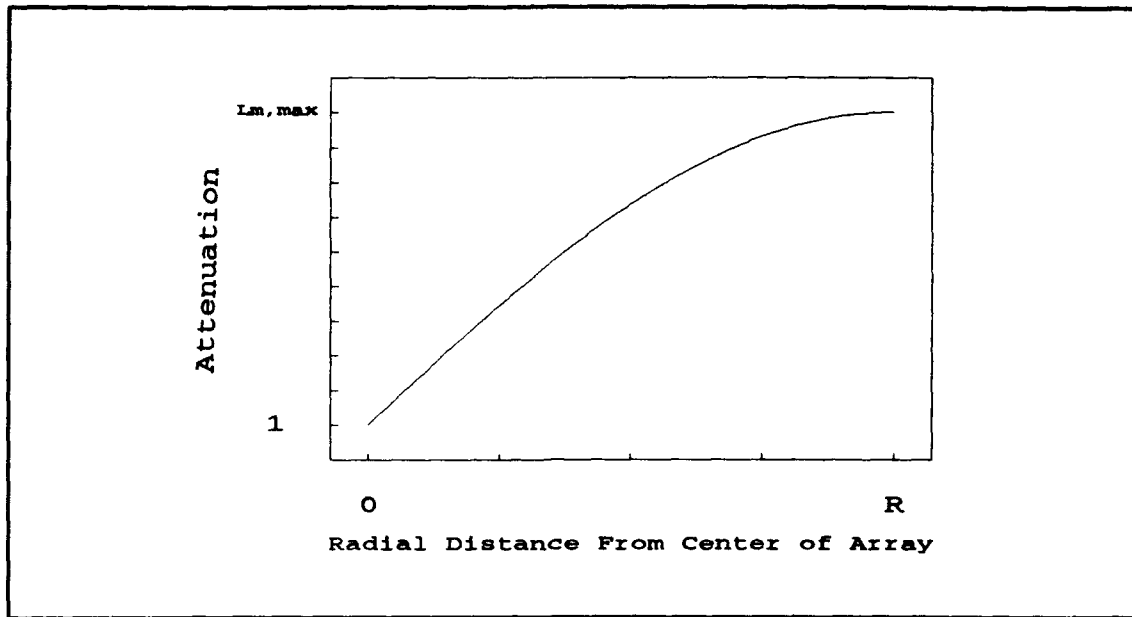
FIGURE 3. COSINE-SQUARED-ON-A-PEDESTAL TAPER

Before substituting Equation 15 into Equation 12, it would be helpful to reduce Equation 15 to a simpler, more easily integrable form. First, make the substitution:

$$\cos^2\alpha = \frac{1}{2}*(1+\cos(2*\alpha))$$

which, when substituted into Equation 15, results in:

$$L_m(r) = [1+\frac{(L_{m,max}-1)}{2}]+\frac{(L_{m,max}-1)}{2}*\cos(\pi*(1-\frac{r}{R}))$$

Simplifying this equation and making the substitution:

$$\cos(\alpha-\beta) = \cos(\alpha)*\cos(\beta)+\sin(\alpha)*\sin(\beta)$$

results in:

$$L_m(r) = \frac{L_{m,max}+1}{2}-(\frac{L_{m,max}-1}{2})*\cos(\frac{\pi*r}{R}) \tag{16}$$

13

Putting this expression for $L_{m,max}$ into Equation 12, repeated here for clarity, results in Equation 17 below.

$$F^1_{SA} = F_{AA} + \frac{2*F_{BB}}{R^2} * \int_0^R r*L_m(r)dr \tag{12}$$

$$F^1_{SA} = F_{AA}$$
$$+ \frac{2*F_{BB}}{R^2} * \int_0^R r*[\frac{L_{m,max}+1}{2} - \frac{L_{m,max}-1}{2}*\cos(\frac{\pi*r}{R})]drd\theta \tag{17}$$

Equation 17 can be solved and ultimately simplifies to its final form of:

$$F^1_{SA} = F_{AA} + F_{BB}*[1+(L_{m,max}-1)*(\frac{1}{2}+\frac{2}{\pi^2})] \tag{18}$$

Equation 2-7 is also dominated by the F_{AA} term and for weighting functions like Hamming (equivalent to $\cos^2$ with $L_{m,max} = 1/.08 = 12.5$ or ≈ 11 dB attenuation), the effect of increasing peripheral module noise figure is negligible compared to the system-noise figure, assuming good receiver design. However, for low, sidelobe Taylor weighting, which is closely matched to cosine-squared-on-a-pedestal up to about -42 dB sidelobes[4], the maximum weighting can be 30 to 50 dB. Because of this similarity, it is assumed that this weighting should give results similar to Taylor weighting up to approximately 35-dB edge attenuation or so. In any event, cosine-squared-on-a-pedestal should be a good demonstrator of the concept. As with the linear taper example, Appendix D contains calculated examples of this effect. Again, much depends on the amount of isolation in the amplifier chain. The first example shown in Appendix D is very insensitive to weighting while the last example is highly sensitive to weighting.

An additional observation that helps to build confidence in cosine-squared-on-a-pedestal's usefulness for exploring more complex weighting structures is the fact that, in each example, the linear and cosine-squared-on-a-pedestal weightings give results that are virtually identical.

This seems to support the hypothesis that, noting the increased complexity of cosine-squared-on-a-pedestal weighting over linear weighting, even more complex weightings (i.e., Taylor weighting) would show similar results to those shown here.

RESULTS AND CONSIDERATIONS

As stated in the introduction, this work was originally initiated as a confirmation and extension of the work by J.B. Hoffman of Technology Service Corporation[1] since circumstances prevented the proper review cycles before its delivery. The approach taken has been to show enough details of the calculations so the reader can follow the logic of the developments without stumbling over leaps in mathematical reasoning. It was also intended to highlight other processes occurring in this area of active-array receiver design.

In his work, Mr. Hoffman developed an expression for noise figure that turns out to be a good approximation that overlooked some of the beamformer network effects, which resulted in inaccurate noise-figure calculations as the module losses are increased. Since one of his conclusions was to operate the modules with approximately 30-dB attenuation, to achieve an acceptable third-order intercept, the effect of this inaccuracy begins to appear. However, comparing the analyses (refer to Appendix C and Reference 1) tends to show slightly lower noise figures at high module losses for the expressions developed here which, in itself, tends to benefit his suggestion.

However, the high module losses suggested by Mr. Hoffman are somewhat disconcerting. If you look at the dynamic range for each case, it becomes apparent that the highest dynamic range occurs between 25- and 30-dB module loss for most cases. Since, as indicated in the introduction, dynamic range is a measure of a receiver's ability to satisfy both good noise-figure and good third-order intercept point, this result seems to support Mr. Hoffman's suggestion. The results of Parts 2 and 3 also tend to track Mr. Hoffman's results, in terms of calculations, except he stops short in two areas. First, if antenna tapering on receive is desired, that taper is added directly to the module loss he already suggests using. This could result in module losses of 60- to 70-dB on receive and, according to the curves in Appendix C, dynamic range would suffer greatly. These kinds of losses seem excessive on a per-module basis. Second (and closely related to the first), Mr. Hoffman uses a 12-dB noise figure as a system benchmark because other low sidelobe systems have similar noise figures because of heavy tapering. However, since the system-noise figure is allowed to grow to this 12-dB level by the inclusion of module losses for the purpose of achieving acceptable third-order intercepts, adding the additional heavy taper losses will only increase the noise figure more and, as mentioned above, could actually push the receiver into a lower dynamic range situation because of the downward curve to the dynamic range at higher losses. The engineer is left with the question of whether it is better to compromise third-order intercept by putting in only attenuation to accomplish tapering or put in both taper and module attenuation or a compromise between the two.

It is felt that more thought needs to be given to the specific requirements of the particular system being evaluated. The design of an individual stand-alone receiver would have to satisfy

different requirements than that of a receiver that is to be part of an array of receivers on an active-array radar antenna, which is the stated ultimate subject of this effort. By looking at the figures in Appendix C, one can see there are approaches that could be used. Cases 1 through 4 are good examples of designs with low noise figures and reasonable dynamic ranges at low module loss. Cases 7 through 10 also show good noise figure with slightly better dynamic range, and third-order intercept point, at low module loss, except that the dynamic range starts to turn down at somewhat lower module losses than for cases 1 through 4. In cases 29 and 30, even higher dynamic ranges are seen at low module loss, except that noise figure is somewhat more compromised than before. The remainder of the cases show variations of these results that could possibly be taken advantage of, depending on system requirements. For example, if smaller dynamic ranges can be tolerated, operating at lower module losses could be traded for better sensitivity by selecting lower noise figures. The requirements may allow operating at lower, more reasonable noise figures with lower third-order intercept points so antenna tapers can be tolerated without excessive noise-figure growth and, in fact, improved dynamic range for those receivers with the added taper. Perhaps something entirely different, like range- and azimuth-sensitive attenuator control [similar to sensitivity time control (STC)], could be implemented to control intermodulation distortion from strong interference signals that are localized. In some cases, operation at high module losses may satisfy a given set of requirements but should not be considered the only method.

Another effect highlighted, but not studied in depth here, is the effect of weighting taper on the overall system dynamic range. The addition of attenuation to the receivers studied here show that, for most designs considered, the dynamic range is more sensitive than noise figure. However, the sensitivity is generally to increase dynamic range, up to ≈ 30 dB attenuator values, where it begins to decrease rapidly. This is considered a benefit rather than a problem. It also provides an additional parameter to adjust, or take advantage of, in the design of active-array receivers, as seen above. It is suggested that an analysis similar to the noise-figure analysis here be done to better characterize this effect.

Another striking observation is that the two weighting tapers used—linear and cosine-squared-on-a-pedestal—gave almost identical results for the three examples shown. As stated earlier, this observation helps to build confidence in cosine-squared-on-a-pedestal's usefulness for exploring more complex weighting structures. This seems to support the earlier hypothesis and assumption that, noting the increased complexity of cosine-squared-on-a-pedestal over linear weighting, even more complex weightings (i.e., Taylor weighting) would show results similar to those shown here—at least those resulting from the use of the cosine-squared-on-a-pedestal as a suitable approximation to more complex weightings.

Another possibly useful analysis would be the study of the unequal-input, signal-intercept point or multiple signal-generated interference. It would be very difficult to describe a realistic signal environment, but perhaps a simple set of signals could provide useful information. The potential benefits to clutter analysis would be extremely useful.

16

REFERENCES

1. Hoffman, J.B., *Preliminary Results of Active Array Noise Figure/Third Order Intercept Tradeoff Analysis*, Technology Service Corporation, Silver Spring, MD, 11 December 1991.

2. Collier, Don, "Optimizing LNA's for Use in Phased Arrays," *Microwave Systems News*, April 1990, pp 37-44.

3. Hayward, W.H., *Introduction to Radio Frequency Design*, Prentice-Hall, Inc., 1982, pp 202-232 and 367-371.

4. Skolnik, Merril, *Radar Handbook*, Second Edition, McGraw-Hill Publishing Company, New York, NY, 1990, pp 10.30 - 10.33.

APPENDIX A

SYSTEM-NOISE FIGURE CALCULATION

APPENDIX A NOMENCLATURE

HEMT   High-electron mobility transistor

HBT   Heterojunction bipolar transistor

MSFET   Metal semiconductor field-effect transistor

This appendix develops an expression for the equivalent system noise figure for an active phased-array radar. This work, along with Appendix B, was used for comparison to work performed in Hoffman's work;[A-1] those results are shown in Appendix C.

The confusing factors for this analysis are what effect that receiver module losses (in the form of taper and fixed attenuation to optimize third-order intercept) and beamformer effects, have on the array noise figure. Assume the generalized receiver chain of Figure A-1.
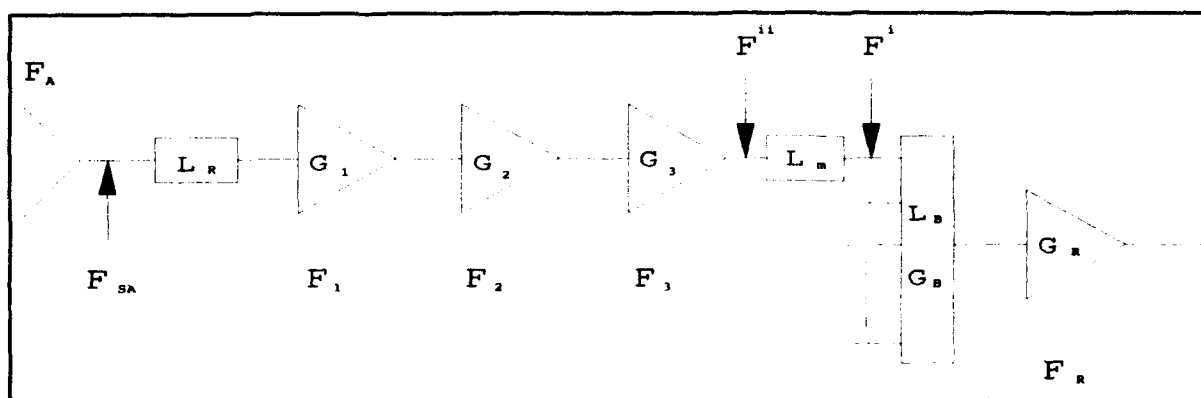
FIGURE A-1. GENERALIZED ARRAY-RECEIVER CHAIN

As a first step, we must calculate the equivalent noise figure (F^i) at the input of one channel of the beamformer network. To better illustrate this, refer to Figure A-2. The loss (L_B) of the beamformer acts on both the signal (S_i) and the noise (N_i) inputs equally. However, the gain of the beamformer is different for signals and noise. The signal gain is 1 per channel while the noise gain is $1/G_B$ per channel since the signal adds coherently (in phase) and the noise adds incoherently (random phase).

[A-1]   Hoffman, J.B., *Preliminary Results of Active Array Noise Figure/Third Order Intercept Tradeoff Analysis*, Technology Service Corporation, Silver Spring, MD, 11 December 1991.
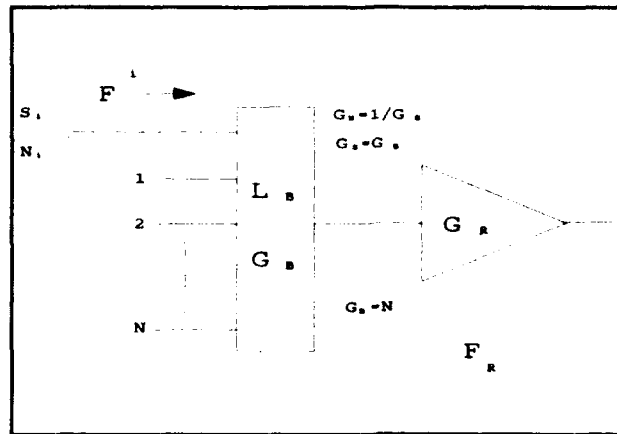
FIGURE A-2. TYPICAL BEAMFORMER

     In addition, more noise is added in the beamformer because of beamformer losses. Since the definition of noise figure is the ratio of input signal-to-noise (S/N) to output S/N, we can follow the signal and noise through the beamformer and write the following equations:

$$S_{o,b} = \frac{S_i}{L_B}$$

and:

$$N_{o,b} = \frac{N_i}{L_B * G_B} + \frac{K * T_{eB} * B}{G_B * L_B}$$

where:

$S_{o,b}$ = *signal at output of beamformer*

$N_{o,b}$ = *noise at output of beamformer*

S_i = *beamformer (circuit) input signal*

N_o = *beamformer (circuit) input noise*

L_B = *beamformer loss*

G_B = *beamformer (array) gain*

K = *Boltzmann's Constant*

B = *system-noise bandwidth*

T_{eB} = *effective passive beamformer temperature*

It should be noted that the effective passive-device temperature (T_{eB}) has been defined at the input of the beamformer so that it is effected by the beamformer loss and gain the same as the input noise (N_i) from previous stages. Continuing to the output of the receiver stage, the output signal and noise become:

$$S_{o,r} = \frac{S_i * G_R}{L_B}$$

and:

$$N_{o,r} = G_R * \left(\frac{N_i}{L_B * G_B} + \frac{K * T_{eB} * B}{L_B * G_B} \right) + G_R * K * T_{eR} * B$$

where:

$S_{o,r}$ = *signal at receiver output*

$N_{o,r}$ = *noise at receiver output*

G_R = *receiver gain*

T_{eR} = *effective receiver noise temperature*

and, again, T_{eR} is defined at the input to the receiver and is the contribution to the output noise power from the receiver. Since definition of the noise figure (F^i) is the input S/N divided by the output S/N, then:

$$F^i = \frac{(\frac{S_i}{N_i})}{[\frac{(\frac{S_i * G_R}{L_B})}{G_R * (\frac{N_i}{L_B * G_B} + \frac{K * T_{eB} * B}{L_B * G_B} + K * T_{eR} * B)}]}$$

where:

F^i = *total equivalent noise figure at input of beamformer, translated receiver with beamformer noise figures*

Reducing yields:

$$F^i = \frac{N_i + K * T_{eB} * B + G_B * L_B * K * T_{eR} * B}{N_i * G_B}$$

Continuing:

$$F^i = \frac{1}{G_B} * [\frac{N_i + K * T_{eB} * B}{N_i} + G_B * L_B * (\frac{K * T_{eR} * B}{N_i})]$$

$$= \frac{1}{G_B} * [\frac{N_i + K * T_{eB} * B}{N_i} + G_B * L_B * (\frac{K * T_{eR} * B + N_i}{N_i} - \frac{N_i}{N_i})]$$

(A-1)

At this time, it should again be noted that the general definition of noise figure is the input S/N ratio divided by the output S/N ratio, or:

$$F = \frac{\dfrac{S_{in}}{N_{in}}}{\dfrac{S_{out}}{N_{out}}}$$

$$= \frac{\dfrac{S_{in}}{N_{in}}}{\dfrac{S_{in}*G}{N_{in}*G + N_{Ae}*G}} \tag{A-2}$$

$$= \frac{N_{in} + N_{Ae}}{N_{in}}$$

where:

N_{Ae} = equivalent added noise referenced at input of device

The noise added in the attenuator (L_B) is:

$$N_{Ae} = K*T_{eB}*B$$

where:

$$T_{eB} = T_0*(L_B-1)$$

Applying these results to Equation (A-2) yields:

$$F_B = \frac{N_i + K*T_0*B*(L_B-1)}{N_i}$$

and:

$$N_i * (F_B - 1) = K * T_0 * B * (L_B - 1)$$
$$= N_i * (L_B - 1)$$

which reduces to:

$$F_B = L_B$$

therefore:

$$L_B = \frac{N_i + K * T_{eB} * B}{N_i}$$

Similarly:

$$F_R = \frac{N_i + K * T_{eR} * B}{N_i}$$

Substituting these last two equations into Equation (A-1) yields:

$$F^i = \frac{1}{G_B} [L_B + G_B * L_B * (F_R - 1)]$$

$$= \frac{L_B}{G_B} + L_B * (F_R - 1)$$

A-3

Applying conventional rules about translating noise figures through cascaded stages yields:

$$F_{SA} = F_A + L_R * [F_1 + \frac{F_2 - 1}{G_1} + \frac{F_3 - 1}{G_1 * G_2} + \frac{F^{ii} - 1}{G_1 * G_2 * G_3}]$$

where, referring to Figure A-1:

F_{SA} = *system noise figure defined at antenna terminals*

F_A = *antenna temperature*

F_1 = *first amplifier input noise figure*

F_2 = *second amplifier input noise figure*

F_3 = *third amplifier input noise figure*

G_1 = *first amplifier gain*

G_2 = *second amplifier gain*

G_3 = *third amplifier gain*

F^{ii} = *total noise figure at point shown on Figure A-1,*

   F^i *translated through module loss*

and:

$$F^{ii} = L_m * F^i$$

Making these substitutions gives:

$$F_{SA} = F_A + L_R * [F_1 + \frac{F_2 - 1}{G_1} + \frac{F_3 - 1}{G_1 * G_2} + \frac{\frac{L_m * L_B}{G_B} + L_m * L_B * (F_R - 1) - 1}{G_1 * G_2 * G_3}]$$

which ultimately reduces to:

$$F_{SA} = F_A + L_R * [F_1 + \frac{F_2 - 1}{G_1} + \frac{F_3 - 1}{G_1 * G_2} + \frac{L_m * L_B * (\frac{1 - G_B}{G_B}) + (L_m * L_B * F_R - 1)}{G_1 * G_2 * G_3}] \quad (A-4)$$

APPENDIX B

THIRD-ORDER INTERCEPT

APPENDIX B NOMENCLATURE

HEMT   High-electron mobility transistor

HBT   Heterojunction bipolar transistor

MSFET   Metal semiconductor field-effect transistor

This appendix derives general expression for the third-order intercept (TOI) of a typical amplifier chain with attenuators and a beamformer network that could be found in active array receivers. This work, along with Appendix A, was used for comparison to work performed by Hoffman.[B-1] The results are shown in Appendix C.

Each amplifier of a chain has associated with it a TOI referenced to either the input or the output and different by the gain of the amplifier. The intent here is to determine the maximum overall chain TOI, given its interdependence on the individual amplifier TOIs. From Collier's work,[B-2] the general form of total TOI is given for a two-node cascade by:

$$I_{T_x} = (\frac{1}{I^X_1} + \frac{1}{I^X_2})^{-1}$$

$$(B-1)$$

where:

I_{T_x} = total TOI at point X

I^X_1 = output TOI of first node referenced at point X

I^X_2 = output TOI of node two referenced at point X

The example given in Reference B-2 showed quite clearly how Equation (B-1) is applied. However, the method of handling passive components, such as attenuators, was not shown. Referring to Figure B-1, the example is modified to include these effects. The TOIs shown are output TOIs.
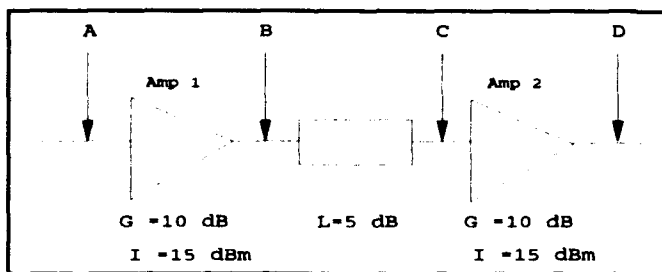
FIGURE B-1. EXAMPLE PORTION OF A TYPICAL
AMPLIFIER CHAIN

[B-1] Hoffman, J.B., *Preliminary Results of Active Array Noise Figure/Third Order Intercept Tradeoff Analysis*, Technology Service Corporation, Silver Spring, MD, 11 December 1991

[B-2] Collier, Don, "Optimizing LNA's for Use in Phased Arrays," *Microwave Systems News*, April 1990, pp 37-44.

A key simplifying assumption is that all passive components (not components such as limiters) considered can be thought of as having an infinite TOI. While this is not strictly true, it is a valid and useful assumption in this case and for the signal levels considered here. Going forward through the chain, at point C the contribution from the left of C can be written:

$$I_{T_C} = \left(\frac{1}{I^C_{T_{Lft}}} + \frac{1}{I^C_{T_{Rgt}}} \right)^{-1}$$

$$I^C_{T_{Lft}} = \frac{\left(\frac{1}{I_1} + \frac{1}{I_A} \right)^{-1}}{L}$$

$$I^C_{T_{Rgt}} = \frac{I_2}{G_2}$$

where:

I_{T_C} = *total TOI at point C*

$I^C_{T_{LFT}}$ = *total TOIs before C, referenced at C*

$I^C_{T_{Rgt}}$ = *total TOIs after C, referenced at C*

I_1 = *output TOI of first amplifier*

= *15 dBm*

I_2 = *output TOI of second amplifier*

= *15 dBm*

G_2 = *gain of amplifier two*

= *10 dB*

I_A = *attenuator output TOI*

= *∞*

L = *attenuator loss*

= *5 dB*

The definitions of parameters relative to the subscripts and superscripts are consistant and maintained from this point on. That is, I^X_1 and I^X_2 are the reflection of the output TOIs of

amplifiers one and two to the point X. Refer to Figure B-1 for the definitions for these general examples. Substituting values for the parameters yields:

$$I^C{}_{T_{Lf}} = (\frac{1}{31.62*.31623} + \frac{1}{\infty})^{-1}$$

$$= (\frac{1}{10} + 0)^{-1}$$

$$= 10 \ mw$$

$$= 10 \ dBm$$

$$I^C{}_{T_{Rgt}} = \frac{31.62}{10}$$

$$= 3.162 \ mw$$

$$= 5.0 \ dBm$$

Combining terms and solving for the total TOI at point C yields:

$$I_{T_C} = (\frac{1}{I^C{}_{T_{Lf}}} + \frac{1}{I^C{}_{R_{gt}}})^{-1}$$

$$= (\frac{1}{10} + \frac{1}{3.162})^{-1}$$

$$= 2.4024 \ mw$$

$$= 3.81 \ dBm$$

If we wanted, we could translate this to point D, yielding:

$$I_{T_D} = I_{T_C}*G_2$$

$$= 2.4024*10$$

$$= 24.024 \ mw$$

$$= 13.81 \ dBm$$

Checking this result by using another approach, we can determine each component of TOI by translating them through the losses and gains to have at point D:

$$I_{T_D} = (\frac{1}{I'_1} + \frac{1}{I_2})^{-1}$$

$$= (\frac{1}{\dfrac{I_1 * G_2}{L}} + \frac{1}{I_2})^{-1}$$

$$= (\frac{1}{100} + \frac{1}{31.62})^{-1}$$

$$= 24.02 \ mw$$

$$= 13.81 \ dBm$$

which is the same results using both approaches.

To determine the chain input TOI point, we can translate this 13.81 dBm back through the chain, thus:

$$I_{T_A} = (13.81 \ dBm) - G_2 + L - G_1$$

$$= -1.19 \ dBm$$

This can also be checked by doing the original analysis going backward:

$$I_{T_B} = (\frac{1}{I_1} + \frac{1}{\dfrac{I_2 * L}{G_2}})^{-1}$$

$$= (\frac{1}{31.62} + \frac{1}{\dfrac{31.62 * 3.162}{10}})^{-1}$$

$$= .13^{-1}$$

$$= 7.59630 \ mw$$

$$= 8.80602 \ dBm$$

$$I_{T_A} = 8.80669 \; dBm - G_1$$

$$= 8.80669 - 10$$

$$= -1.19331 \; dBm$$

or by using the formula:

$$I_{T_A} = \left(\frac{1}{\dfrac{I_1}{G_1}} + \frac{1}{\dfrac{I_2 * L}{G_1 * G_2}} \right)^{-1}$$

$$= \left(\frac{1}{3.1623} + \frac{1}{\dfrac{100}{100}} \right)^{-1}$$

$$= .75975 \; mw$$

$$= -1.19331 \; dBm$$

which confirms the results.

These examples show that it does not matter where the relation is applied in the chain as long as the gains and losses are adequately accounted for. Each of the individual TOIs can be referred/translated to the point of interest separately and combined using the formula at that point of interest.

Applying this technique to the same receiver chain used in Appendix A (reproduced in Figure B-2 with appropriate labels) the individual TOIs (defined at the antenna terminals) are:

$$I^{SA}_R = \frac{I_R * I_R * L_m * L_B}{G_R * G_B * G_3 * G_2 * G_1}$$

$$I^{SA}_3 = \frac{I_3 * L_R}{G_3 * G_2 * G_1}$$

$$I^{SA}_2 = \frac{I_2 * L_R}{G_2 * G_1}$$

$$I^{SA}_1 = \frac{I_1 * L_R}{G_1}$$

FIGURE B-2. REPRESENTATIVE RECEIVER DESIGN, THE Is ARE OUTPUT TOIs

Combining these components yields the total system TOI referenced to the antenna terminals:

$$I_{T_{SA}} = (\frac{I_R * L_R * L_m * L_B}{G_R * G_B * G_3 * G_2 * G_1} + \frac{I_3 * L_R}{G_3 * G_2 * G_1} + \frac{I_2 * L_R}{G_2 * G_1} + \frac{I_1 * L_R}{G_1})^{-1} \qquad \text{(B-2)}$$

It is easiest to determine each component of Equation (B-2) in dBm, then convert to mw to do the sum. It is concluded that the gain (G_B) of the beamformer can be used because the whole array would be functioning to reach TOI for the off-array receiver amplifier. Each array module is assumed to provide the same signal level to the beamformer. In practice, this may not be true; receiver weighting (taper) may result in different characteristics. Also, different placement of the attenuator (L_m) would yield different results, although mostly for noise figure.

APPENDIX C

RESULTS

APPENDIX C NOMENCLATURE

HEMT   High-electron mobility transistor

HBT   Heterojunction bipolar transistor

MSFET   Metal semiconductor field-effect transistor

This appendix presents the result of applying the noise figure, third-order intercept, and dynamic-range equations that were developed in this effort to the parameters used in Reference 1 with an antenna contribution (F_A) of 0.53416 as determined using the approach utilized in Appendix D. The difference is that the starting noise figure was read as 2.77 dB at that time versus 2.75 dB in Appendix D. This explains why this number is different, although only slightly, from that used in Appendix D. For each result, the parameters will be restated first, as taken from Reference C-1, along with the page number in Reference C-1 that corresponds to the presented case. The graphed results will then be presented in Figures C-1 through C-6. The reader must compare these results with those of Reference C-1; however, three examples of Hoffman's[C-1] results (see the following text) are shown for immediate comparison.

In general, the results of the two analyses agree very closely. The noise-figure results at low-module loss agree quite closely. Any errors, with the exception of case 28, are thought to be because of initial inaccuracy in reading the noise-figure graphs to calculate the effects of antenna temperature. See the introduction above, page C-56, and Appendix D. At high-module loss (40 dB) the differences vary from ≈ 0.5 to ≈ 2.5 dB difference. These are still small differences because of the similarity in the equations used. The noise figures shown here are all smaller because of the negative term arising from the effects of beamformer gain. Therefore, the noise figures presented here are somewhat better (at high-module loss) than in the original analysis.

Third-order intercepts are virtually identical in Reference C-1 and here because it is believed that the same equations were used. For this reason, little can be said except that the original work has been confirmed in this area. It should be mentioned that this third-order effect is a result of two input signals of equal magnitude. A complete analysis should also look at the more likely events of nonequal magnitude signal interference and greater-than-two signal interference cases. A thorough analysis would be very difficult and is beyond the scope of this analysis.

Finally, dynamic-range questions arise concerning active, phased-array antennas. The analysis of Reference C-1 did not address dynamic-range questions. The curves presented here, showing dynamic range, show considerable dependance on module loss, as one would expect. The dynamic range can typically change ≈ 13 dB or more for a module loss from 0 to 30 dB. An analysis of system-dynamic range versus antenna-weighting taper (similar to the noise-figure versus taper analysis presented here earlier) should be undertaken. Antenna taper would cause the outer elements to experience increased dynamic range, in most cases considered here up to a 30-dB weight. Because the dynamic range increases, this may not be an issue; but if time had permitted, that analysis would have been done. Cases 1, 4, and 7 of Hoffman's[C-1] results are shown for comparison and are shown immediately after those cases as presented here.

[C-1] Hoffman, J.B., *Preliminary Results of Active Array Noise Figure/Third Order Intercept Tradeoff Analysis*, Technology Service Corporation, Silver Spring, MD, 11 December 1991.

Case 1:   HEMT 3-Stage Configuration. F_i = 0.8 dB, G_i = 15 dB, TOI_i
= 28 dBm, L_R = 0.5 dB, L_A = 3 dB, G_B = 40 dB, F_R = 4 dB,
G_R = 10 dB, TOI_R = 55 dBm, Reference Page 27.
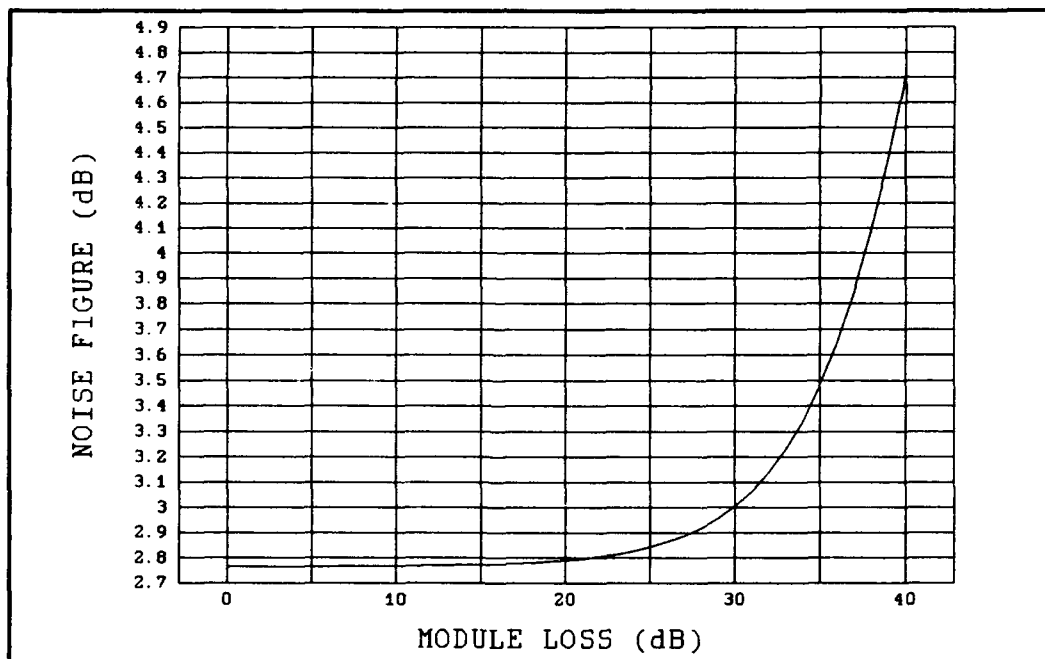
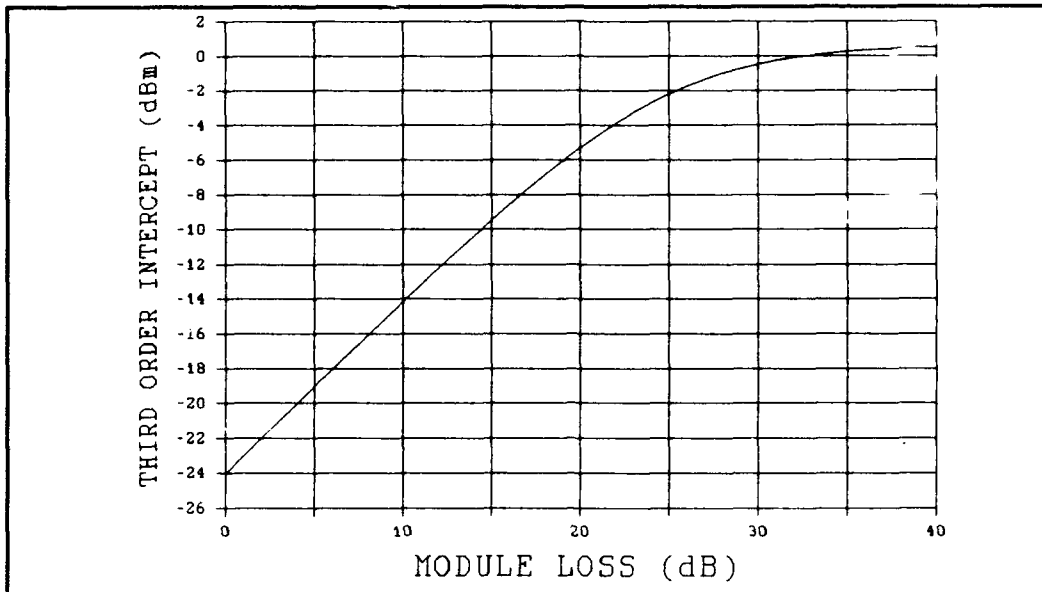Figure C-1A. Case 1, HEMT 3-Stage Noise Figure, Reference
Page 27.
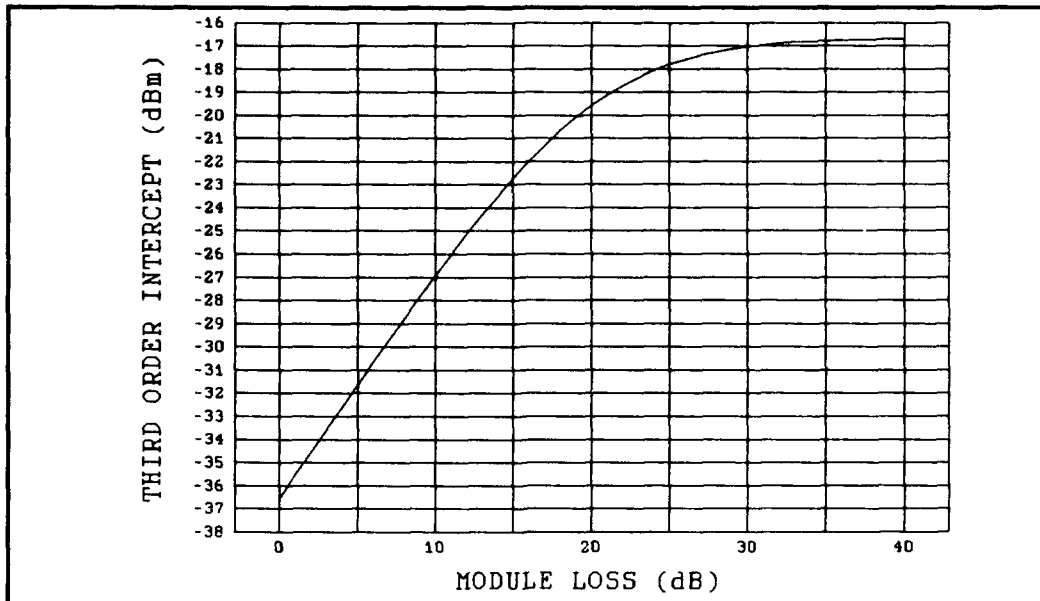
Figure C-1B. Case 1, HEMT 3-Stage Third Order Intercept, Reference Page 27.
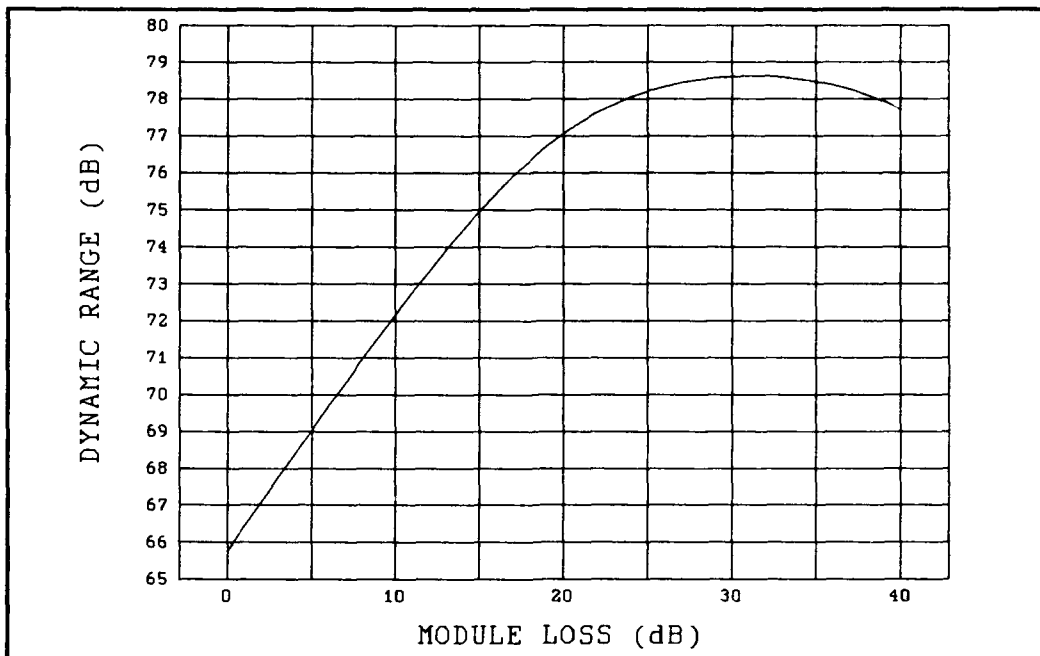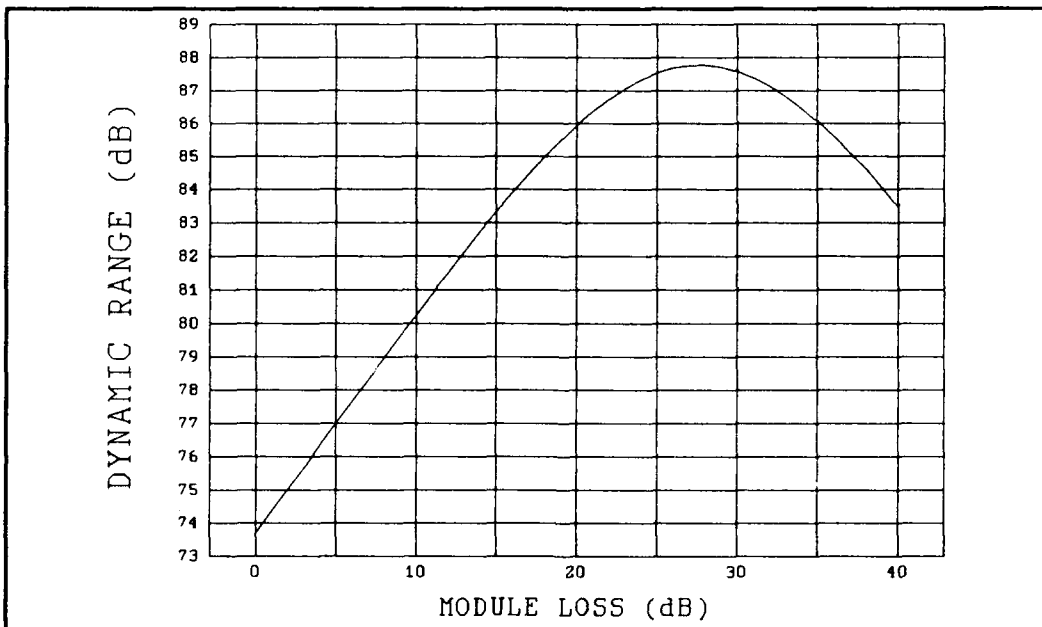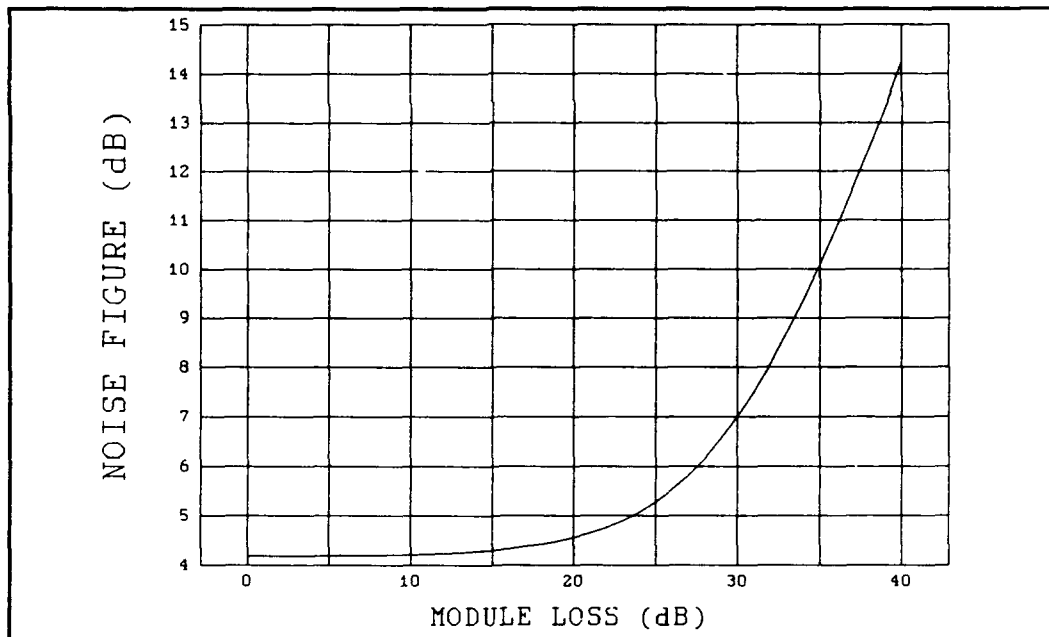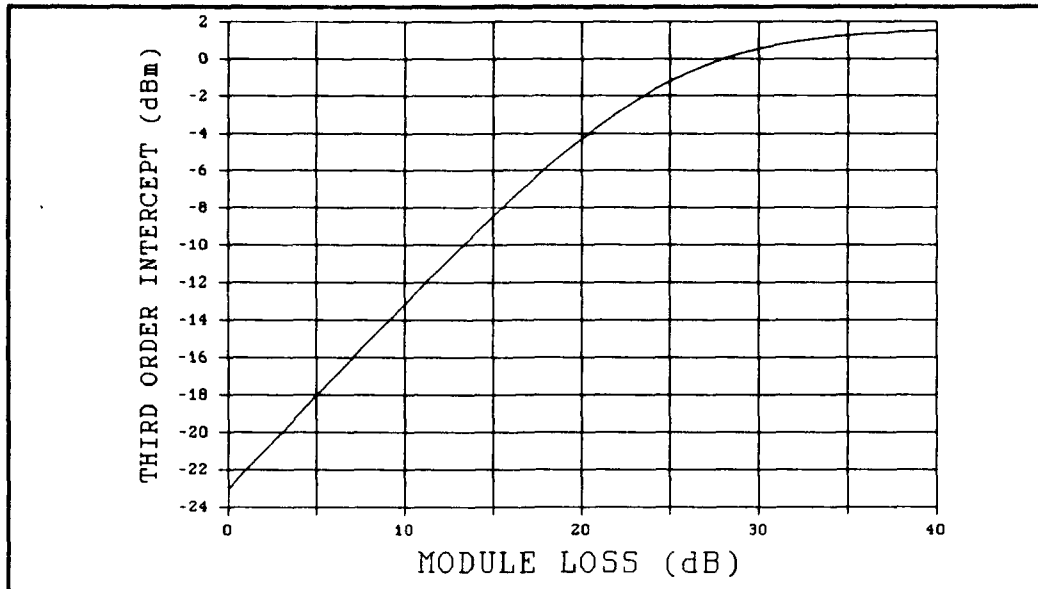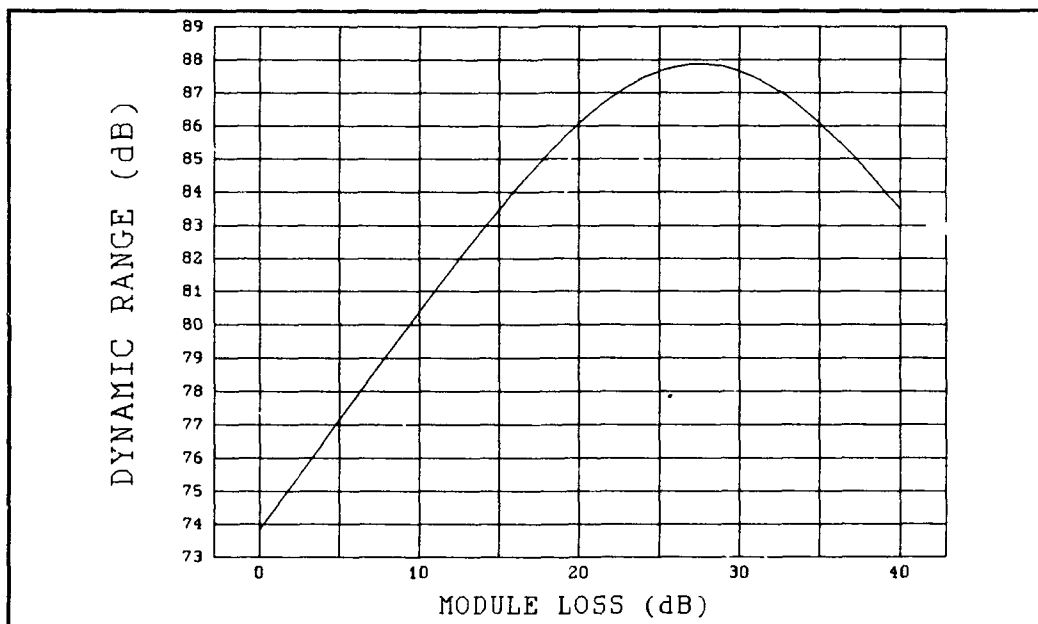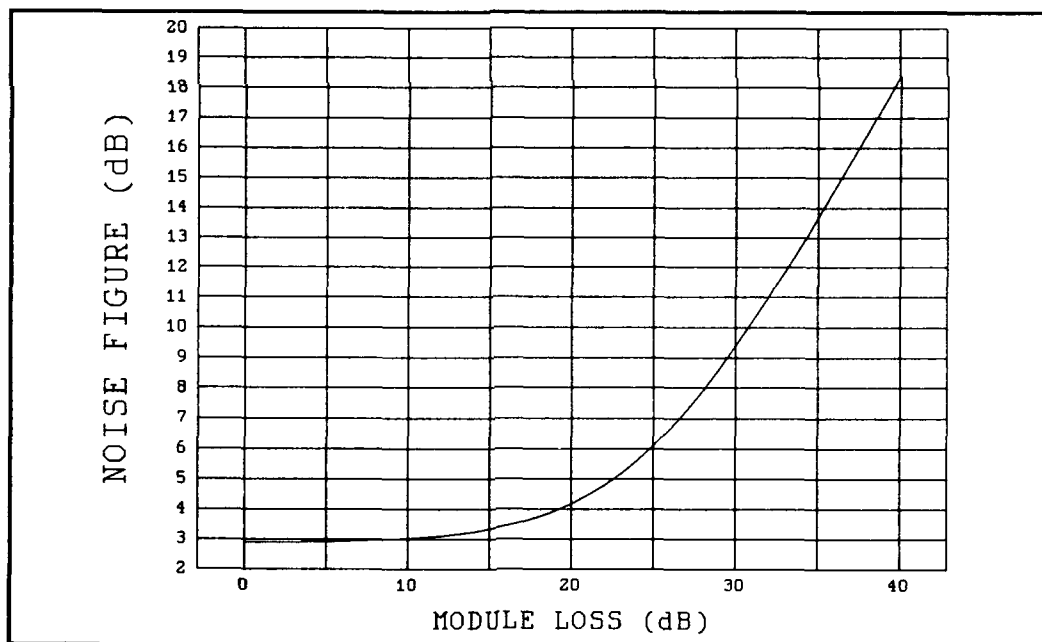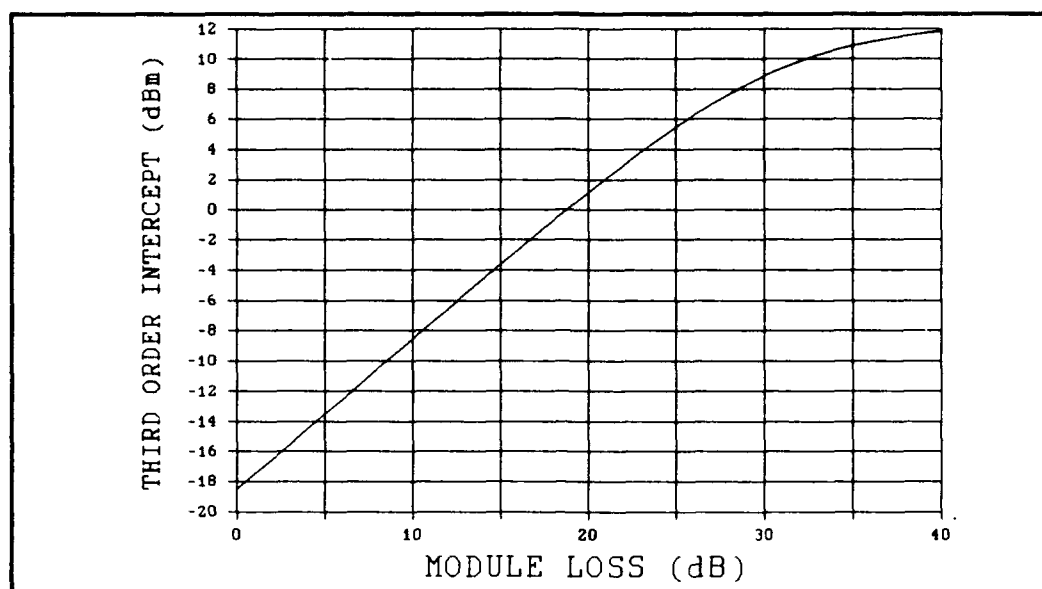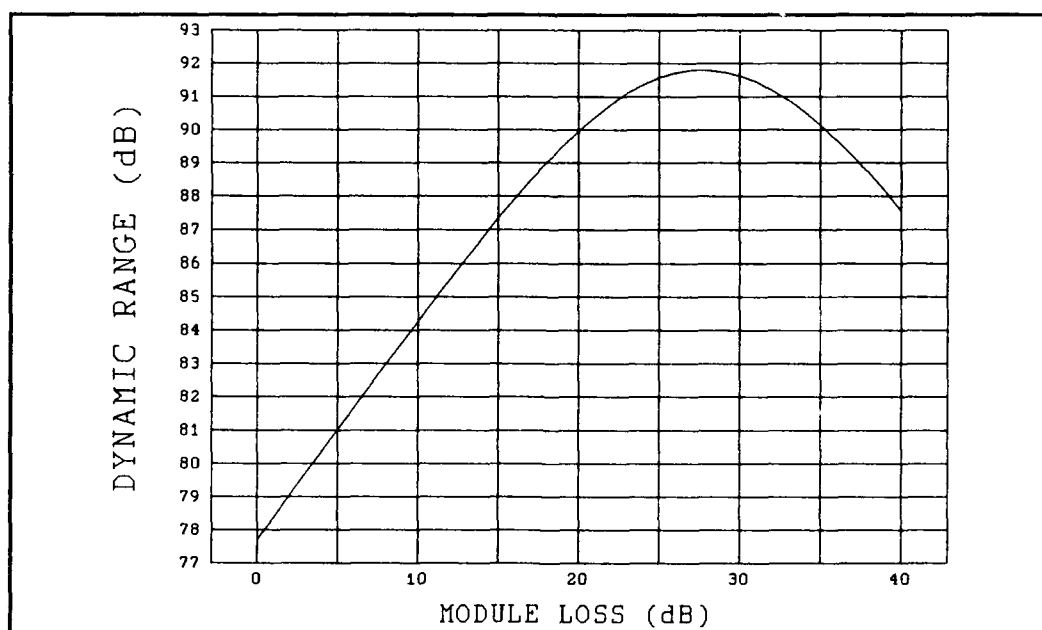

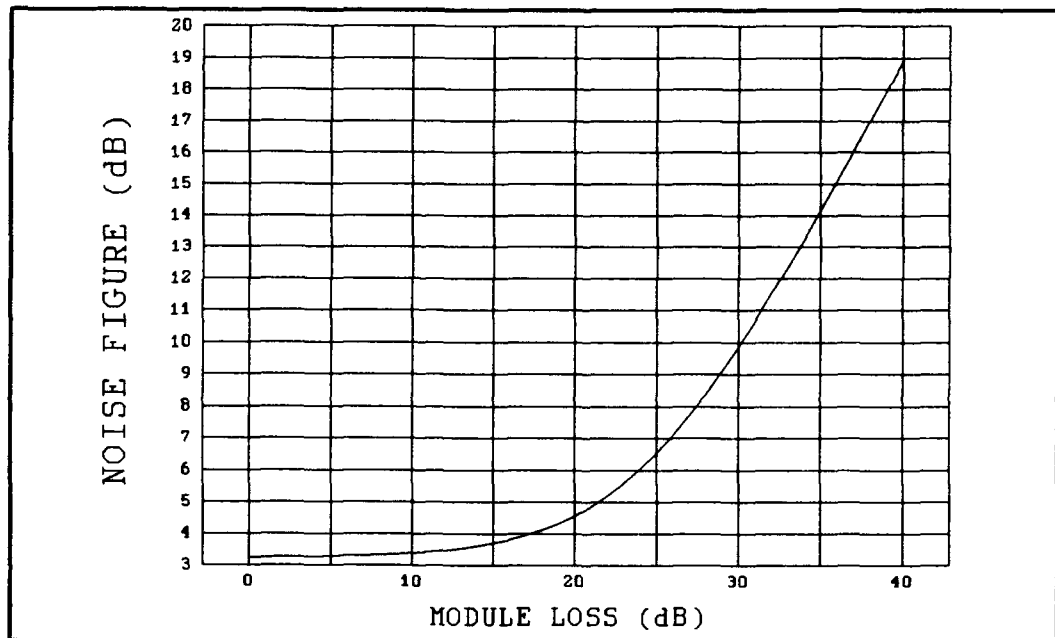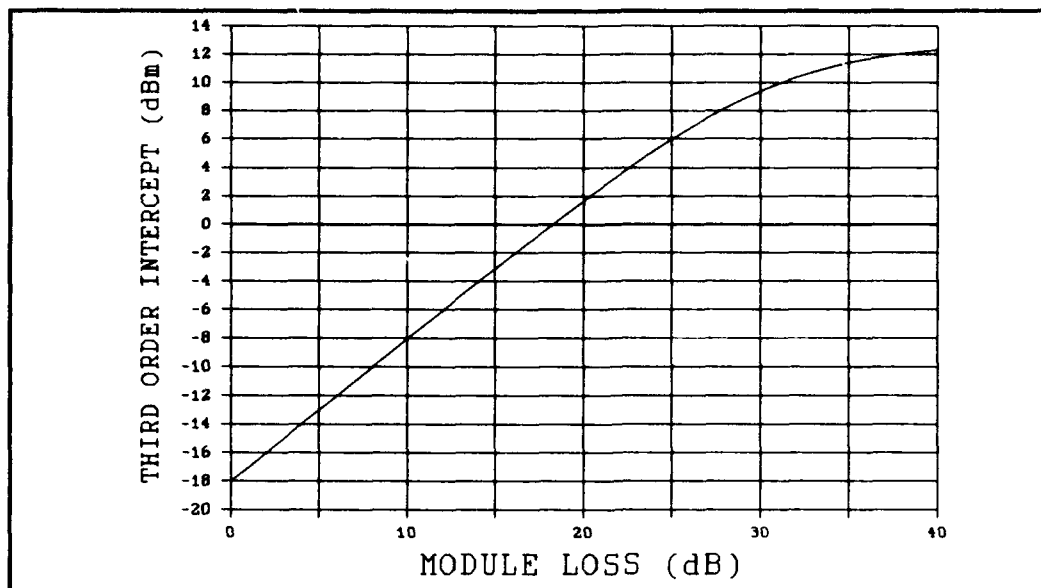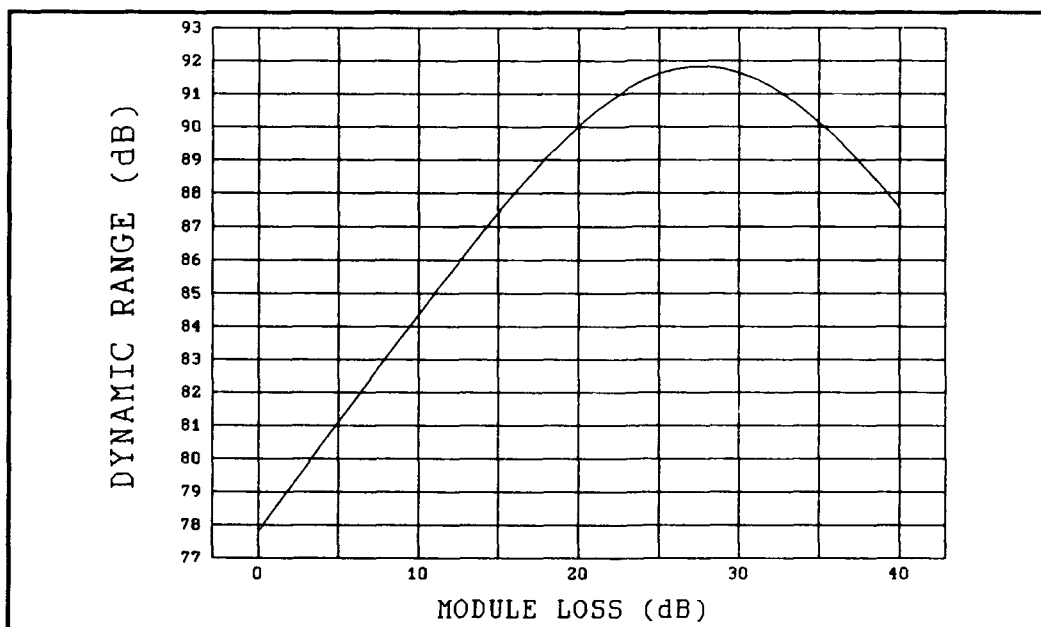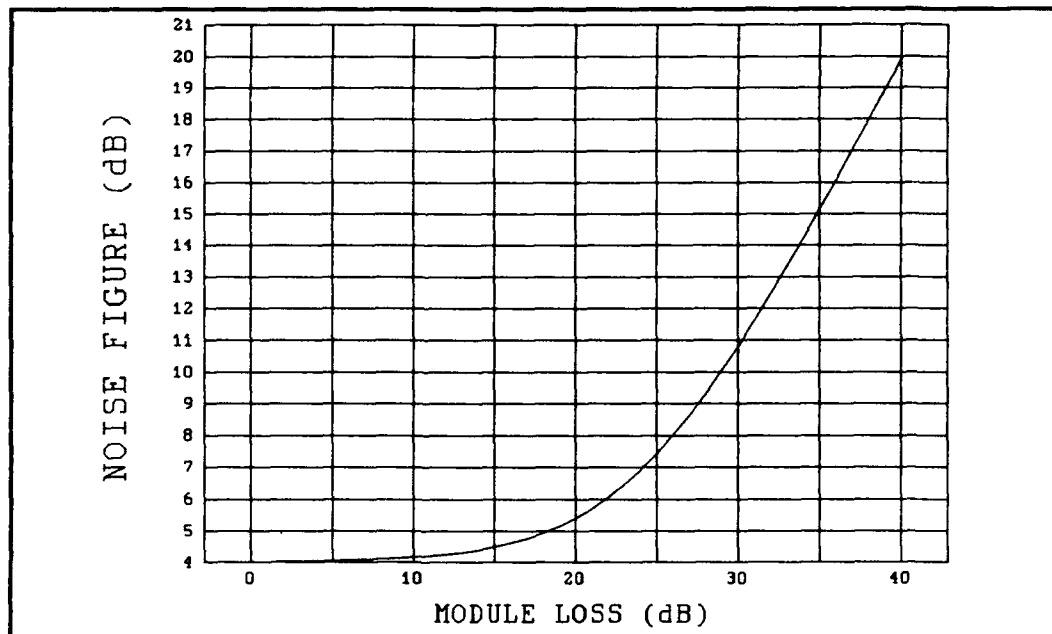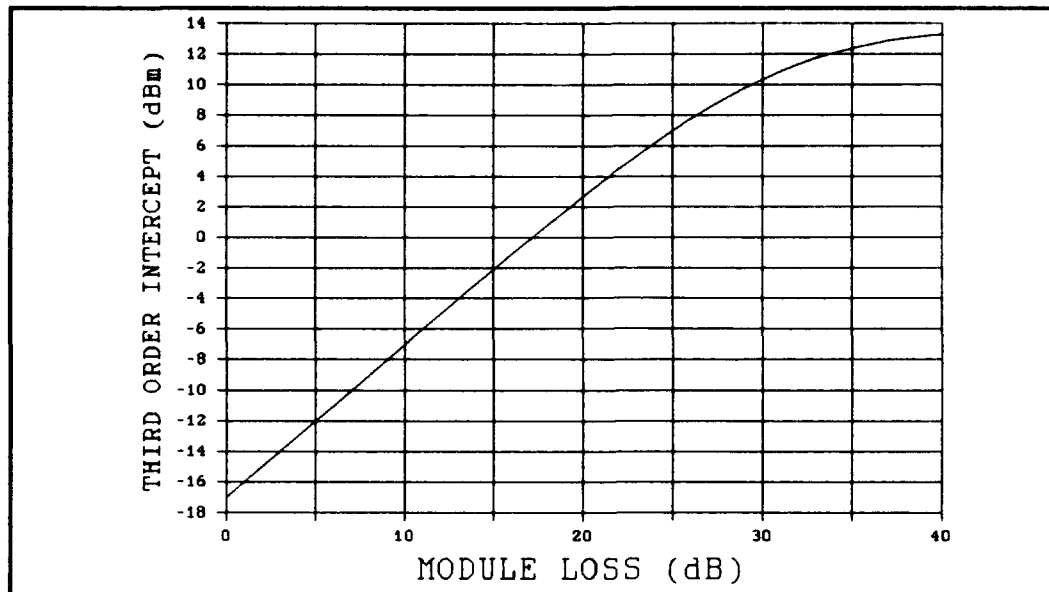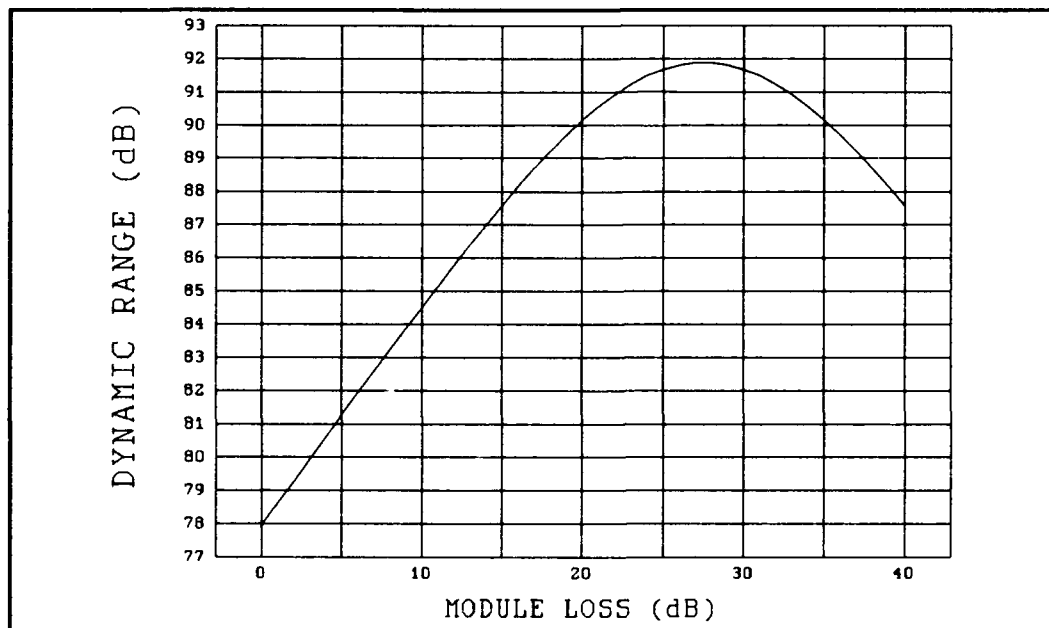**Figure C-1C. Case 1, HEMT 3-Stage Dynamic Range, Reference Page 27.**
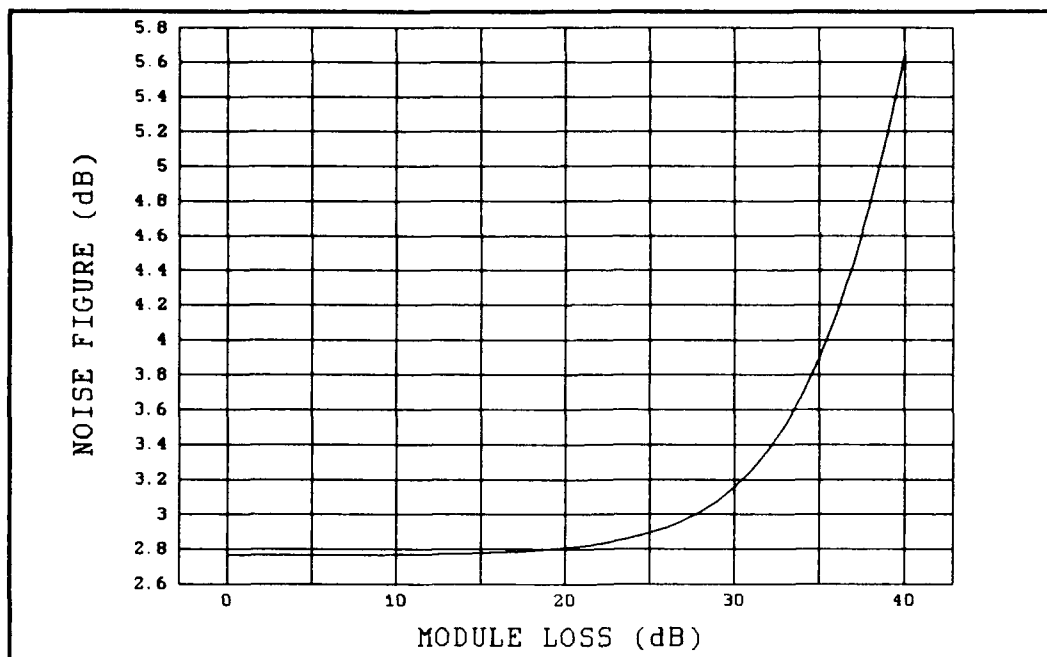
Figure C-1D. Hoffman's[C-1] Results, Case 1, HEMT 3-Stage Noise Figure, Reference Page 27, Shown For Comparison.
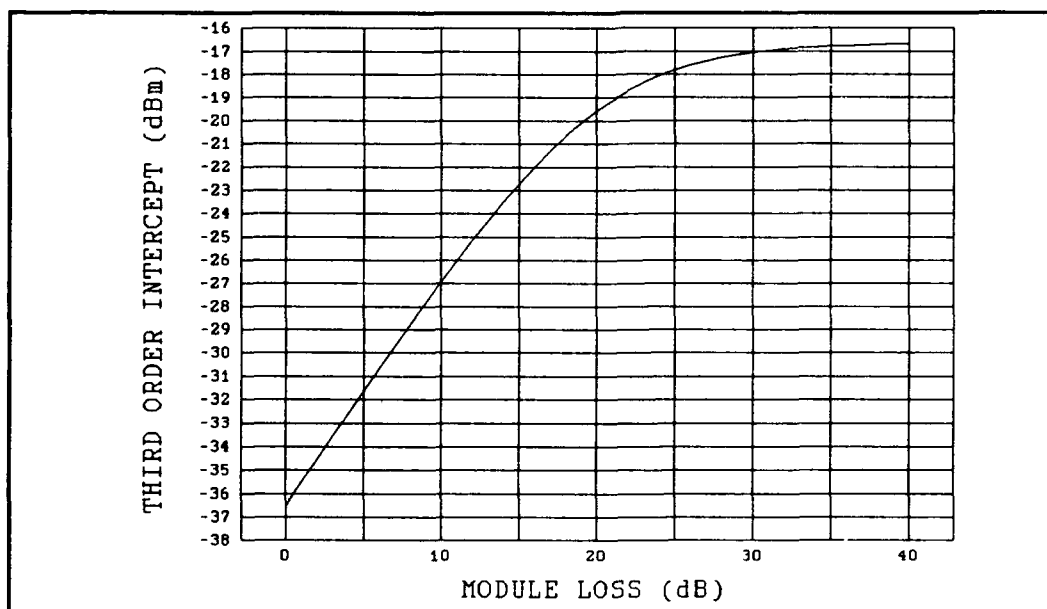
Figure C-1E. Hoffman's[C-1] Results, Case 1, HEMT 3-Stage Third-Order Intercept, Reference Page 27, Shown For Comparison.

Case 2: HEMT 3-Stage Configuration. F_i = 0.8 dB, G_i = 15 dB, TOI_i = 28 dBm, L_R = 1 dB, L_A = 3 dB, G_B = 40 dB, F_R = 4 dB, G_R = 10 dB, TOI_R = 55 dBm, Reference Page 28.
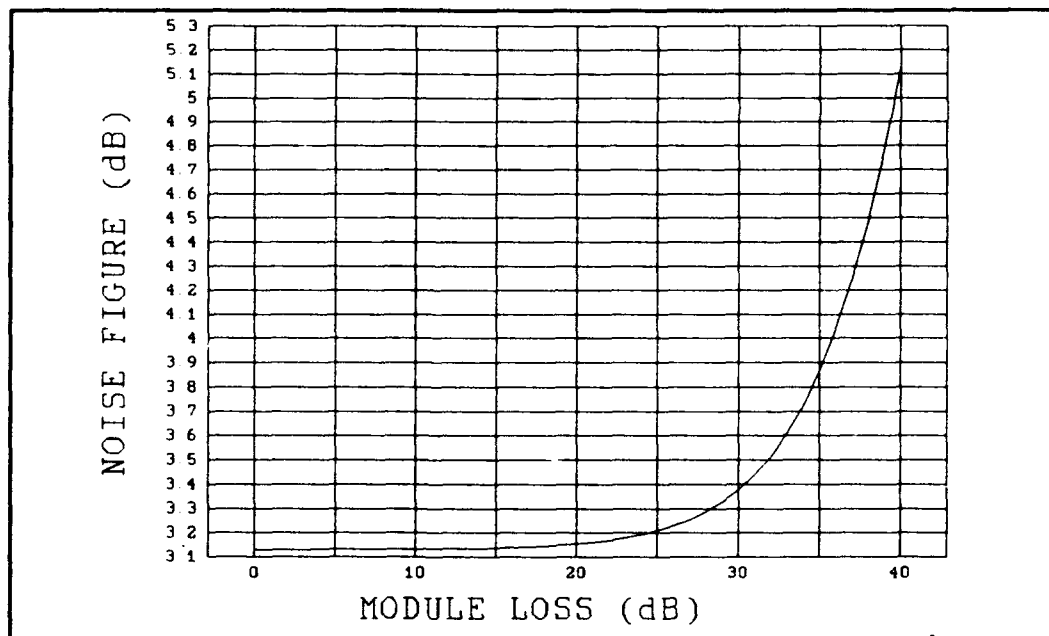
Figure C-2A. Case 2, HEMT 3-Stage Noise Figure, Reference Page 28.
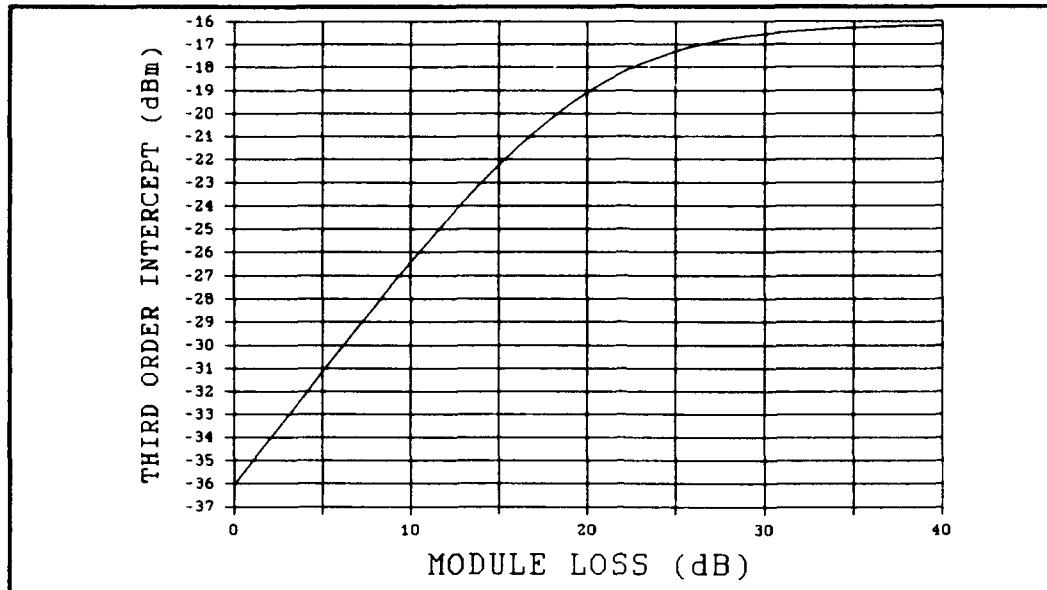
Figure C-2B. Case 2, HEMT 3-Stage Third-Order Intercept, Reference Page 28.
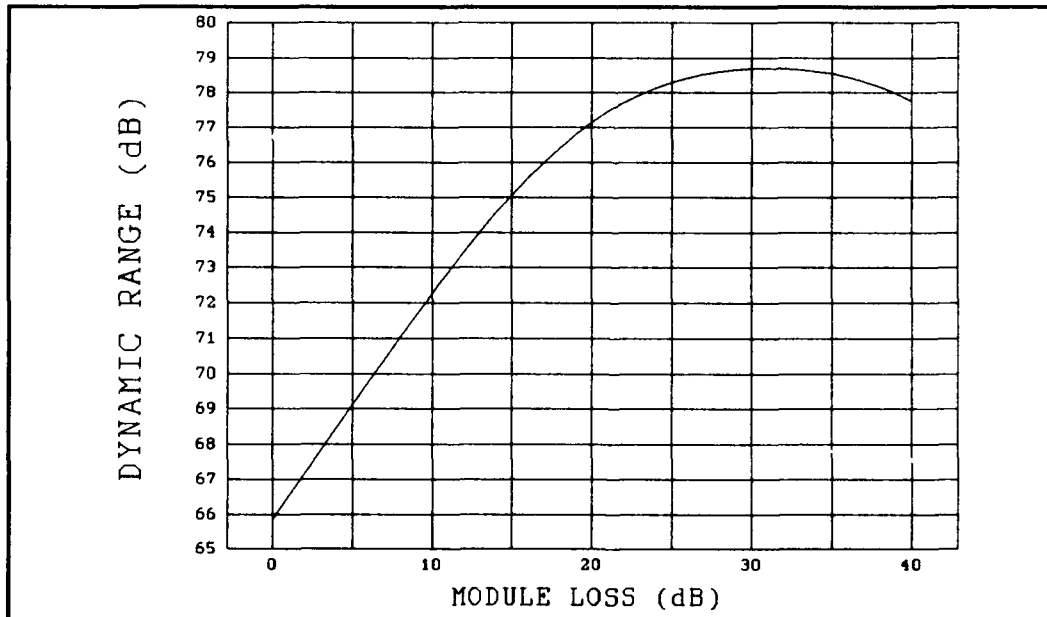
Figure C-2C. Case 2, HEMT 3-Stage Dynamic Range, Reference Page 28.

Case 3: HEMT 3-Stage Configuration. $F_i = 0.8$ dB, $G_i = 15$ dB, $TOI_i = 28$ dBm, $L_R = 2$ dB, $L_A = 3$ dB, $G_B = 40$ dB, $F_R = 4$ dB, $G_R = 10$ dB, $TOI_R = 55$ dBm, Reference Page 29.
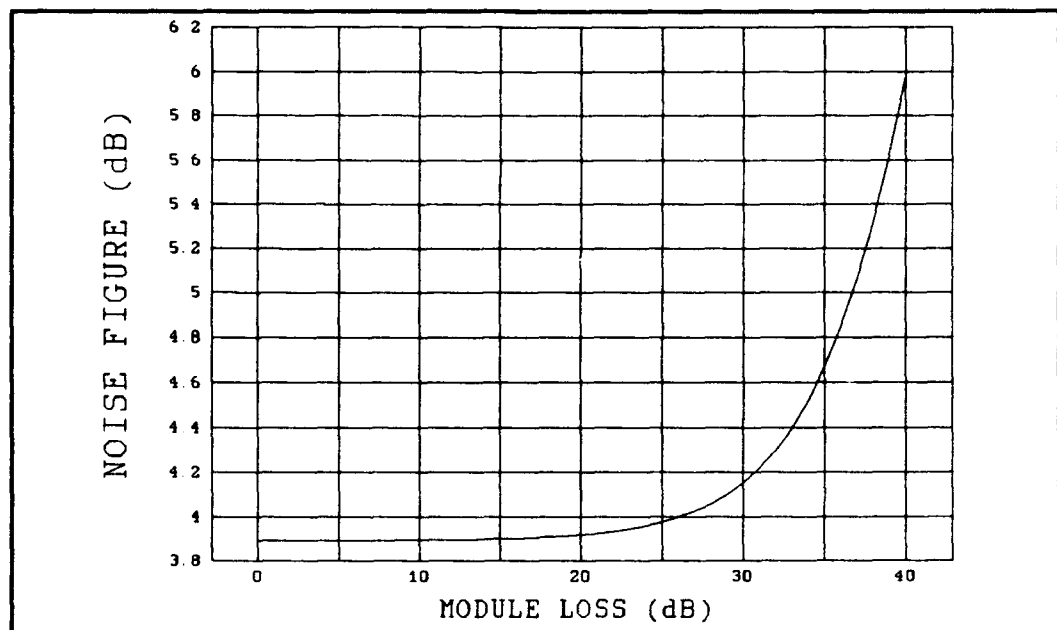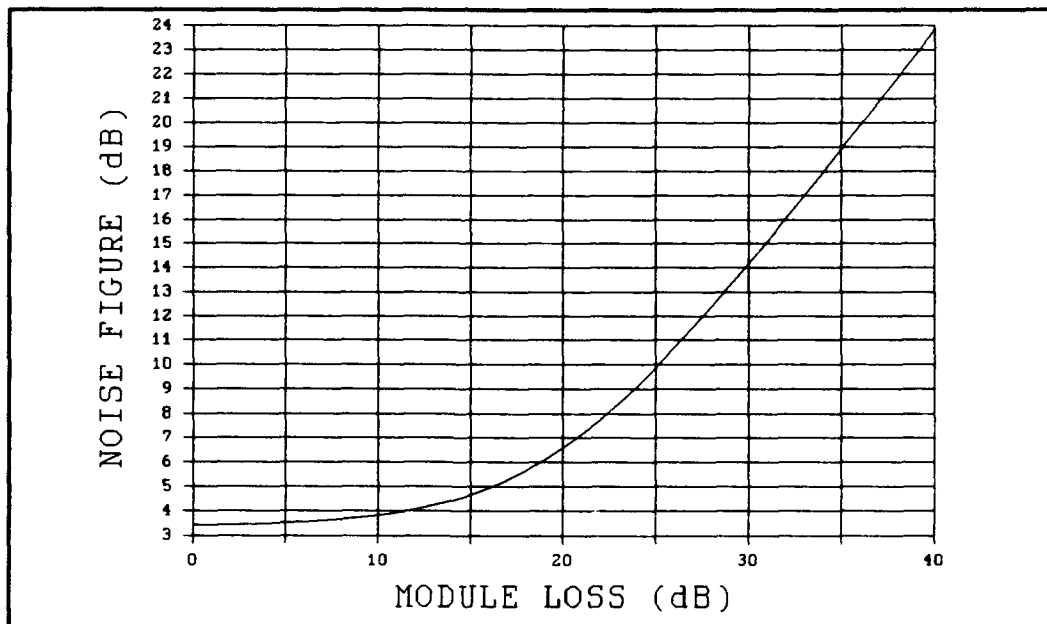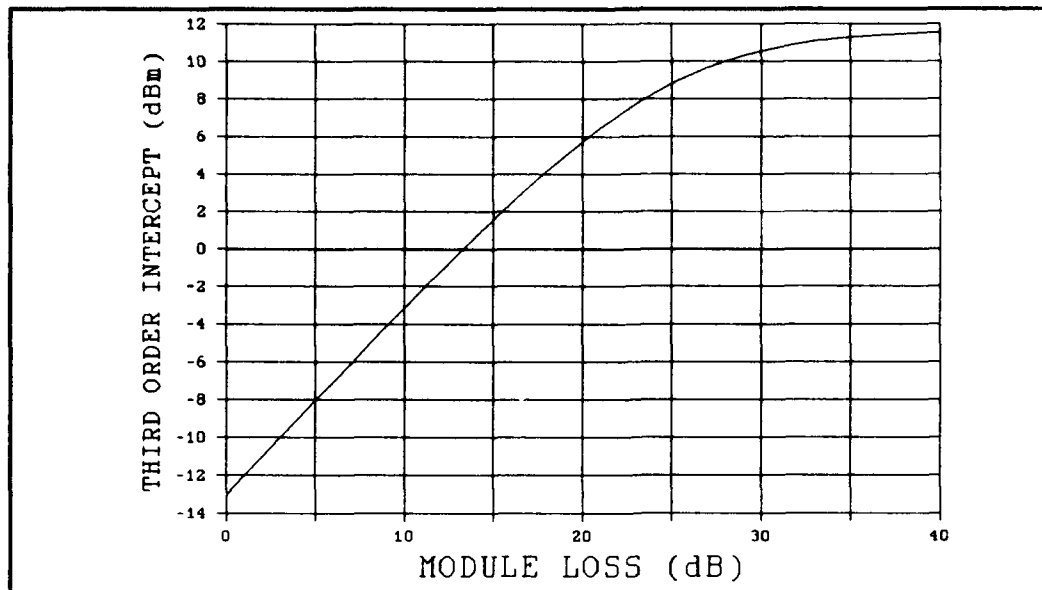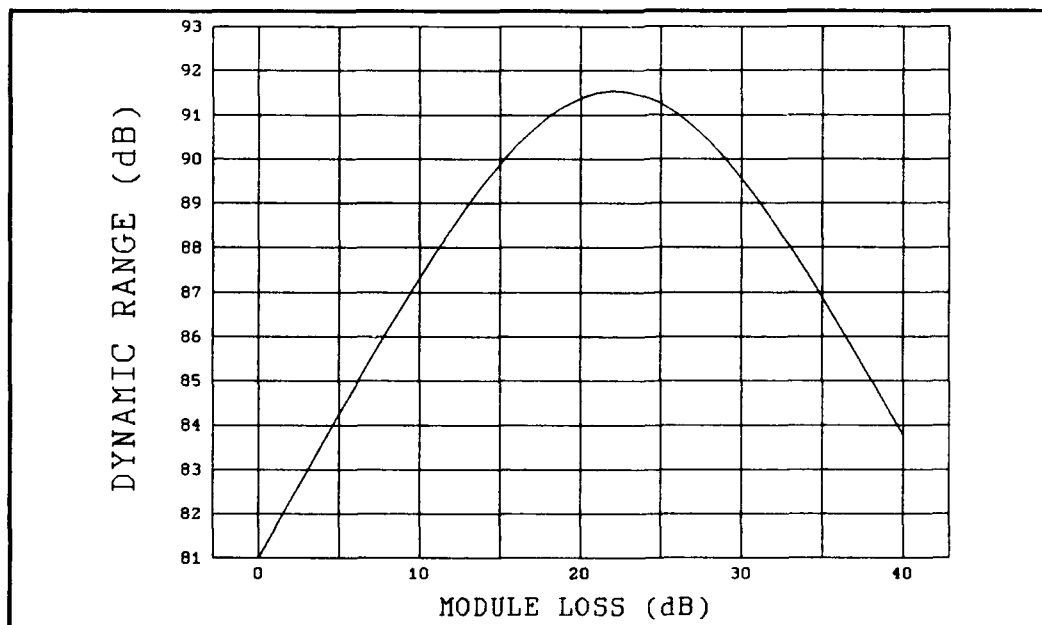

Figure C-3A. Case 3, HEMT 3-Stage Noise Figure, Reference Page 29.
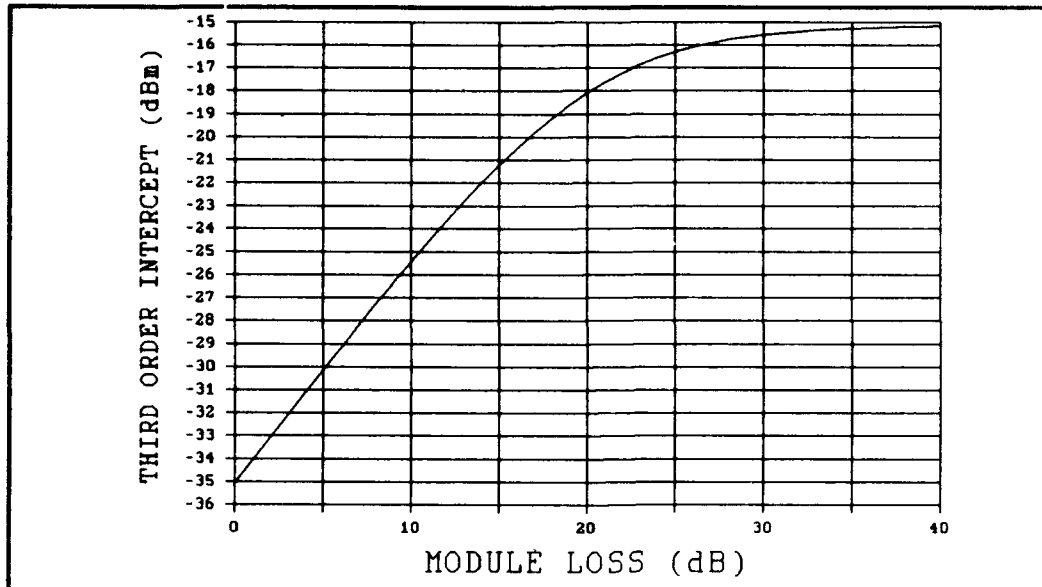
Figure C-3B. Case 3, HEMT 3-Stage Third-Order Intercept, Reference Page 29.
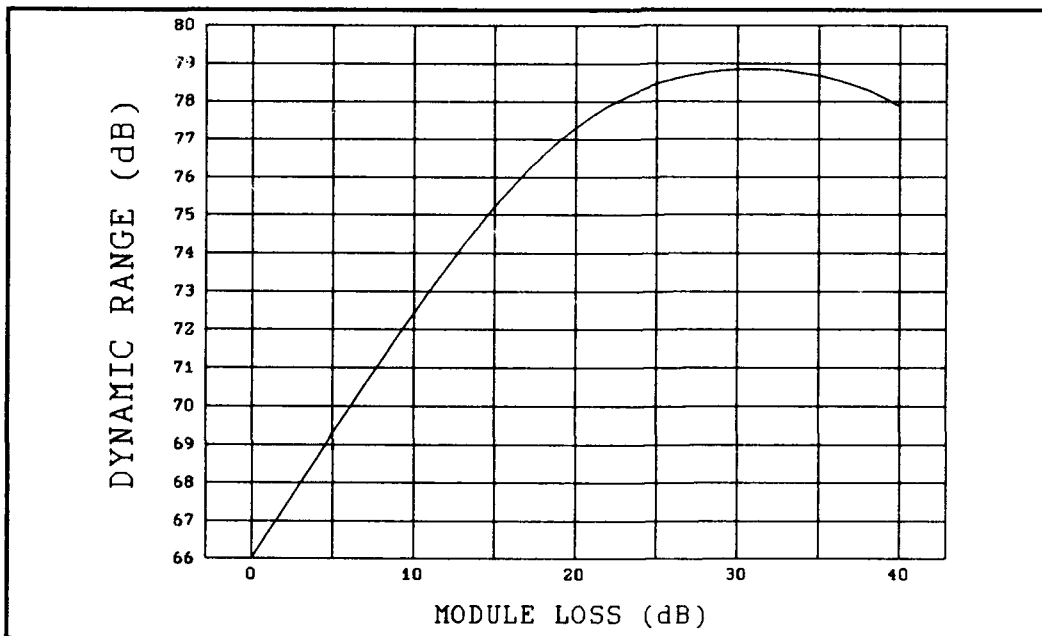
Figure C-3C. Case 3, HEMT 3-Stage Dynamic Range, Reference Page 29.

Case 4: MESFET 3-Stage Configuration. F_i = 1.1 dB, G_i = 11 dB, TOI_i = 33 dBm, L_R = 0.5 dB, L_A = 3 dB, G_B = 40 dB, F_R = 4 dB, G_R = 10 dB, TOI_R = 55 dBm, Reference Page 30.
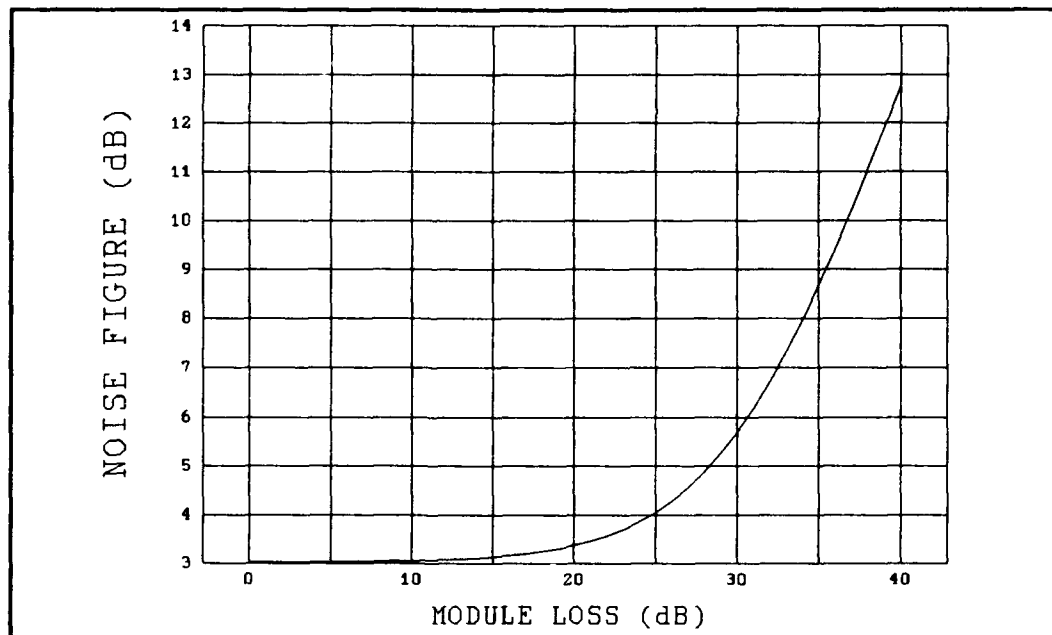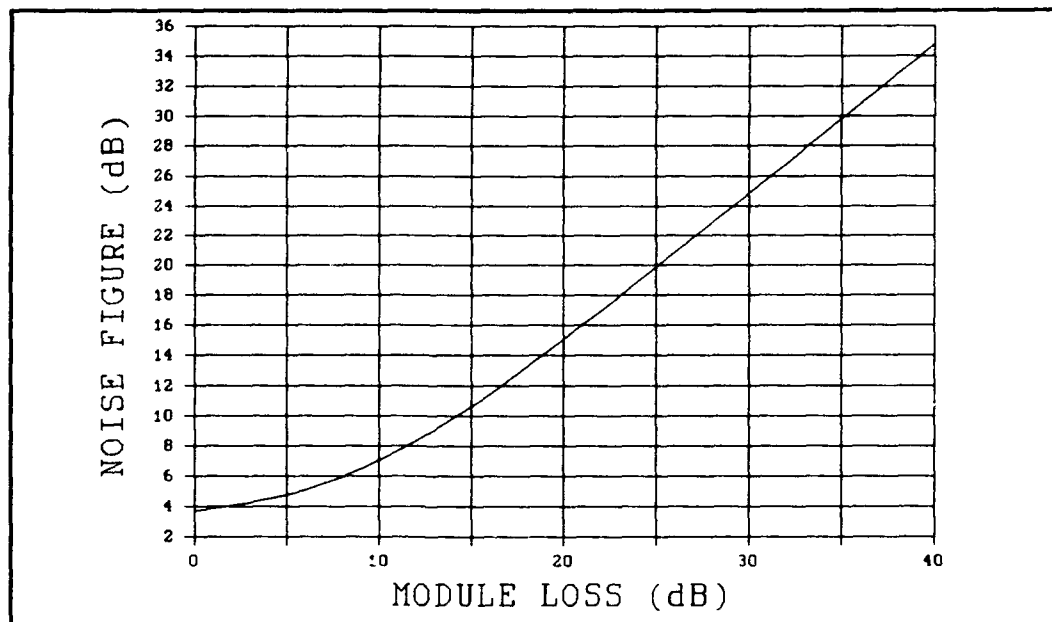

Figure C-4A. Case 4, MESFET 3-Stage Noise Figure, Reference Page 30.
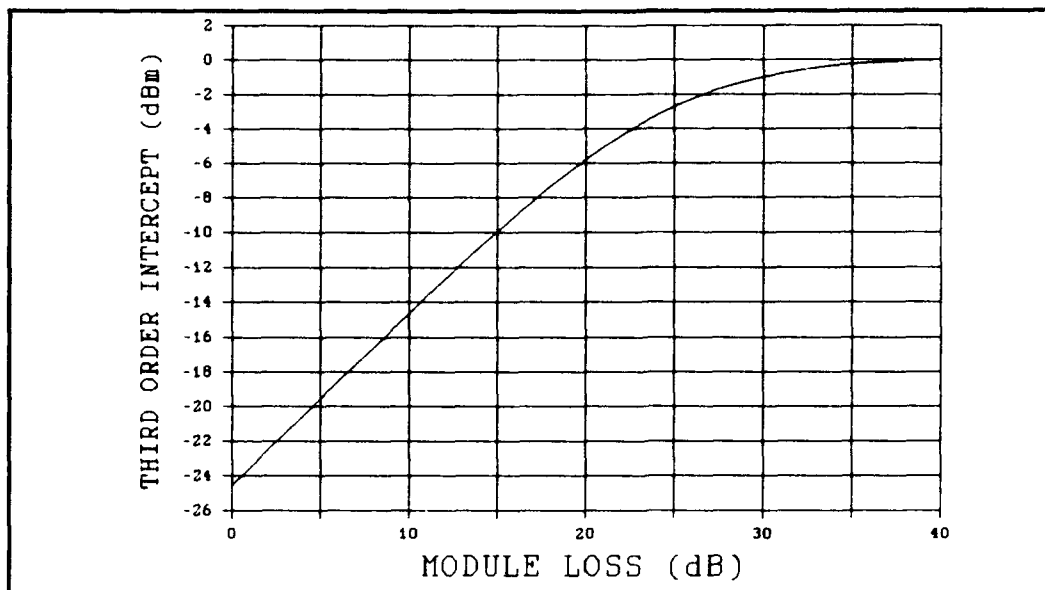
Figure C-4B. Case 4, MESFET 3-Stage Third–Order Intercept, Reference Page 30.
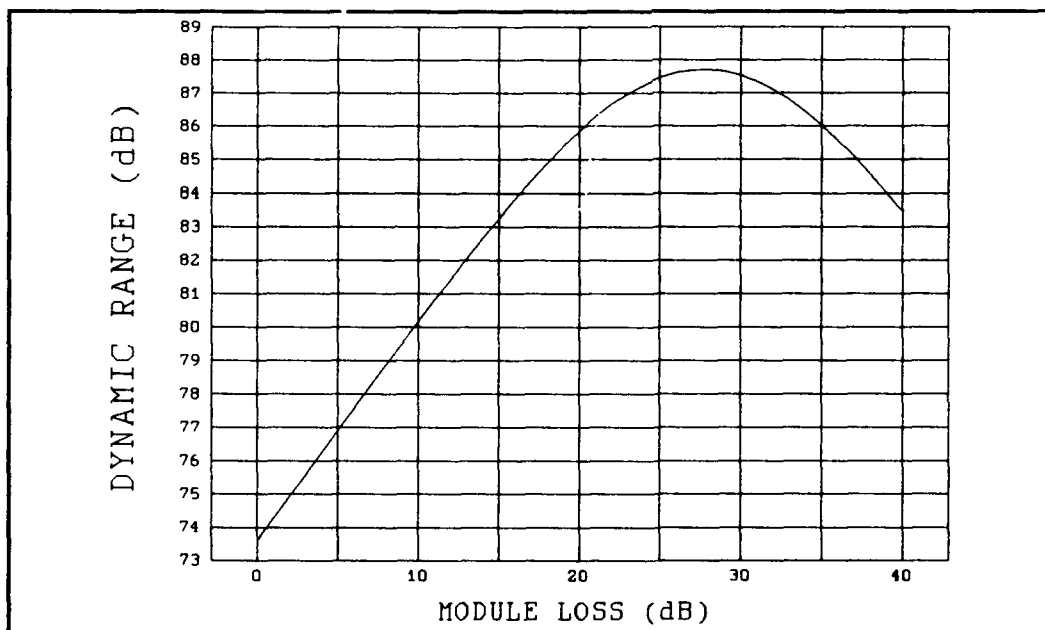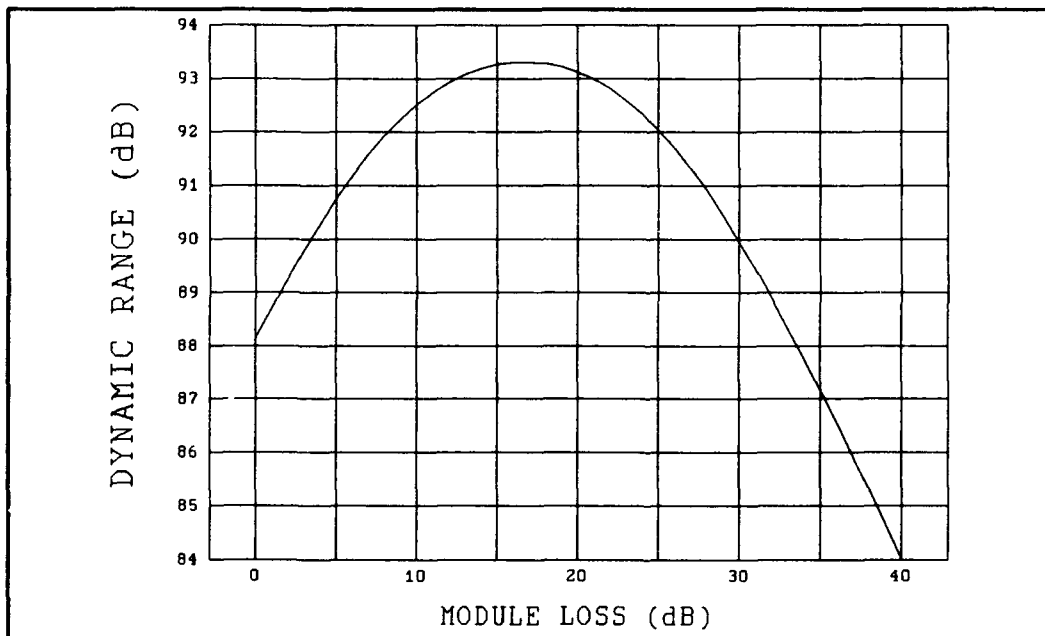

Figure C-4C. Case 4, MESFET 3-Stage Dynamic Range, Reference Page 30.
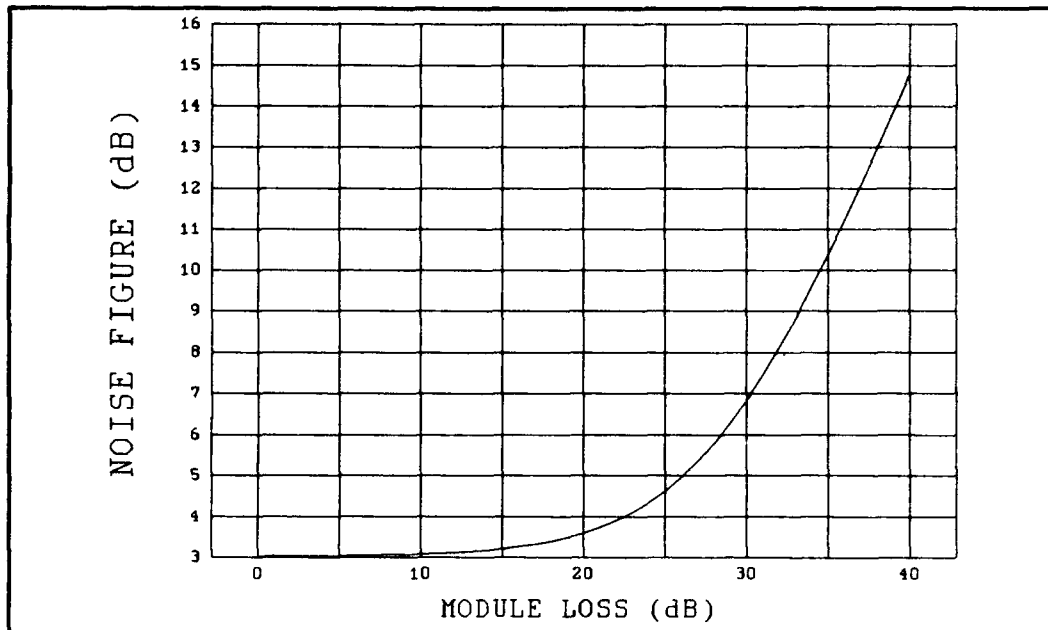
Figure C-4D. Hoffman's[C-1]Results, Case 4, MESFET 3-Stage
Noise Figure, Reference Page 30, Shown For Comparison.
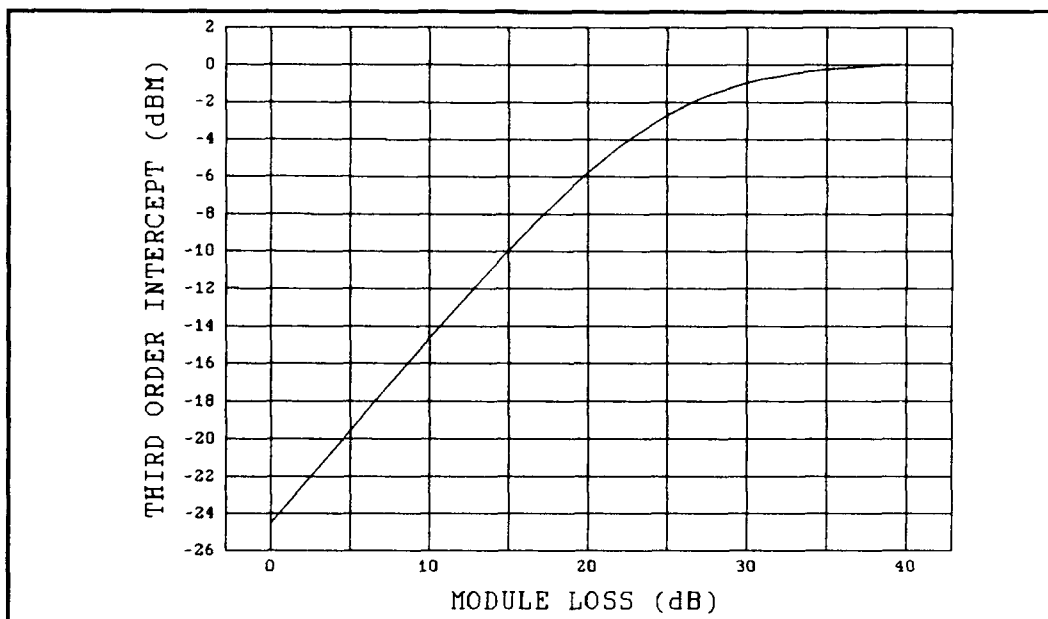
Figure C-4E. Hoffman's[C-1]Results, Case 4, MESFET 3-Stage
Third Order Intercept, Reference Page 30, Shown For
Comparison.

Case 5:   MESFET 3-Stage Configuration. F_i = 1.1 dB, G_i = 11 dB, TOI_i = 33 dBm, L_R = 1.0 dB, L_A = 3 dB, G_B = 40 dB, F_R = 4 dB, G_R = 10 dB, TOI_R = 55 dBm, Reference Page 31.
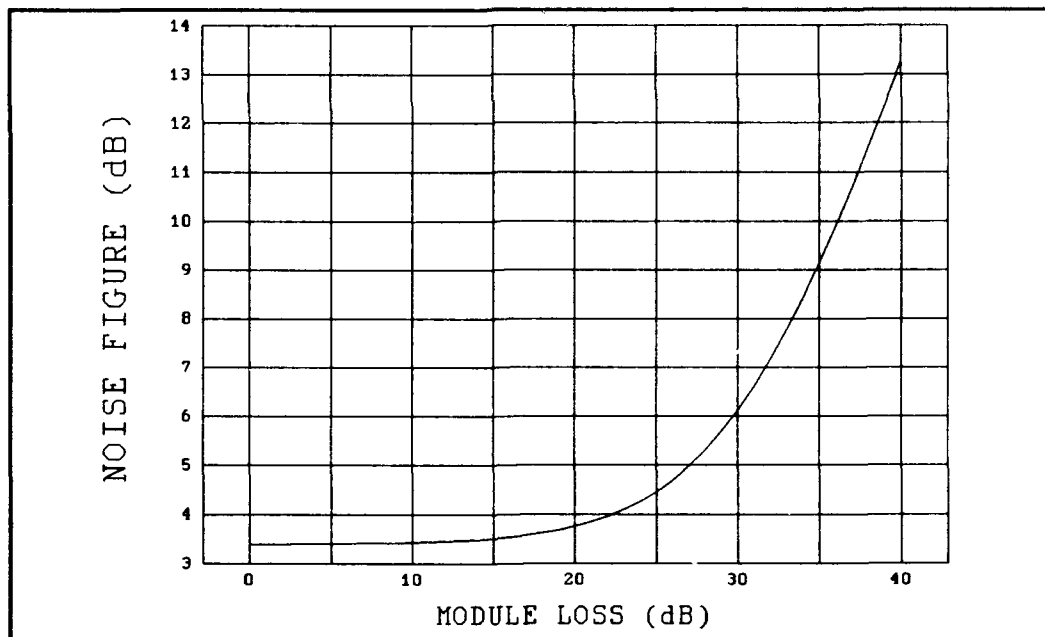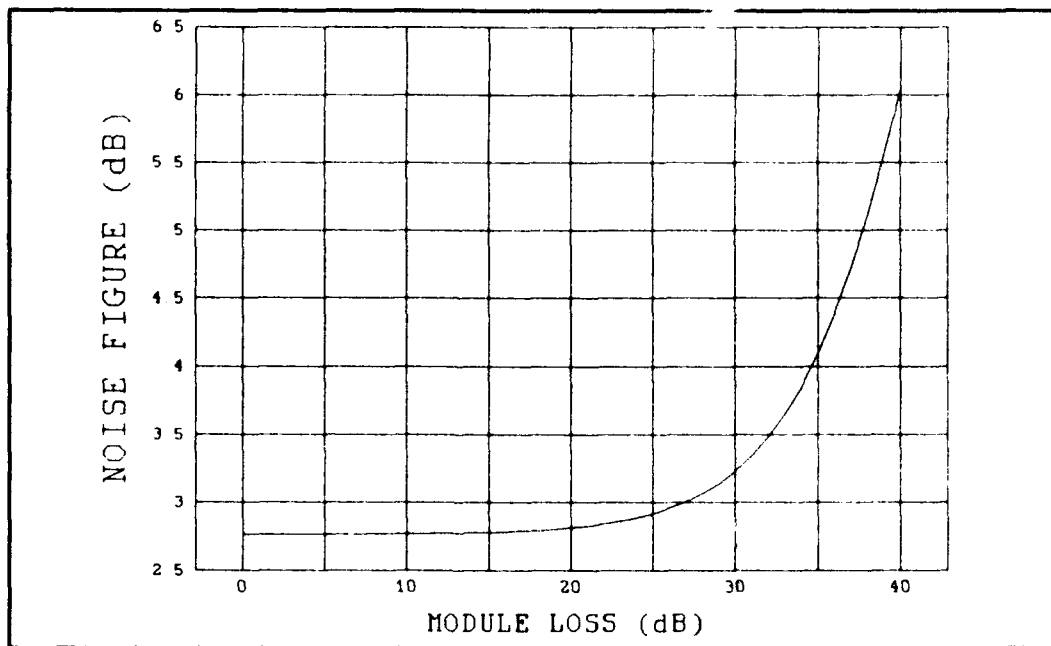

Figure C-5A. Case 5, MESFET 3-Stage Noise Figure, Reference Page 31.

Figure C-5B. Case 5, MESFET 3-Stage Third-Order Intercept, Reference Page 31.

Figure C-5C. Case 5, MESFET 3-Stage Dynamic Range, Reference Page 31.

Case 6:   MESFET 3-Stage Configuration. F_i = 1.1 dB, G_i = 11 dB,
           TOI_i = 33 dBm, L_R = 2.0 dB, L_A = 3 dB, G_B = 40 dB, F_R = 4
           dB, G_R = 10 dB, TOI_R = 55 dBm, Reference Page 32.

Figure C-6A.   Case 6, MESFET 3-Stage Noise Figure,
Reference Page 32.

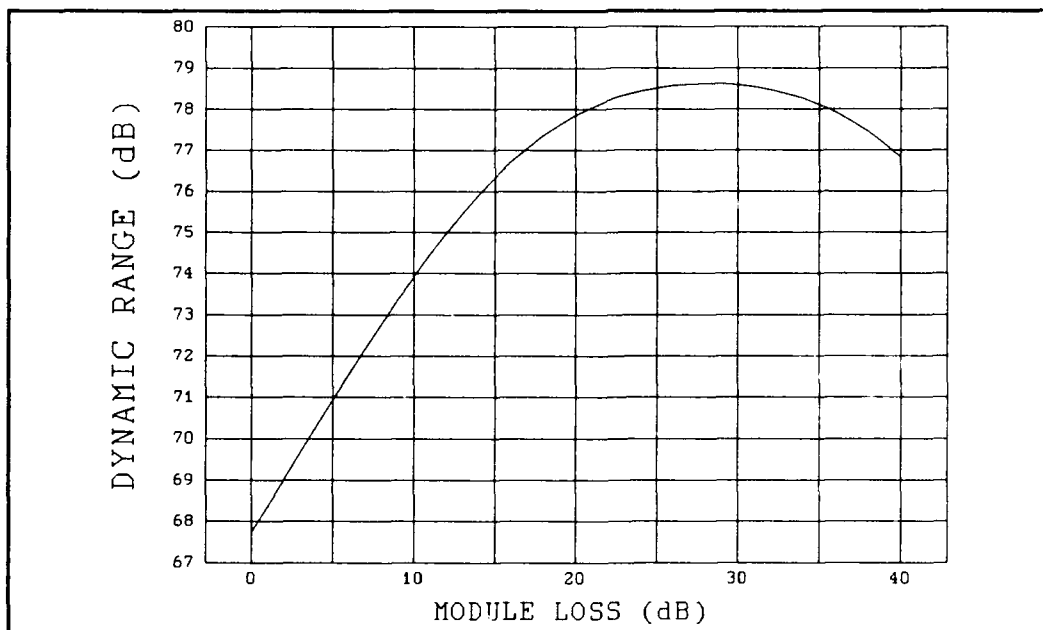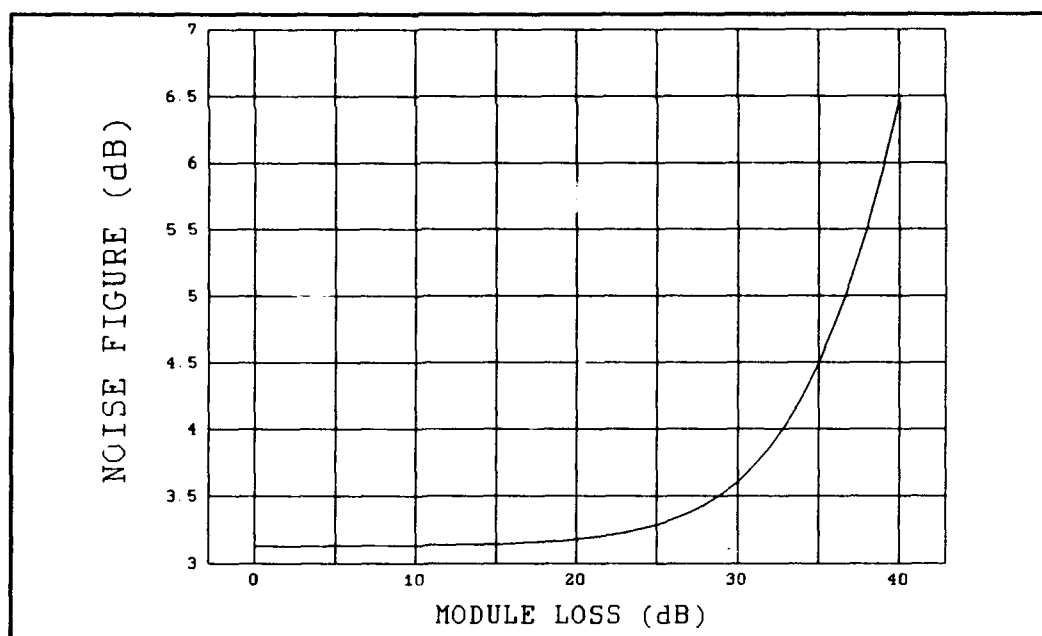**Figure C-6B. Case6, MESFET 3-Stage Third-Order Intercept, Reference Page 32.**

Figure C-6C. MESFET 3-Stage Dynamic Range, Reference Page 32.

Case 7:   HEMT/HBT 2-Stage Configuration. F_1 = 0.8 dB, F_2 = 4 dB,
          G_1 = 15 dB, G_2 = 12 dB, TOI_1 = 28 dBm, TOI_2 = 45 dBm, L_R =
          0.5 dB, L_A = 3 dB, G_B = 40 dB, F_R = 4 dB, G_R = 10 dB, TOI_R
          = 55 dBm, Reference Page 33.

Figure C-7A. Case 7, HEMT/HBT 2-Stage Noise Figure, Reference Page 33.

**Figure C-7B.** Case 7, HEMT/HBT 2-Stage Third-Order Intercept, Reference Page 33.

Figure C-7C. Case 7, HEMT/HBT 2-Stage Dynamic Range, Reference Page 33.
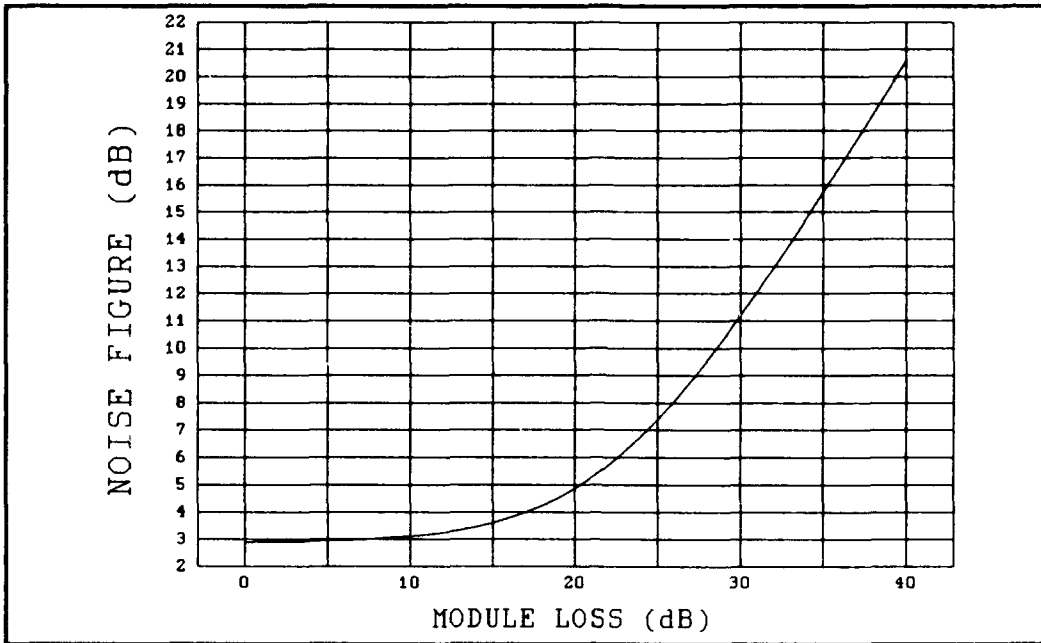
Figure C-7D. Hoffman's[C-1]**Results, Case 7, HEMT/HBT 2-Stage Noise Figure, Reference Page 33, Shown For Comparison.**
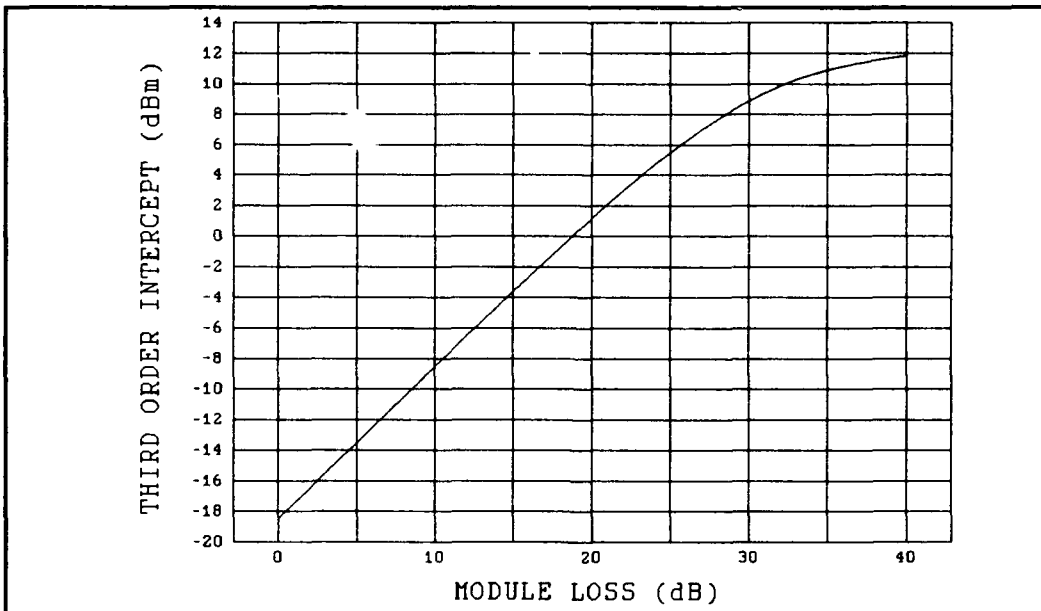
Figure C-7E. Hoffman's[C-1]**Results, Case 7, HEMT/HBT 2-Stage Third Order Intercept, Reference Page 33, Shown For Comparison.**

Case 8:   HEMT/HBT 2-Stage Configuration. F_1 = 0.8 dB, F_2 = 4 dB, G_1 = 15 dB, G_2 = 12 dB, TOI_1 = 28 dBm, TOI_2 = 45 dBm, L_R = 1.0 dB, L_A = 3 dB, G_B = 40 dB, F_R = 4 dB, G_R = 10 dB, TOI_R = 55 dBm, Reference Page 34.

Figure C-8A. Case 8, HEMT/HBT 2-Stage Noise Figure, Reference Page 34.

**Figure C-8B. Case 8, HEMT/HBT 2-Stage Third-Order Intercept, Reference Page 34.**

Figure C-8C. Case 8, HEMT/HBT 2-Stage Dynamic Range, Reference Page 34.

Case 9:   HEMT/HBT 2-Stage Configuration. F_1 = 0.8 dB, F_2 = 4 dB, G_1 = 15 dB, G_2 = 12 dB, TOI_1 = 28 dBm, TOI_2 = 45 dBm, L_R = 2.0 dB, L_A = 3 dB, G_B = 40 dB, F_R = 4 dB, G_R = 10 dB, TOI_R = 55 dBm, Reference Page 35.

Figure C-9A. Case 9, HEMT/HBT 2-Stage Noise Figure, Reference Page 35.

Figure C-9B. Case 9, HEMT/HBT 2-Stage Third-Order
Intercept, Reference Page 35.

Figure C-9C. Case 9, HEMT/HBT 2-Stage Dynamic Range,
Reference Page 35.

Case 10: MESFET 2-Stage Configuration. $F_i = 1.1$ dB, $G_i = 11$ dB, $TOI_i = 33$ dBm, $L_R = 1.0$ dB, $L_A = 3$ dB, $G_B = 40$ dB, $F_R = 4$ dB, $G_R = 10$ dB, $TOI_R = 55$ dBm, Reference Page 36.


Figure C-10A Case 10, MESFET 2-Stage Noise Figure, Reference P _ 36.

Figure C-10B. Case 10, MESFET 2-Stage Third-Order Intercept, Reference Page 36.

Figure C-10C. Case 10, MESFET 2-Stage Dynamic Range, Reference Page 36.

Case 11: **MESFET 1-Stage Configuration.** $F_1 = 1.1$ dB, $G_1 = 11$ dB, $TOI_i = 33$ dBm, $L_R = 1.0$ dB, $L_A = 3$ dB, $G_B = 40$ dB, $F_R = 4$ dB, $G_R = 10$ dB, $TOI_R = 55$ dBm, Reference Page 37.

Figure C-11A. Case 11, MESFET 1-Stage Noise Figure, Reference Page 37.
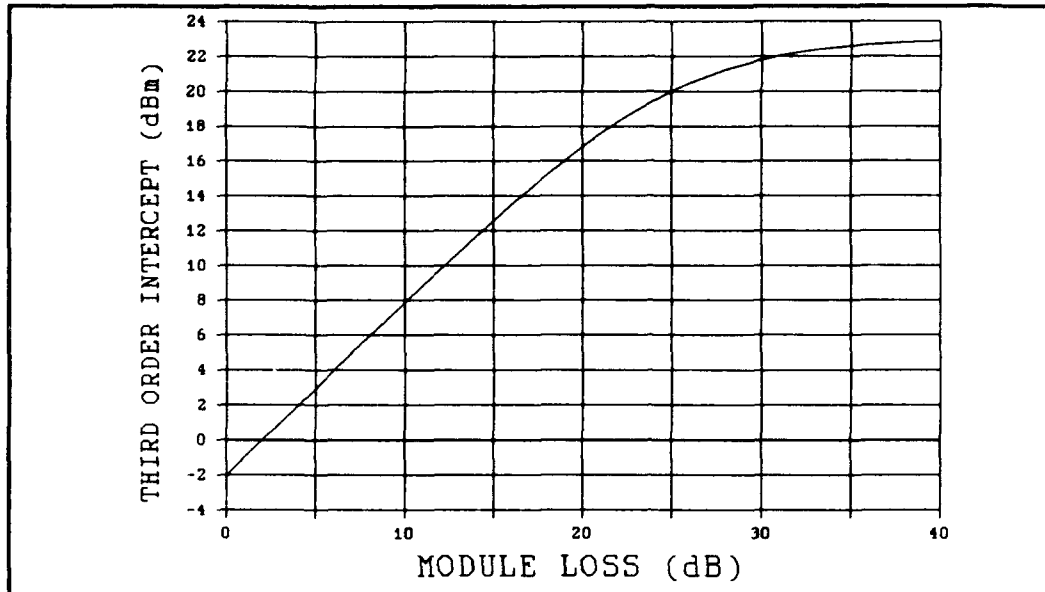
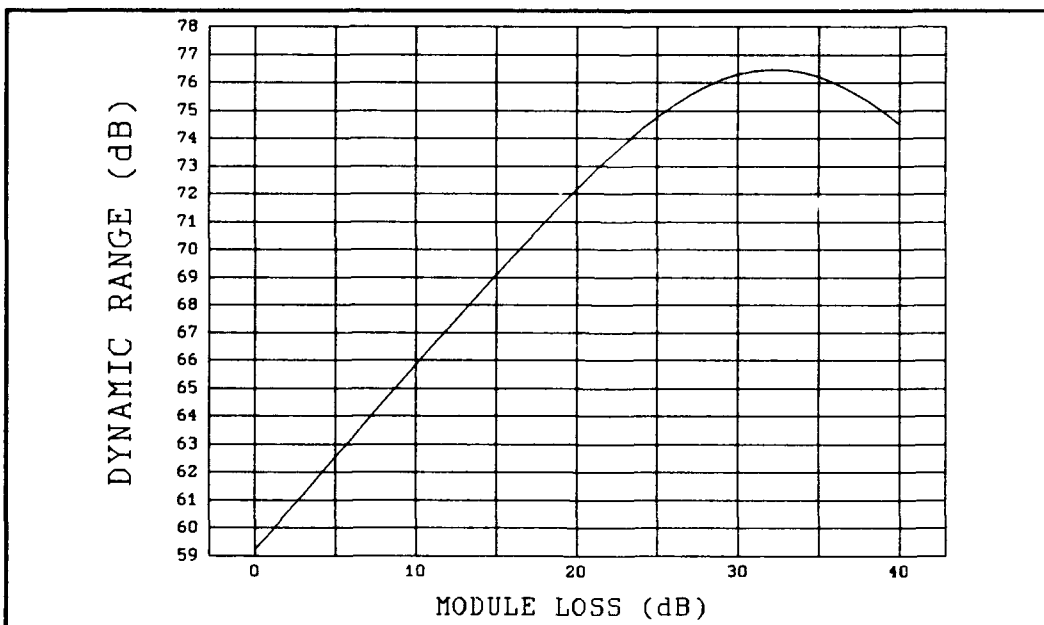**Figure C-11B.** Case 11, **MESFET** 1-Stage Third Order Intercept, Reference Page 37.

Figure C-11C. Case 11, **MESFET** 1-Stage Dynamic Range, Reference Page 37.

Case 12:   HEMT 3-Stage Configuration. F_i = 0.8 dB, G_i = 15 dB, TOI$_i$
= 28 dBm, L_R = 0.5 dB, L_A = 6 dB, G_B = 40 dB, F_R = 4 dB,
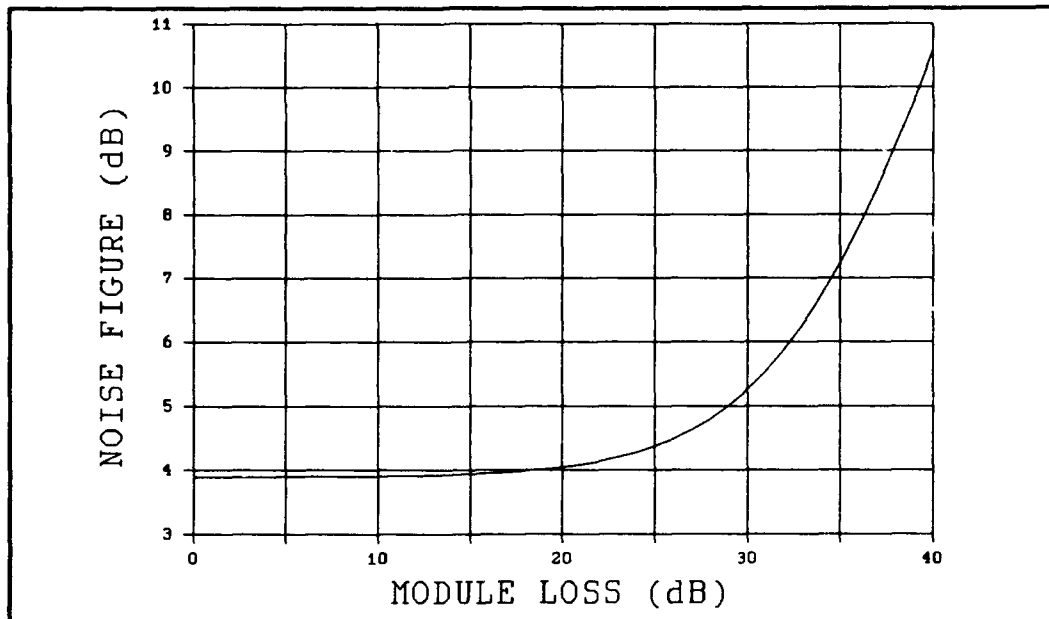G_R = 10 dB, TOI$_R$ = 55 dBm, Reference Page 38.

Figure C-12A. Case 12, HEMT 3-Stage Noise Figure,
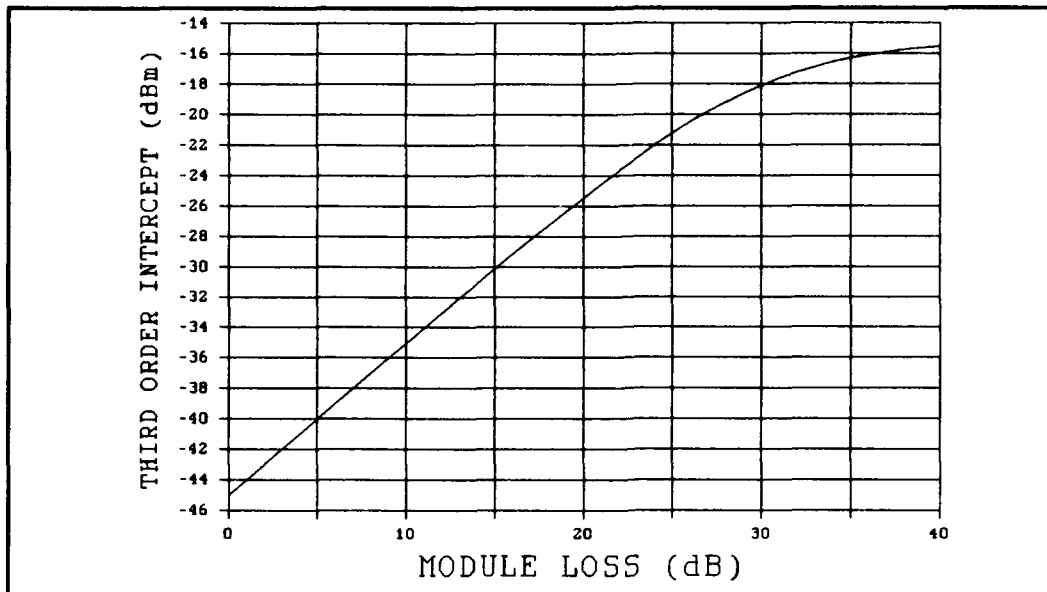Reference Page 38.
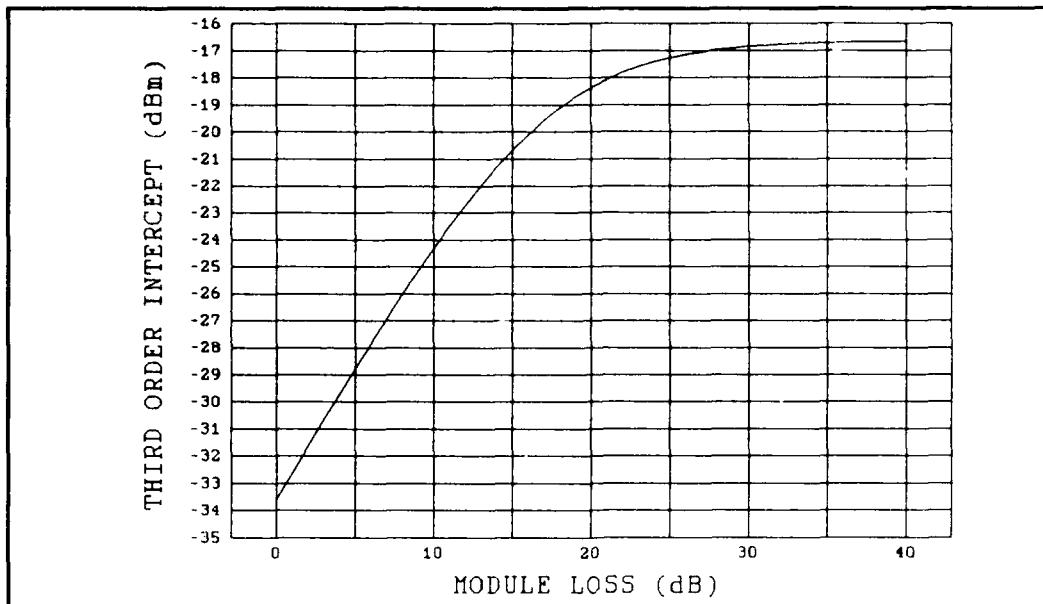
Figure C-12B. Case 12, HEMT 3-Stage Third — Order Intercept, Reference Page 38.

Figure C-12C. Case 12, HEMT 3-Stage Dynamic Range, Reference Page 38.

Case 13:   HEMT 3-Stage Configuration. F_i = 0.8 dB, G_i = 15 dB, TOI_i
            = 28 dBm, L_R = 1.0 dB, L_A = 6 dB, G_B = 40 dB, F_R = 4 dB,
            G_R = 10 dB, TOI_R = 55 dBm, Reference Page 39.

Figure C-13A. Case 13, HEMT 3-Stage Noise Figure,
Reference Page 39.
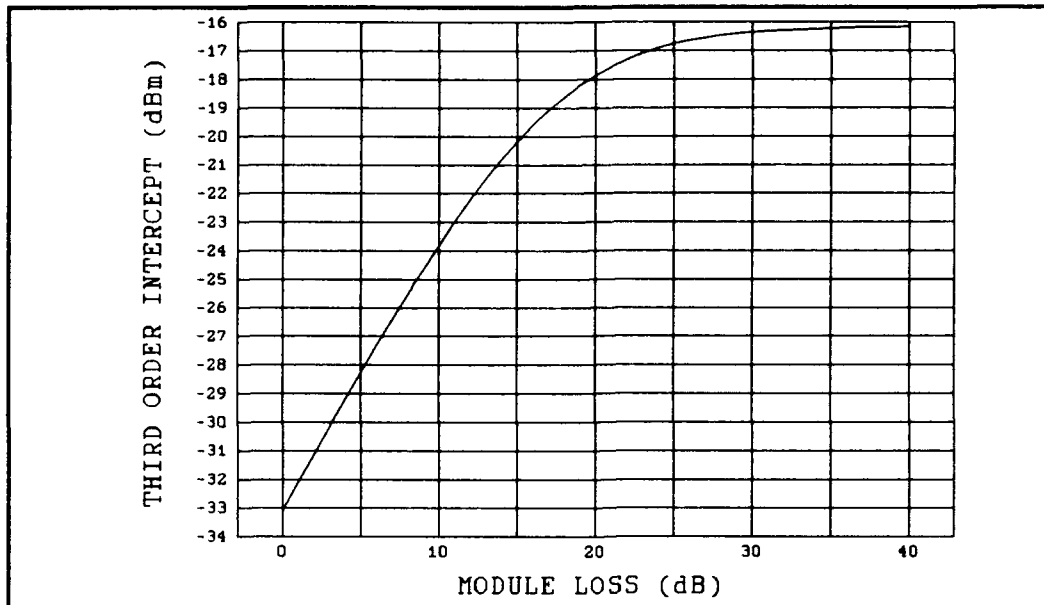
Figure C-13B. Case 13, HEMT 3-Stage Third-Order Intercept, Reference Page 39.
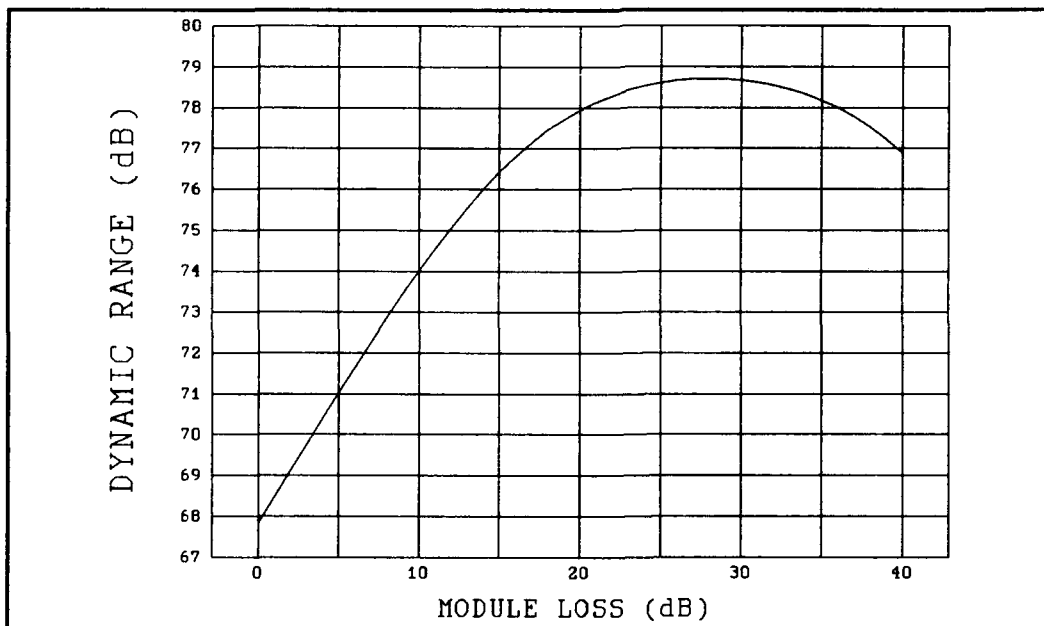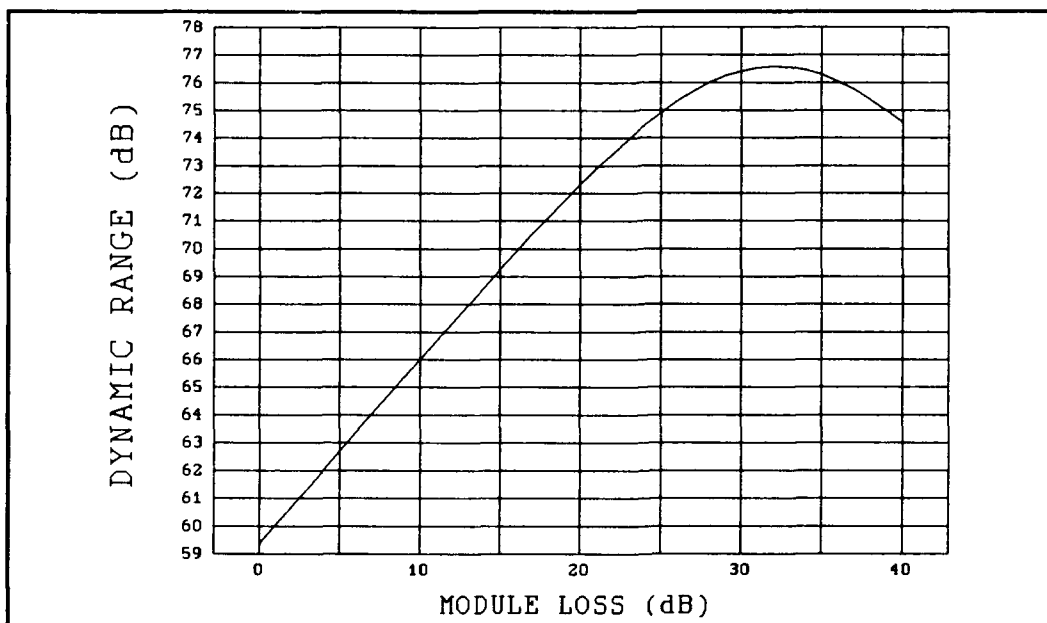

Figure C-13C. Case 13, HEMT 3-Stage Dynamic Range, Reference Page 39.

Case 14: HEMT 3-Stage Configuration. F_i = 0.8 dB, G_i = 15 dB, TOI$_i$ = 28 dBm, L_R = 2.0 dB, L_A = 6 dB, G_B = 40 dB, F_R = 4 dB, G_R = 10 dB, TOI$_R$ = 55 dBm, Reference Page 40.
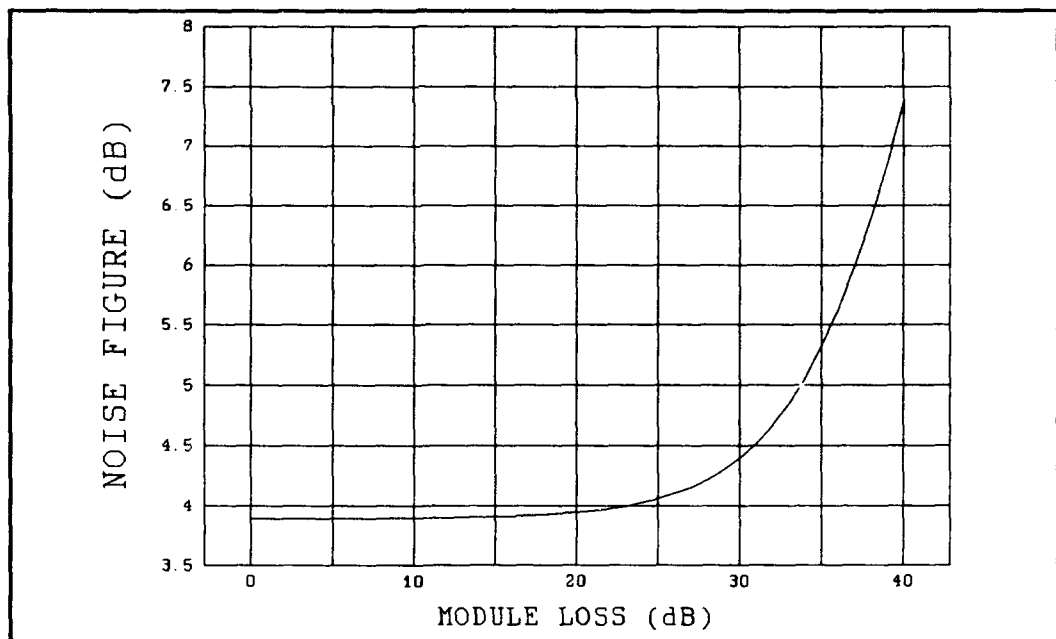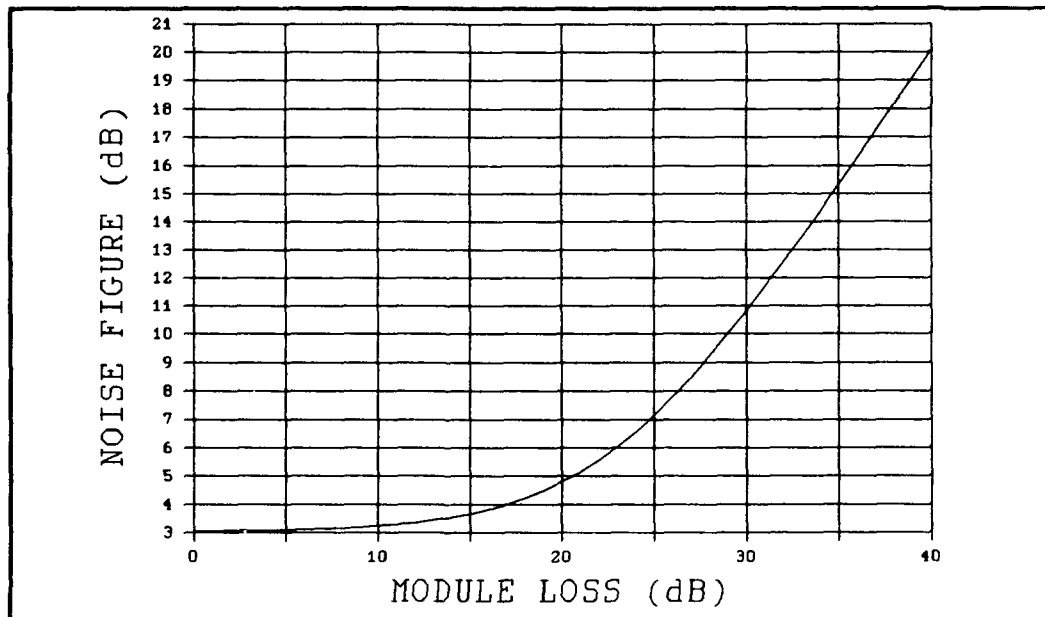

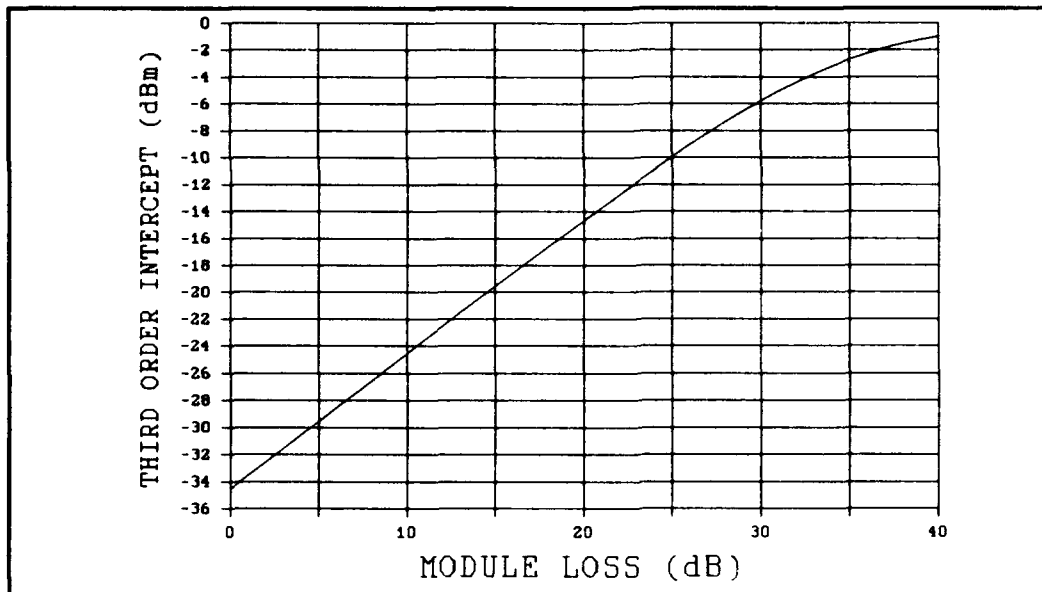Figure C-14A. Case 14, HEMT 3-Stage Noise Figure, Reference Page 40.
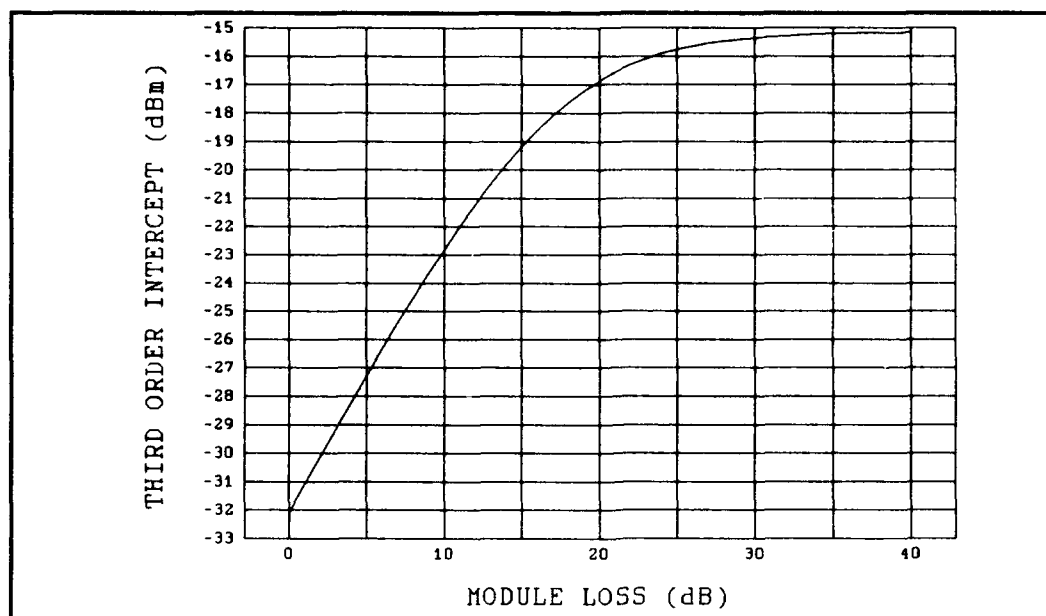
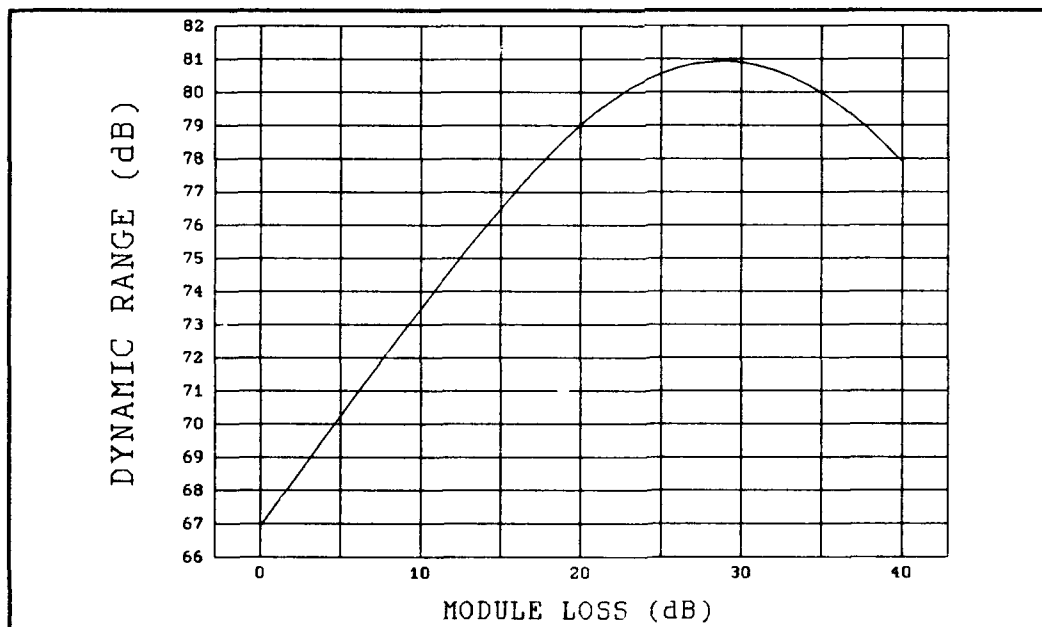**Figure C-14B. Case 14, HEMT 3-Stage Third-Order Intercept, Reference Page 40.**
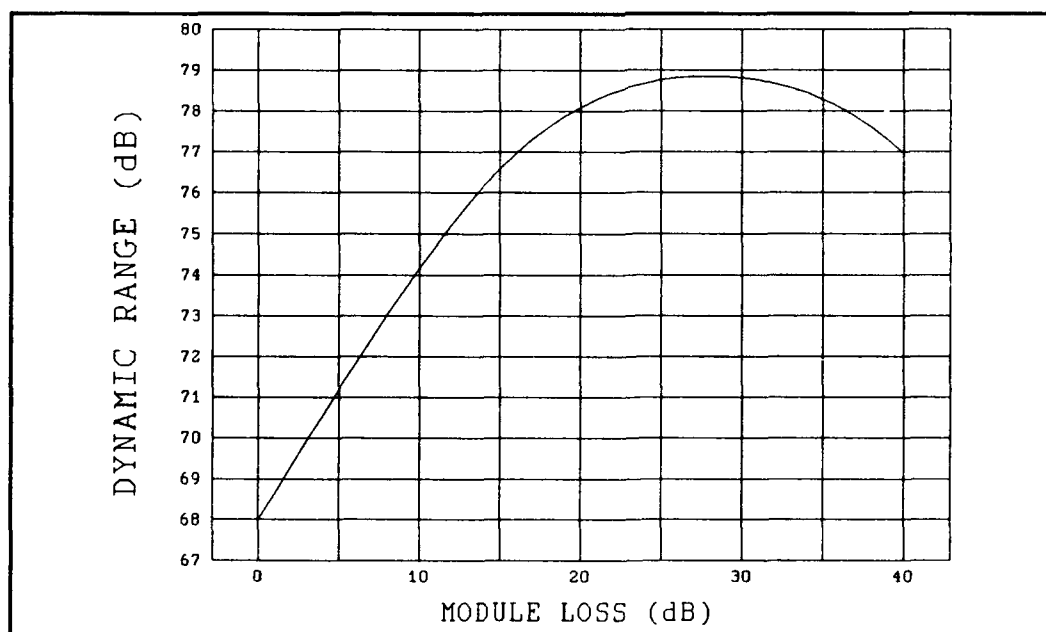
Figure C-14C. Case 14, HEMT 3-Stage Dynamic Range, Reference Page 40.

Case 15: HEMT 3-Stage Configuration. F_i = 0.8 dB, G_i = 15 dB, TOI_i = 28 dBm, L_R = 0.5 dB, L_A = 3 dB, G_B = 40 dB, F_R = 10 dB, G_R = 10 dB, TOI_R = 45 dBm, Reference Page 41.
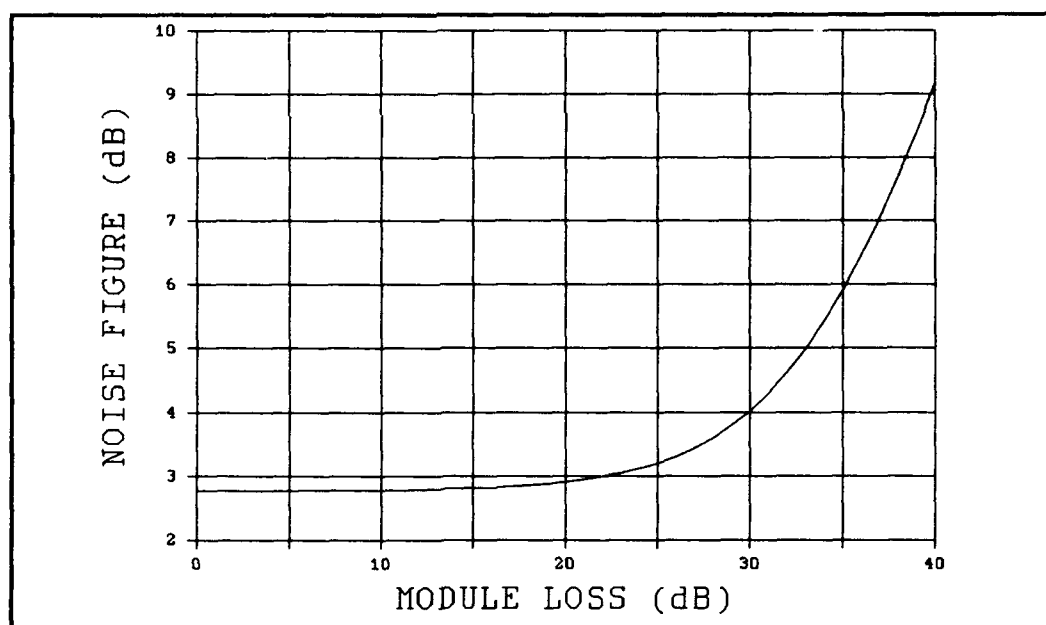
Figure C-15A. Case 15, HEMT 3-Stage Noise Figure, Reference Page 41.
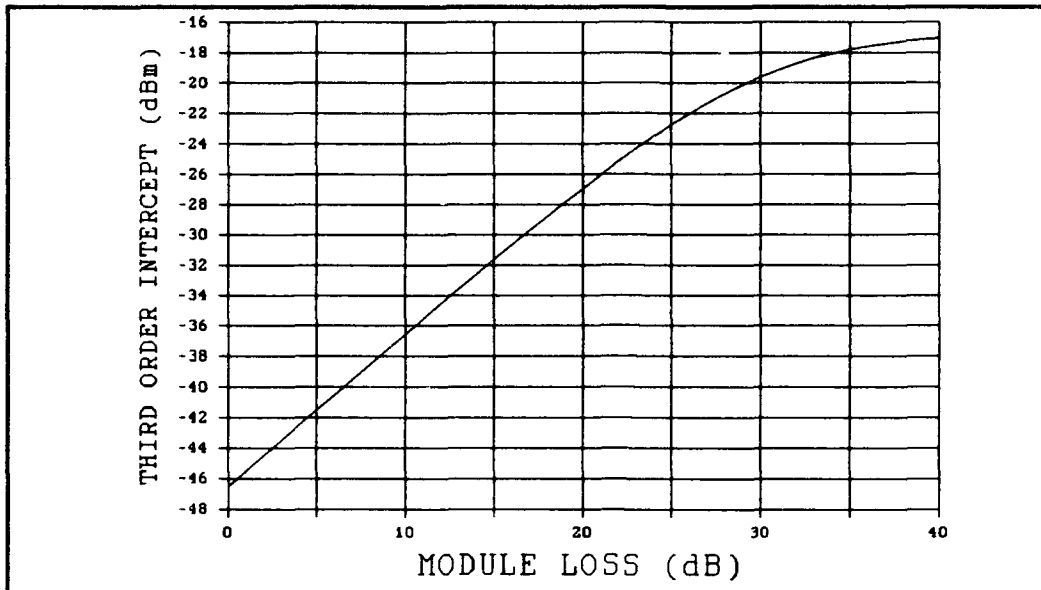
Figure C-15B. Case 15, HEMT 3-Stage Third-Order Intercept, Reference Page 41.
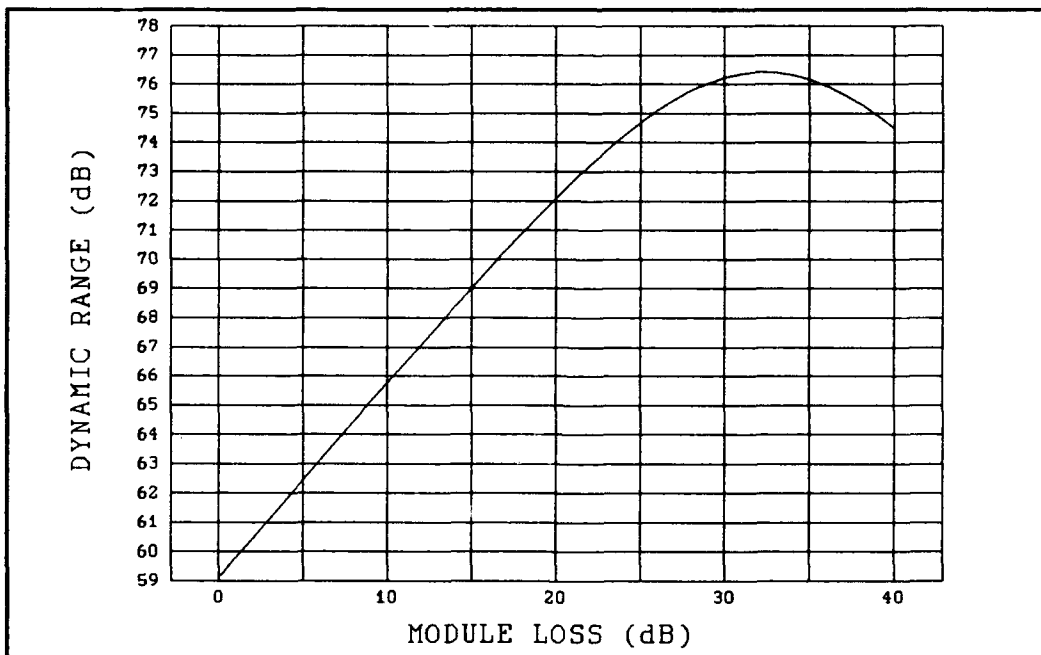
Figure C-15C. Case 15, HEMT 3-Stage Dynamic Range, Reference Page 41.

Case 16: HEMT 3-Stage Configuration. F_i = 0.8 dB, G_i = 15 dB, TOI_i = 28 dBm, L_R = 1.0 dB, L_A = 3 dB, G_B = 40 dB, F_R = 10 dB, G_R = 10 dB, TOI_R = 45 dBm, Reference Page 42.
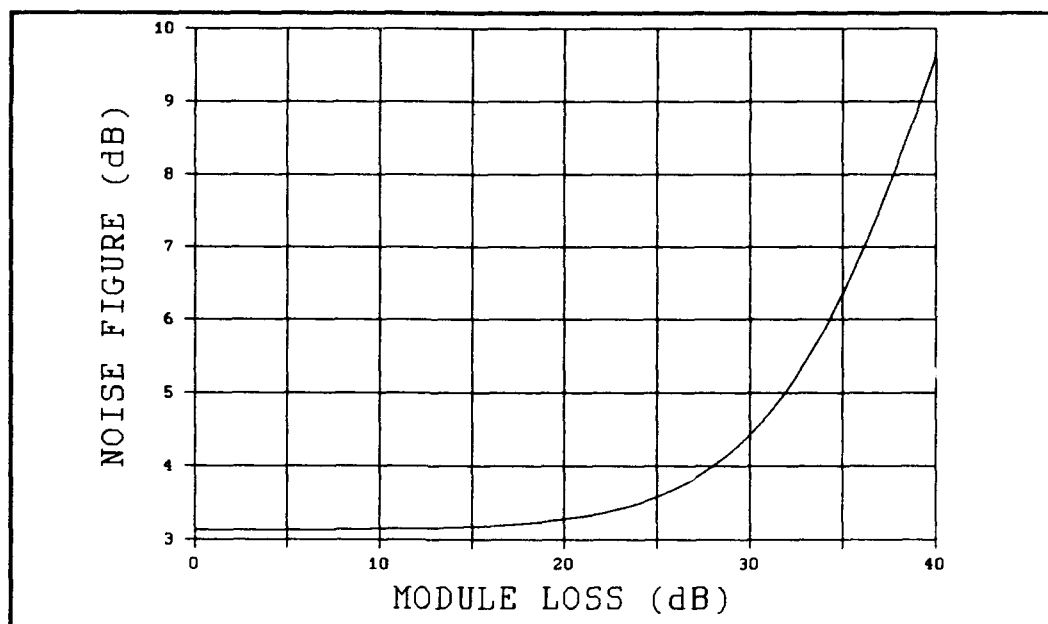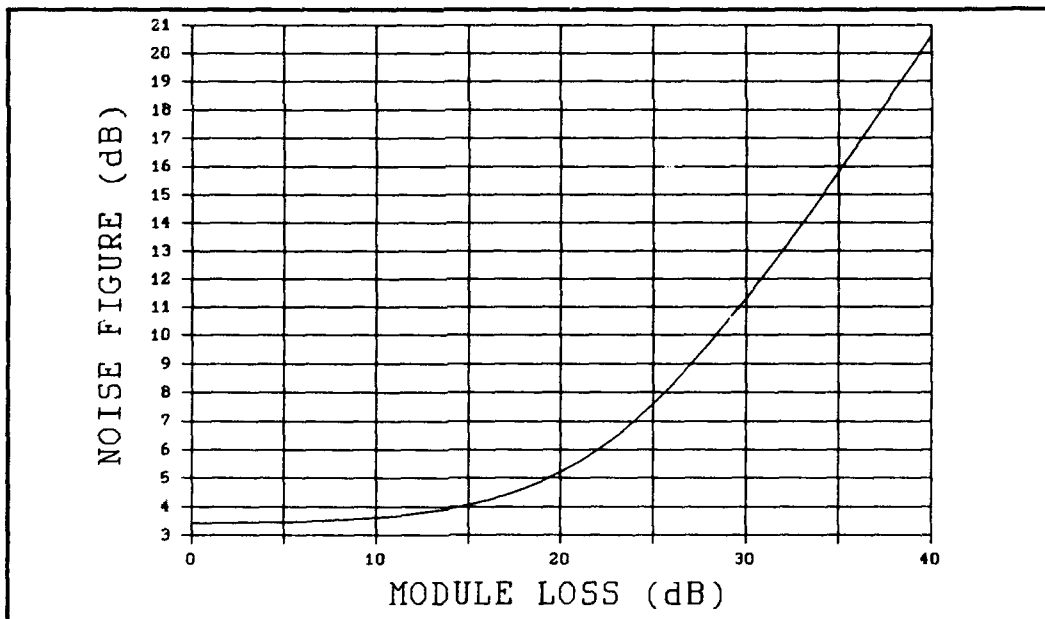

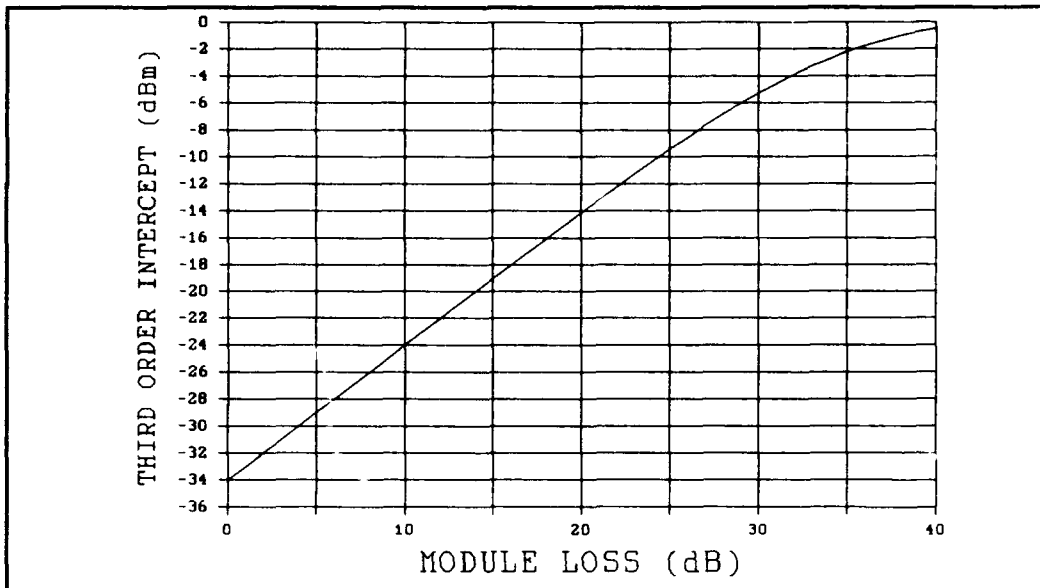Figure C-16A. Case 16, HEMT 3-Stage Noise Figure, Reference Page 42.
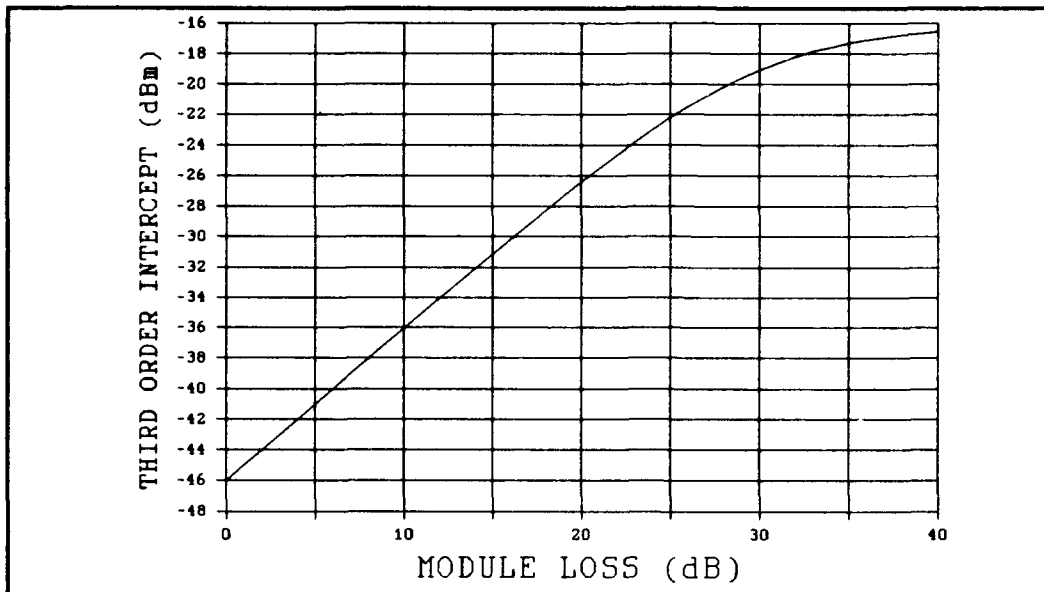
Figure C-16B. Case 16, HEMT 3-Stage Third-Order Intercept, Reference Page 42.
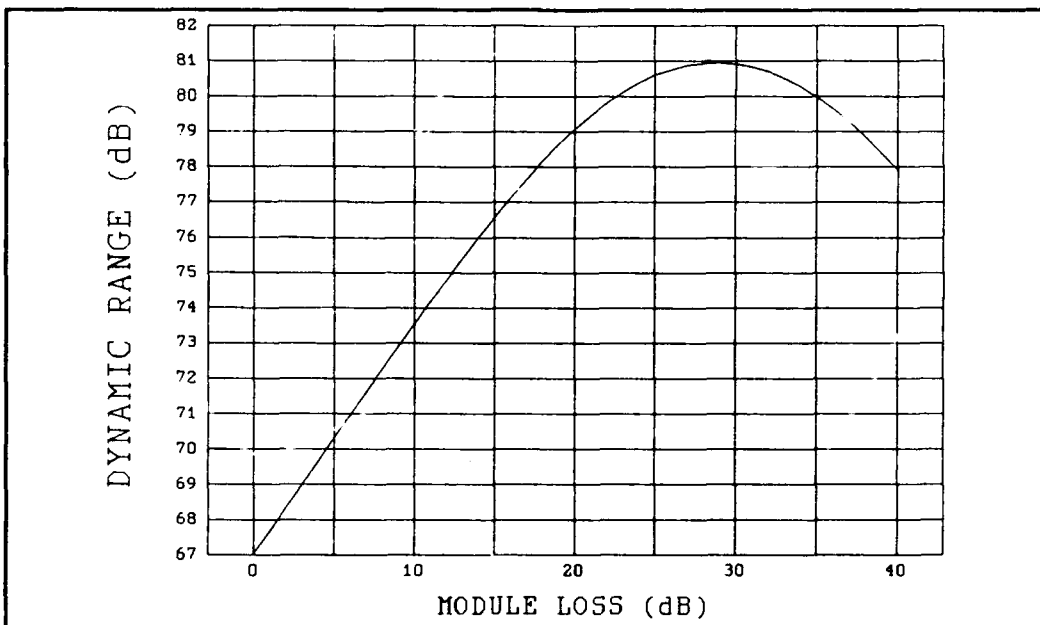

Figure C-16C. Case 16, HEMT 3-Stage Dynamic Range, Reference Page 42.

Case 17: HEMT 3-Stage Configuration. F_i = 0.8 dB, G_i = 15 dB, TOI_i = 28 dBm, L_R = 2.0 dB, L_A = 3 dB, G_B = 40 dB, F_R = 10 dB, G_R = 10 dB, TOI_R = 45 dBm, Reference Page 43.
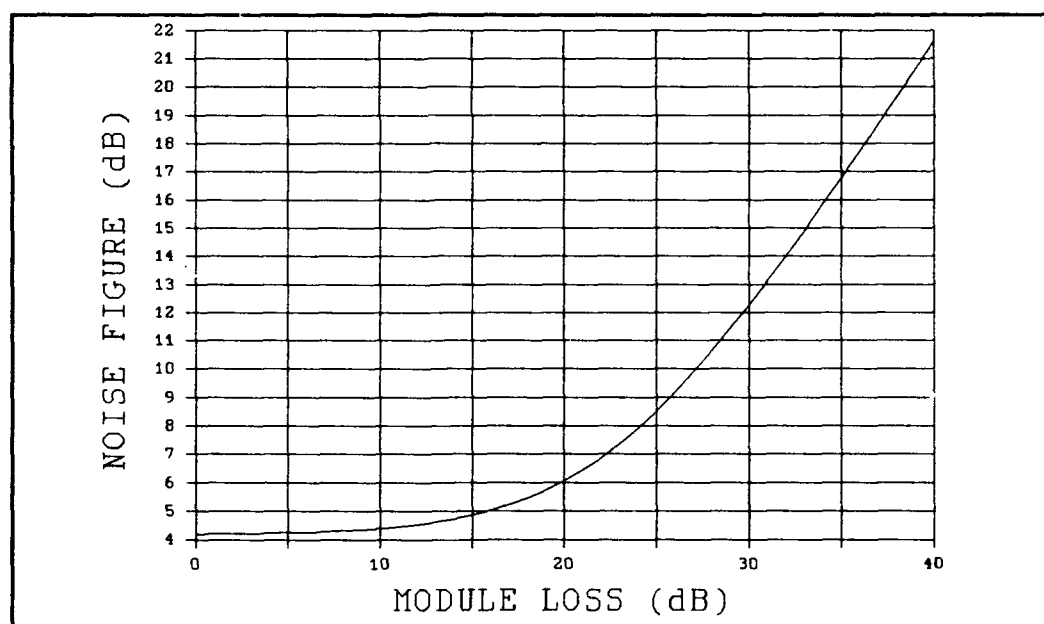

Figure C-17A. Case 17, HEMT 3-Stage Noise Figure, Reference Page 43.

Figure C-17B. Case 17, HEMT 3-Stage Third – Order Intercept, Reference Page 43.

Figure C-17C. Case 17, HEMT 3-Stage Dynamic Range, Reference Page 43.

Case 18: MESFET 3-Stage Configuration. F_i = 1.1 dB, G_i = 11 dB, TOI_i = 33 dBm, L_R = 0.5 dB, L_A = 3 dB, G_B = 40 dB, F_R = 10 dB, G_R = 10 dB, TOI_R = 45 dBm, Reference Page 44.

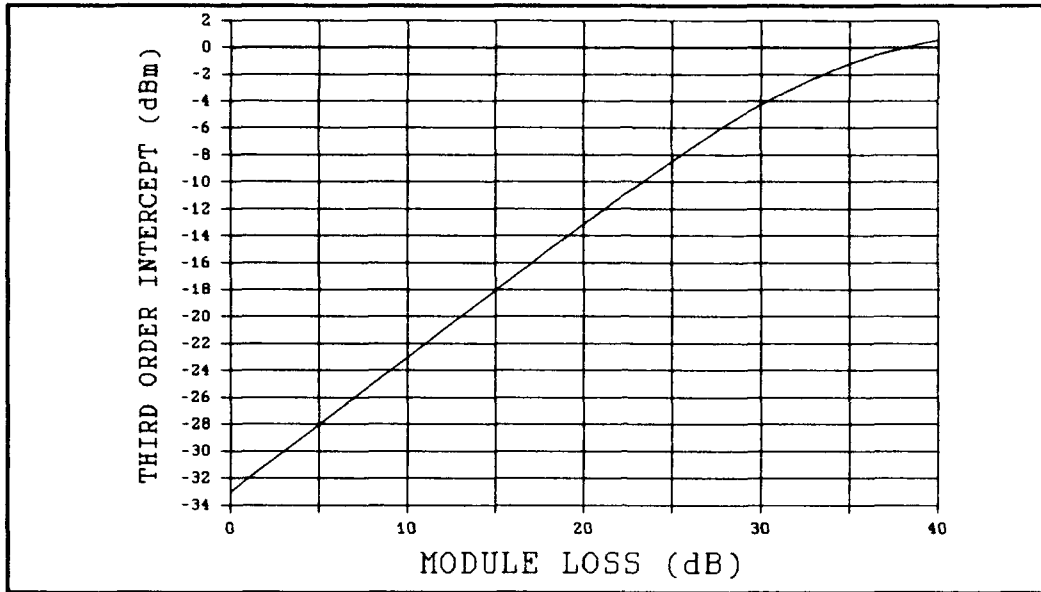Figure C-18A. Case 18, MESFET 3-Stage Noise Figure, Reference Page 44.

Figure C-18B. Case 18, MESFET 3-Stage Third-Order Intercept, Reference Page 44.
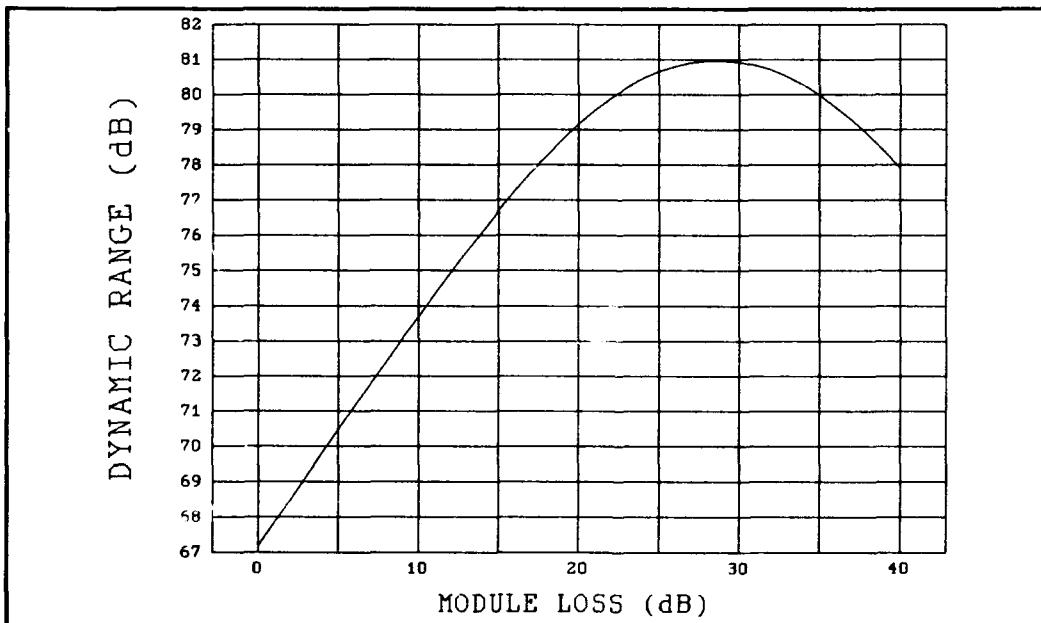

Figure C-18C. Case 18, MESFET 3-Stage Dynamic Range, Reference Page 44.

Case 19:   MESFET 3-Stage Configuration. F_i = 1.1 dB, G_i = 11 dB, TOI_i = 33 dBm, L_R = 1.0 dB, L_A = 3 dB, G_s = 40 dB, F_R = 10 dB, G_R = 10 dB, TOI_R = 45 dBm, Reference Page 45.


Figure C-19A.   Case 19, MESFET 3-Stage Noise Figure, Reference Page 45.

Figure C-19B. Case 19, MESFET 3-Stage Third-Order Intercept, Reference Page 45.

Figure C-19C. Case 19, MESFET 3-Stage Dynamic Range, Reference Page 45.

Case 20: MESFET 3-Stage Configuration. F_i = 1.1 dB, G_i = 11 dB, TOI_i = 33 dBm, L_R = 2.0 dB, L_A = 3 dB, G_B = 40 dB, F_R = 10 dB, G_R = 10 dB, TOI_R = 45 dBm, Reference Page 46.

Figure C-20A. Case 20, MESFET 3-Stage Noise Figure, Reference Page 46.

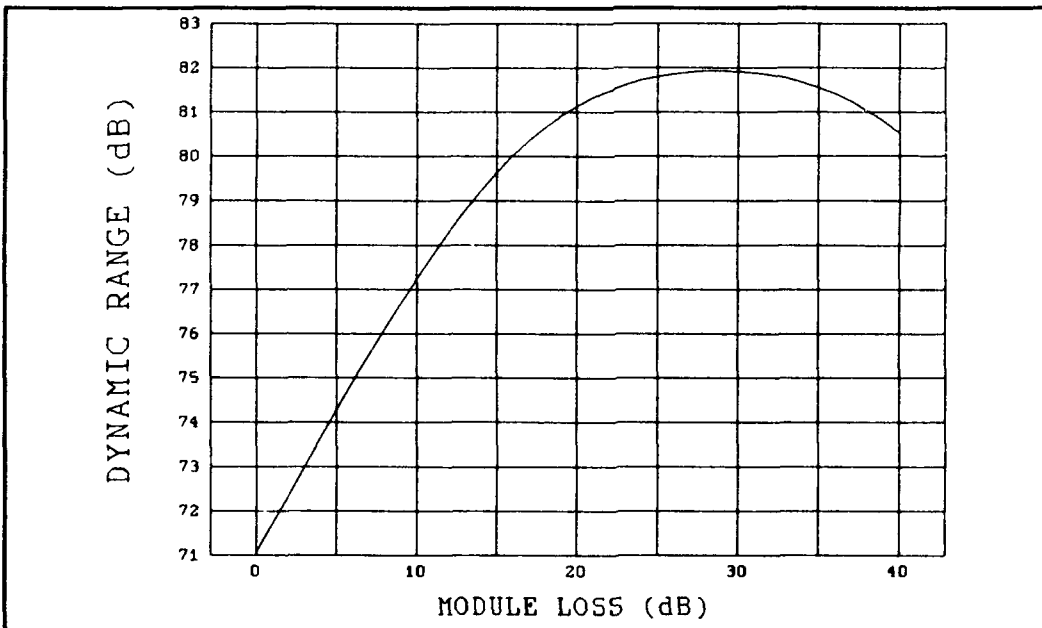Figure C-20B. Case 20, MESFET 3-Stage Third-Order Intercept, Reference Page 46.

Figure C-20C. Case 20, MESFET 3-Stage Dynamic Range, Reference Page 46.

Case 21: HEMT/HBT 2-Stage Configuration. F_1 = 0.8 dB, F_2 = 4 dB, G_1 = 15 dB, G_2 = 12 dB, TOI_1 = 28 dBm, TOI_2 = 45 dBm, L_R = 0.5 dB, L_A = 3 dB, G_B = 40 dB, F_R = 10 dB, G_R = 10 dB, TOI_R = 45 dBm, Reference Page 47.
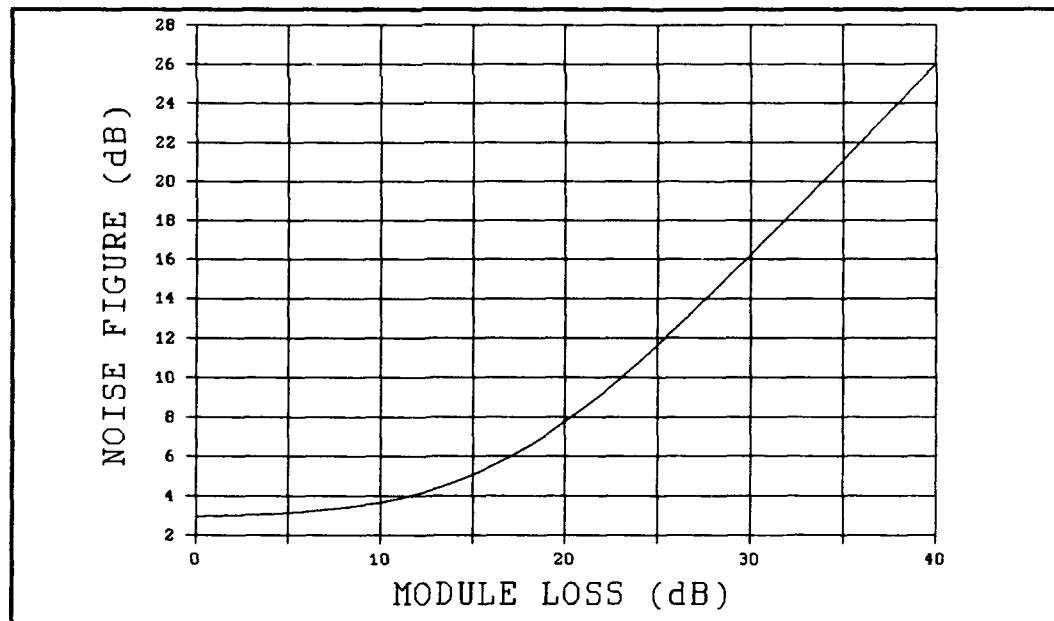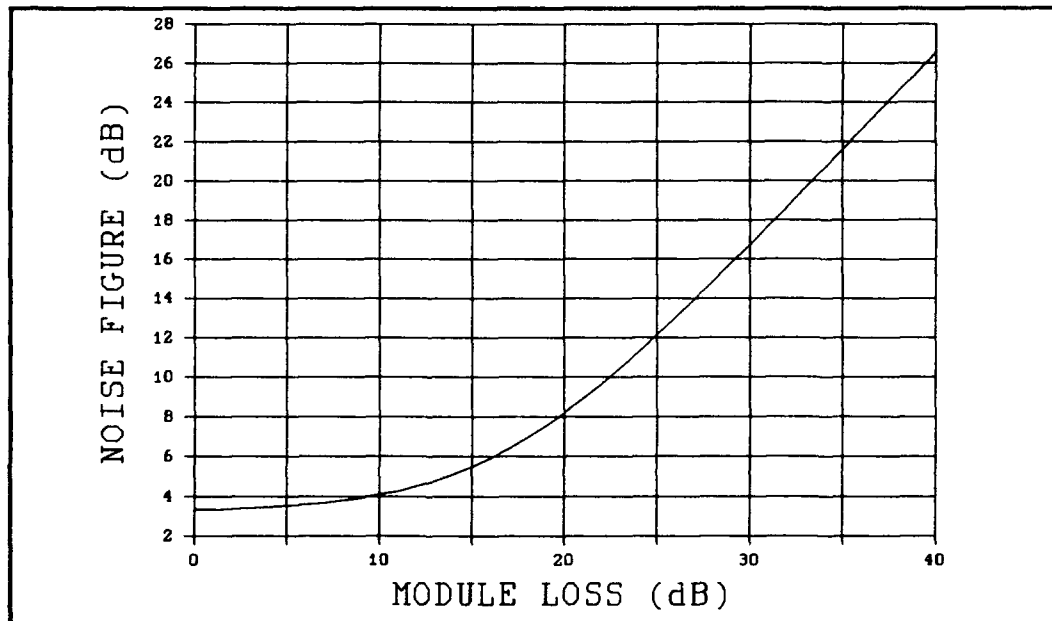

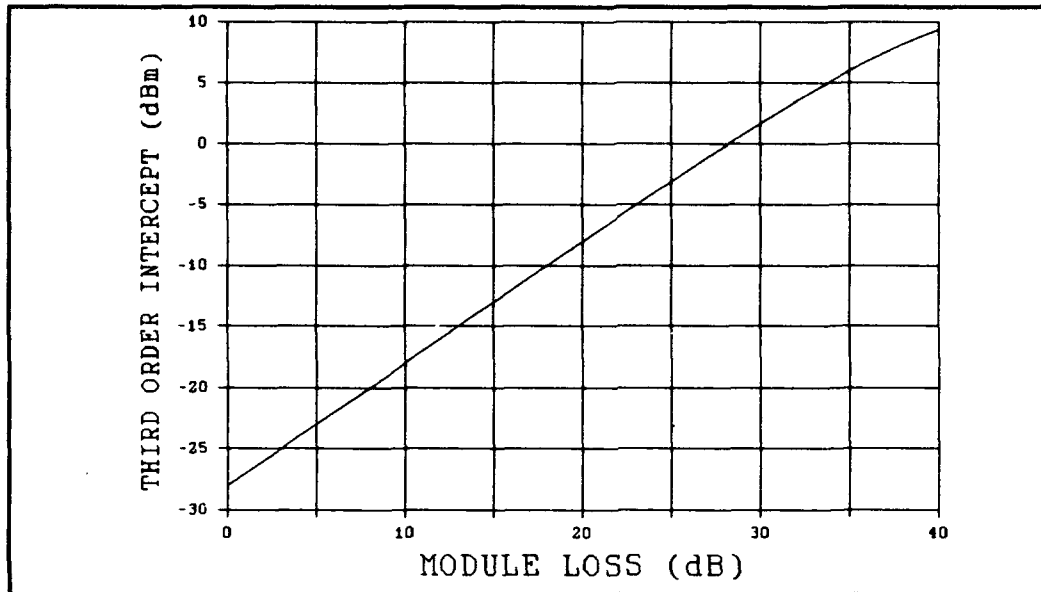Figure C-21A. Case 21, HEMT/HBT 2-Stage Noise Figure, Reference Page 47
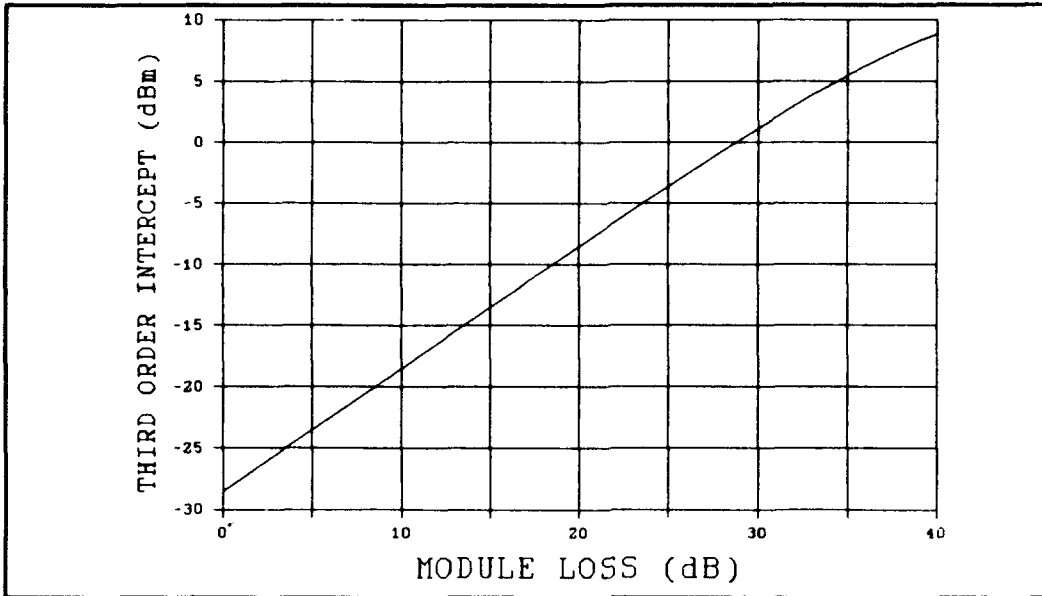
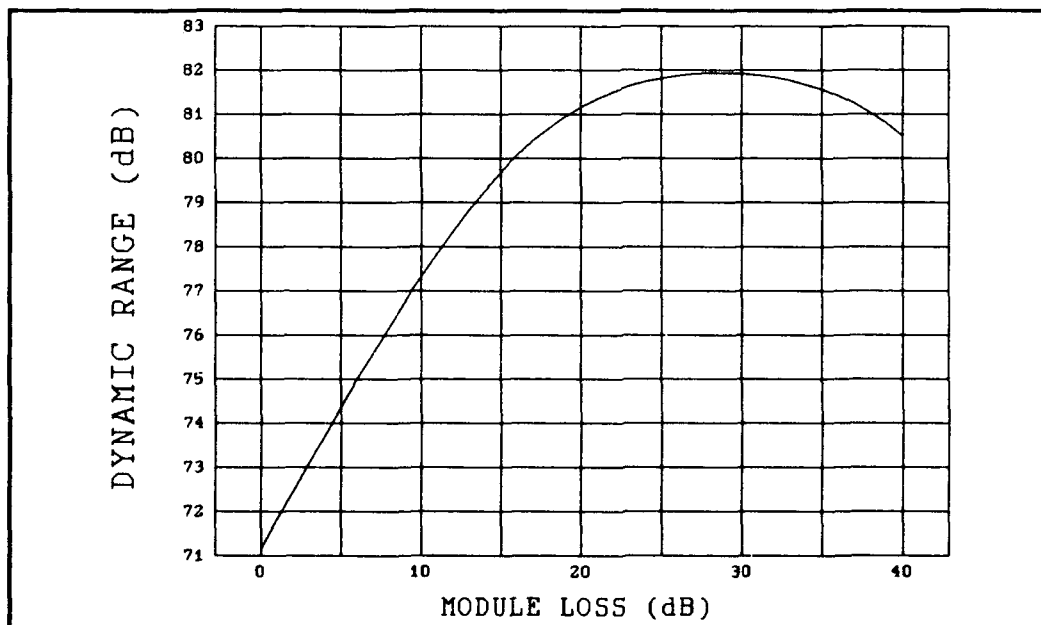**Figure C-21B. Case 21, HEMT/HBT 2-Stage Third-Order Intercept, Reference Page 47.**

Figure C-21C. Case 21, HEMT/HBT 2-Stage Dynamic Range, Reference Page 47.

Case 22: HEMT/HBT 2-Stage Configuration. F_1 = 0.8 dB, F_2 = 4 dB,
G_1 = 15 dB, G_2 = 12 dB, TOI_1 = 28 dBm, TOI_2 = 45 dBm, L_R =
1.0 dB, L_A = 3 dB, G_B = 40 dB, F_R = 10 dB, G_R = 10 dB, TOI_R
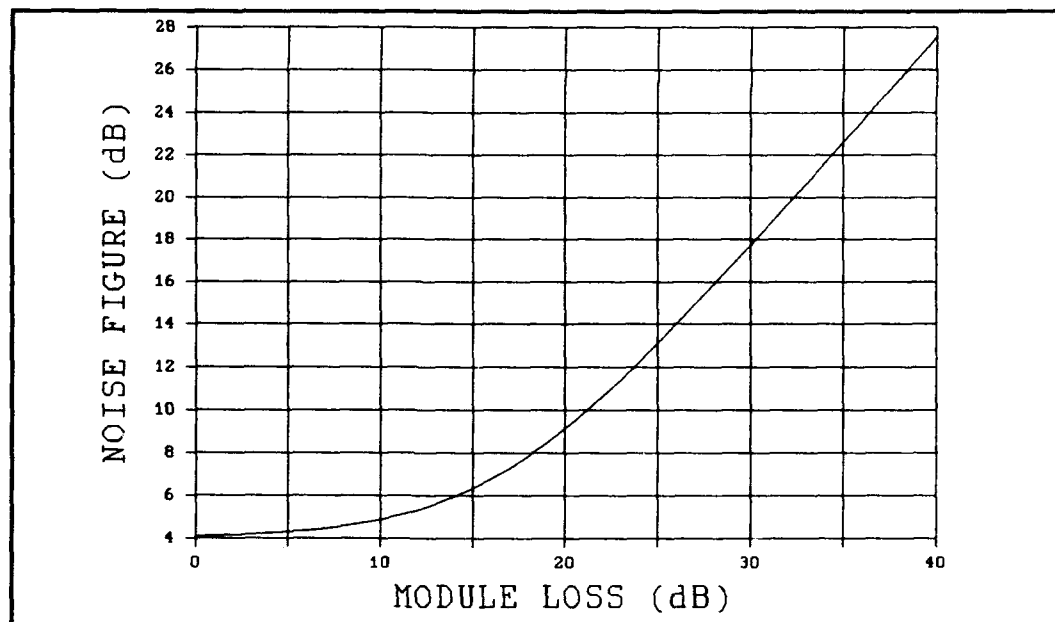= 45 dBm, Reference Page 48.

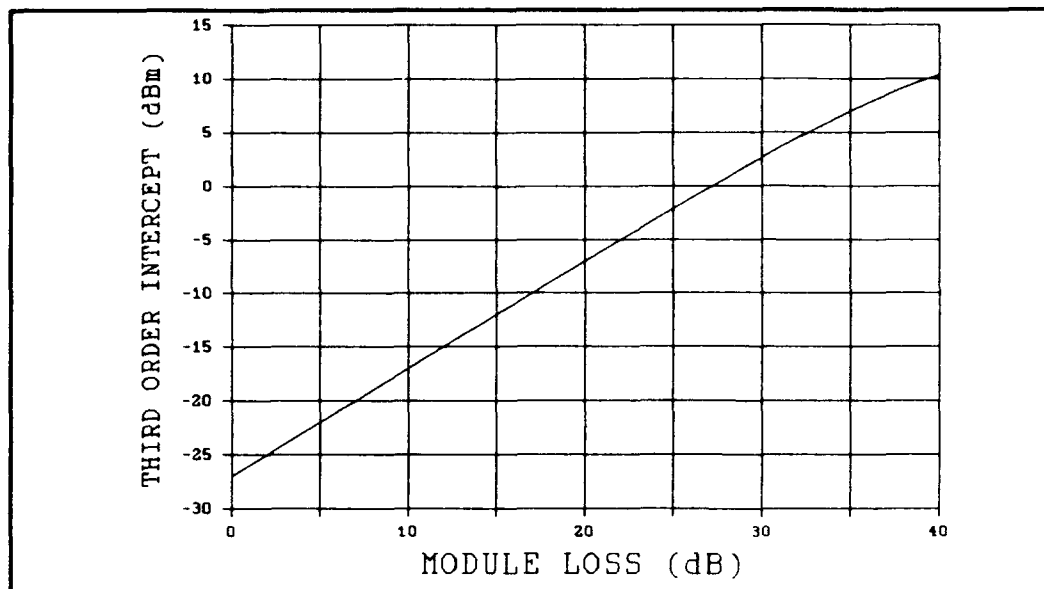Figure C-22A. Case 22, HEMT/HBT 2-Stage Noise Figure,
Reference Page 48.

Figure C-22B. Case 22, HEMT/HBT 2-Stage Third-Order Intercept, Reference Page 48.

Figure C-22C. Case 22, HEMT/HBT 2-Stage Dynamic Range, Reference Page 48.

Case 23: HEMT/HBT 2-Stage Configuration. F_1 = 0.8 dB, F_2 = 4 dB, G_1 = 15 dB, G_2 = 12 dB, TOI_1 = 28 dBm, TOI_2 = 45 dBm, L_R = 2.0 dB, L_A = 3 dB, G_B = 40 dB, F_R = 10 dB, G_R = 10 dB, TOI_R = 45 dBm, Reference Page 49.

Figure C-23A. Case 23, HEMT/HBT 2-Stage Noise Figure, Reference Page 49.

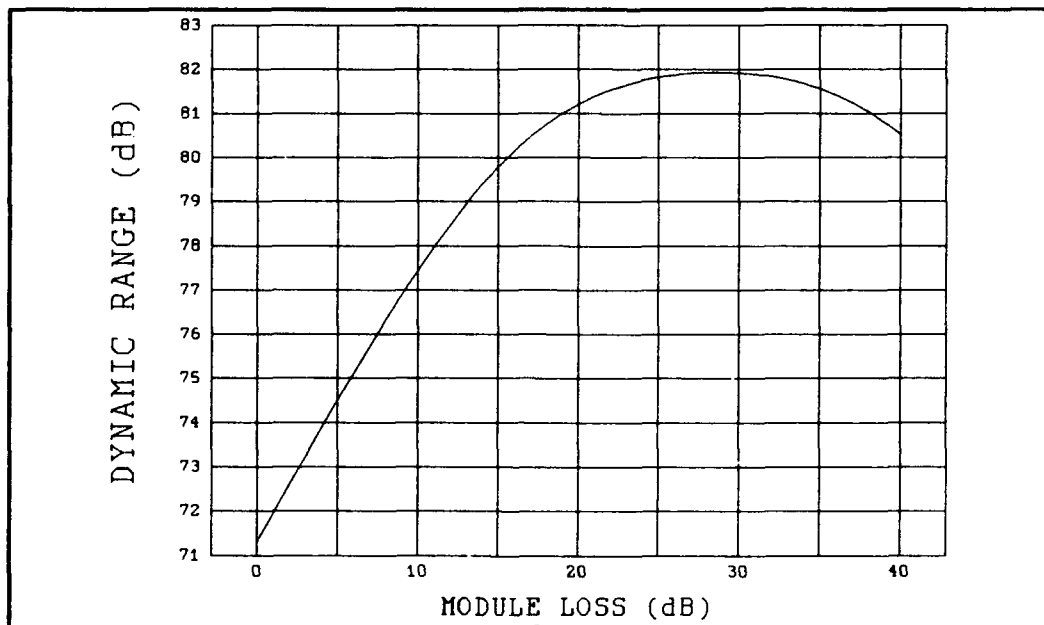Figure C-23B. Case 23, HEMT/HBT 2-Stage Third-Order Intercept, Reference Page 49.

Figure C-23C. Case 23, HEMT/HBT 2-Stage Dynamic Range, Reference Page 49.

Case 24: MESFET 2-Stage Configuration. F_i = 1.1 dB, G_i = 11 dB, TOI_i = 33 dBm, L_R = 1.0 dB, L_A = 3 dB, G_B = 40 dB, F_R = 10 dB, G_R = 10 dB, TOI_R = 45 dBm, Reference Page 50.
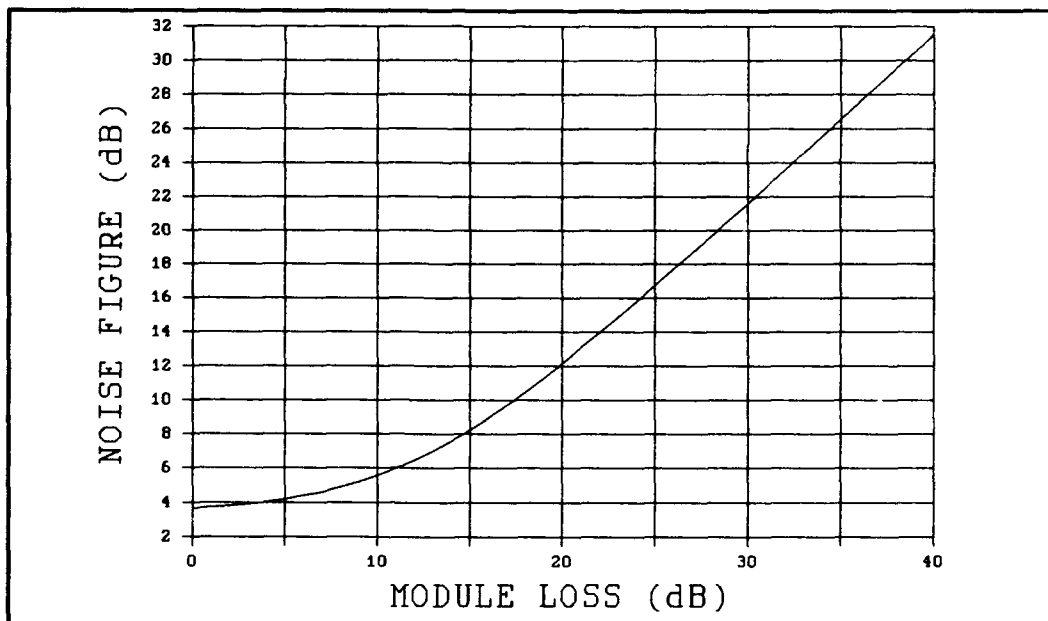

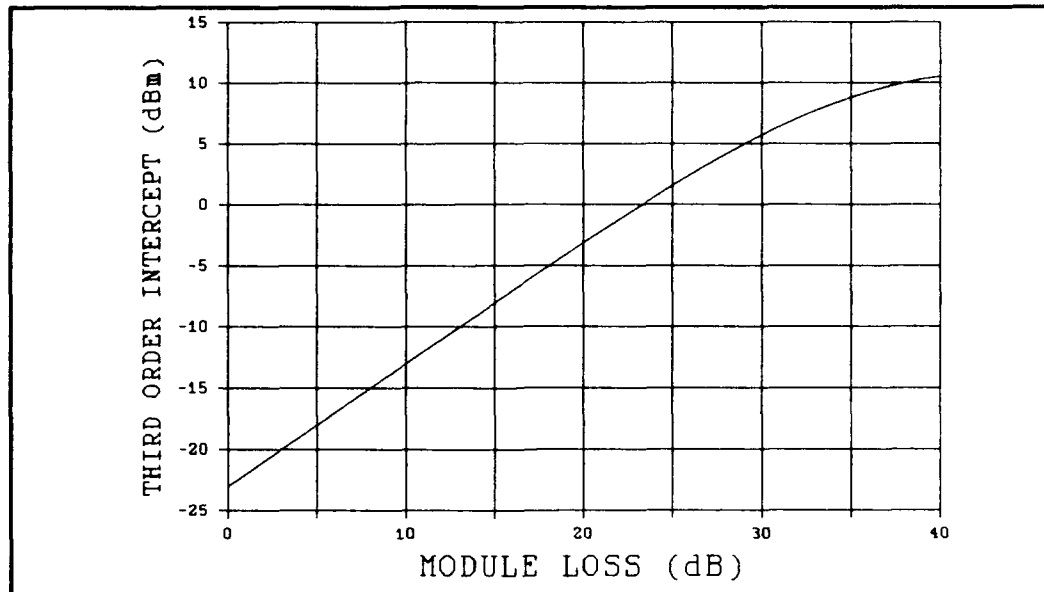Figure C-24A. Case 24, MESFET 2-Stage Noise Figure, Reference Page 50.

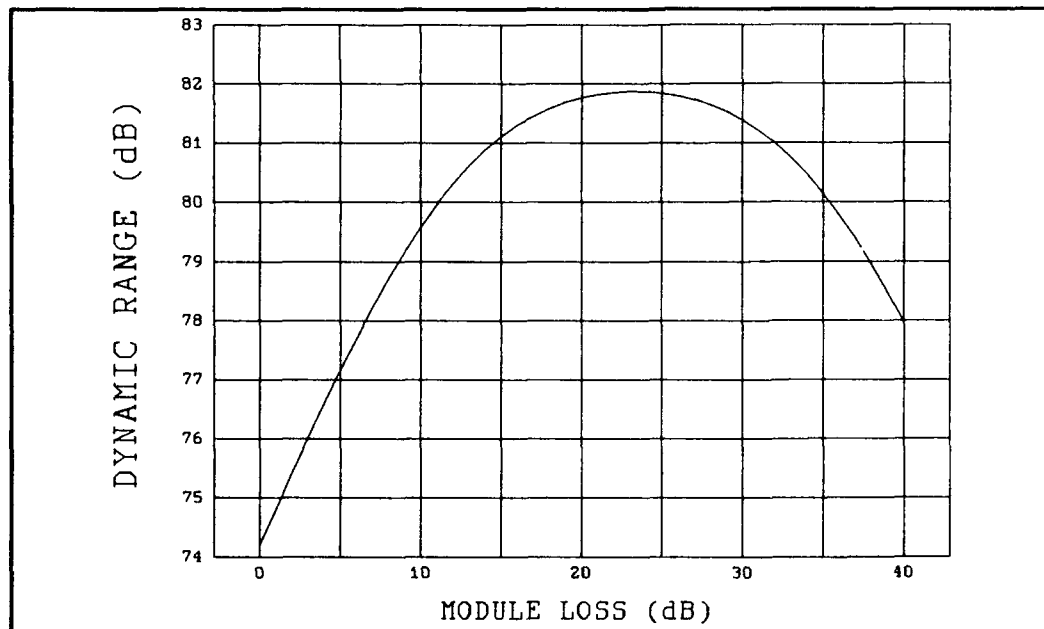**Figure C-24B. Case 24, MESFET 2-Stage Third-Order Intercept, Reference Page 50.**

Figure C-24C. Case 24, MESFET 2-Stage Dynamic Range, Reference Page 50.

Case 25: MESFET 1-Stage Configuration. F_i = 1.1 dB, G_i = 11 dB, TOI_i = 33 dBm, L_R = 1.0 dB, L_A = 3 dB, G_B = 40 dB, F_R = 10 dB, G_R = 10 dB, TOI_R = 45 dBm, Reference Page 51.
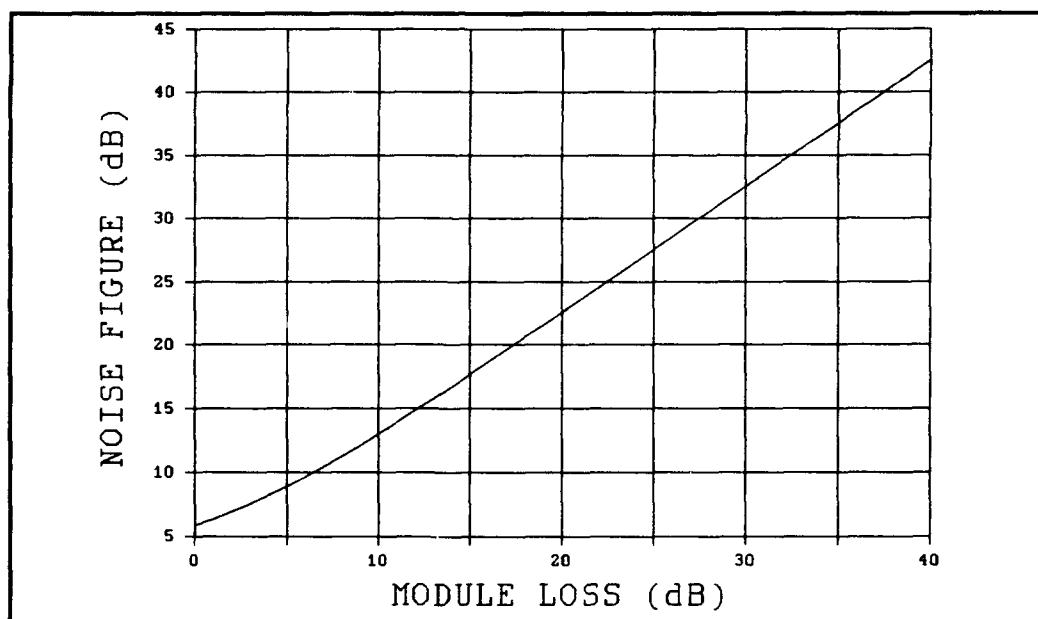

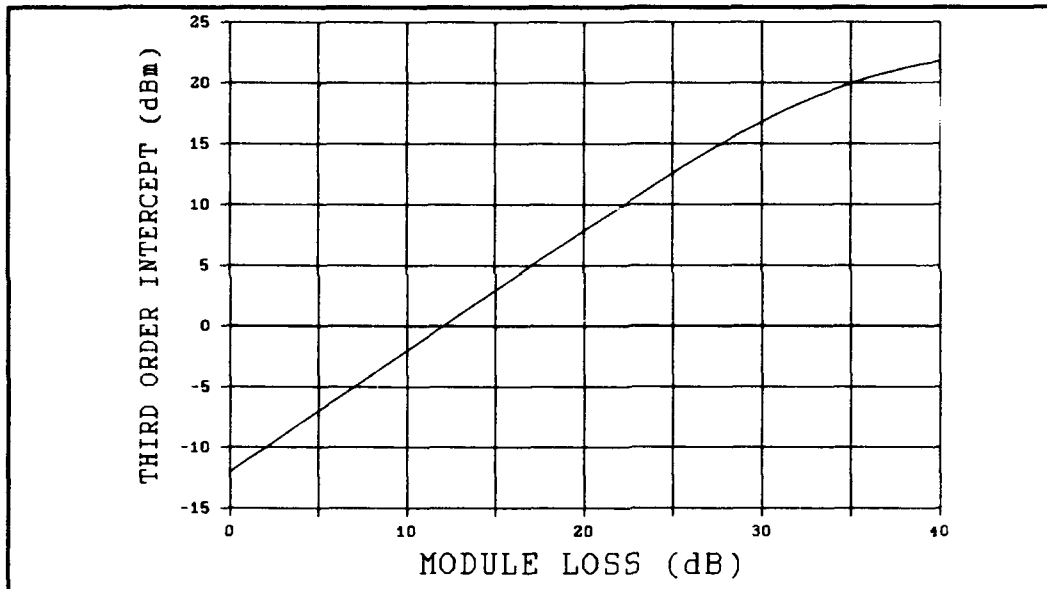Figure C-25A. Case 25, MESFET 1-Stage Noise Figure, Reference Page 51.

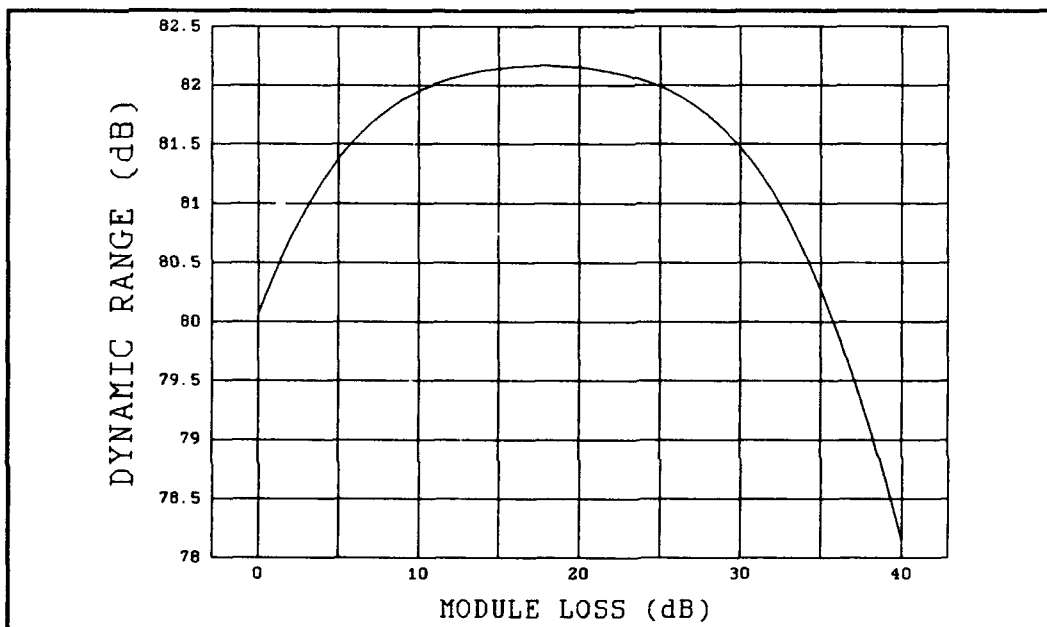Figure C-25B. Case 25, MESFET 1-Stage Third-Order Intercept, Reference Page 51.

Figure C-25C. Case 25, MESFET 1-Stage Dynamic Range, Reference Page 51.

Case 26:   HEMT/HBT 2-Stage Configuration. F_1 = 0.8 dB, F_2 = 4 dB, G_1 = 15 dB, G_2 = 12 dB, TOI_1 = 28 dBm, TOI_2 = 35 dBm, L_R = 0.5 dB, L_A = 3 dB, G_B = 40 dB, F_R = 10 dB, G_R = 10 dB, TOI_R = 55 dBm, Reference Page 52.

Figure C-26A. Case 26, HEMT/HBT 2-Stage Noise Figure, Reference Page 52.

Figure C-26B.   Case 26, HEMT/HBT 2-Stage Third-Order Intercept, Reference Page 52.

Figure C-26C. Case 26, HEMT/HBT 2-Stage Dynamic range, Reference Page 52.

Case 27: HEMT/HBT 2-Stage Configuration. $F_1 = 0.8$ dB, $F_2 = 4$ dB, $G_1 = 15$ dB, $G_2 = 12$ dB, $TOI_1 = 28$ dBm, $TOI_2 = 35$ dBm, $L_R = 1.0$ dB, $L_A = 3$ dB, $G_B = 40$ dB, $F_R = 10$ dB, $G_R = 10$ dB, $TOI_R = 55$ dBm, Reference Page 53.
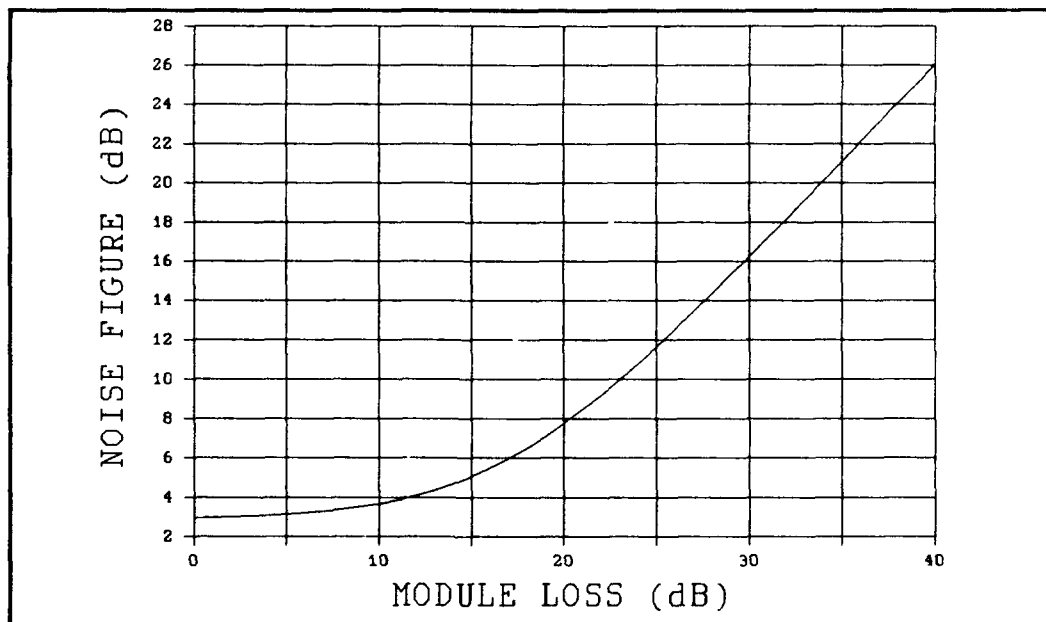

Figure C-27A. Case 27, HEMT/HBT 2-Stage Noise Figure, Reference Page 53.
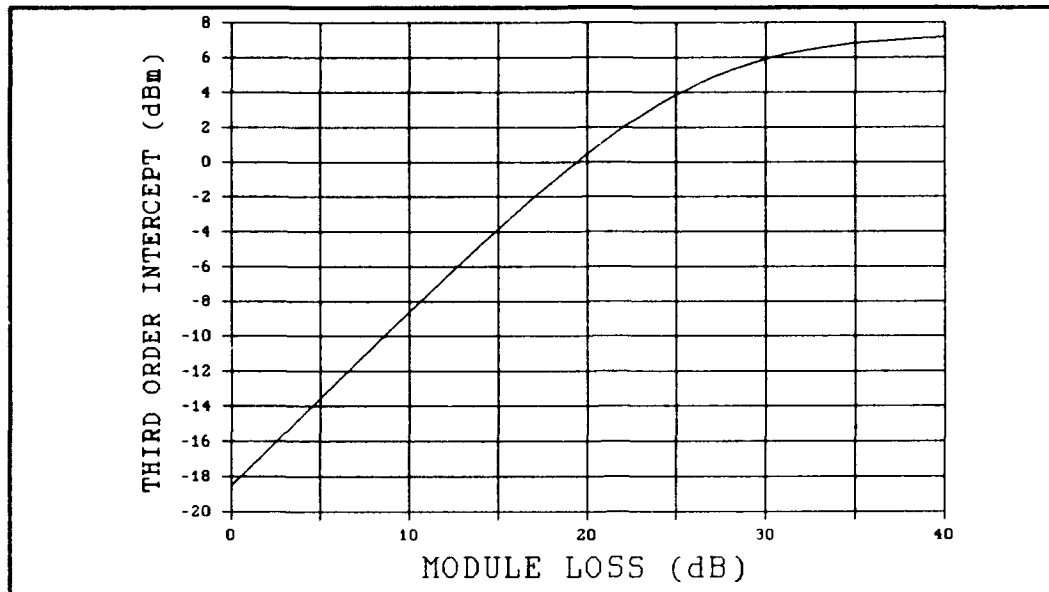
Figure C-27B. Case 27, HEMT/HBT 2-Stage Third-Order Intercept, Reference Page 53.
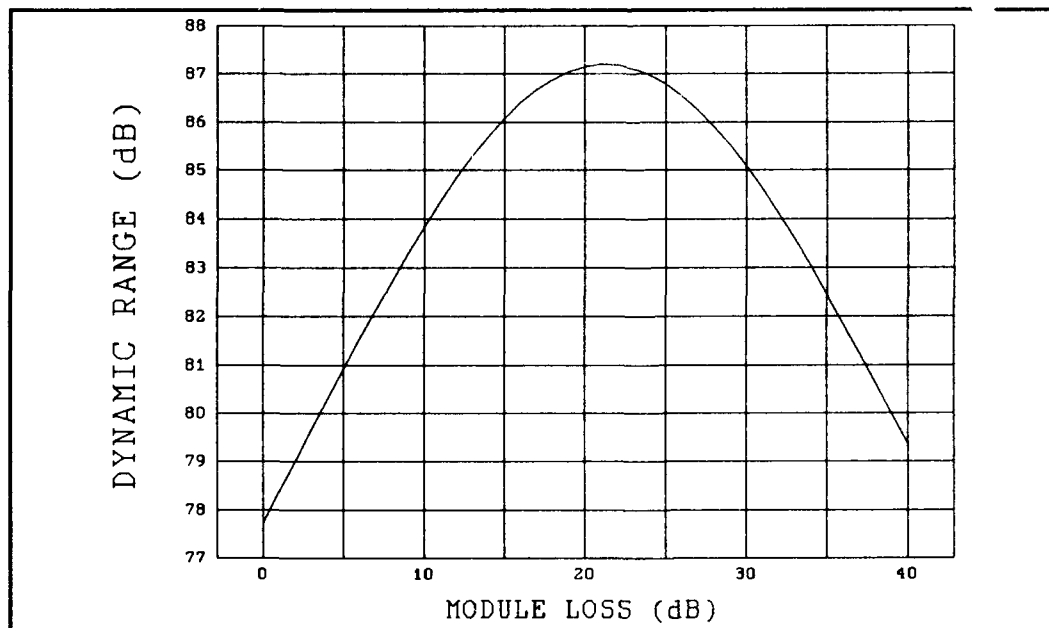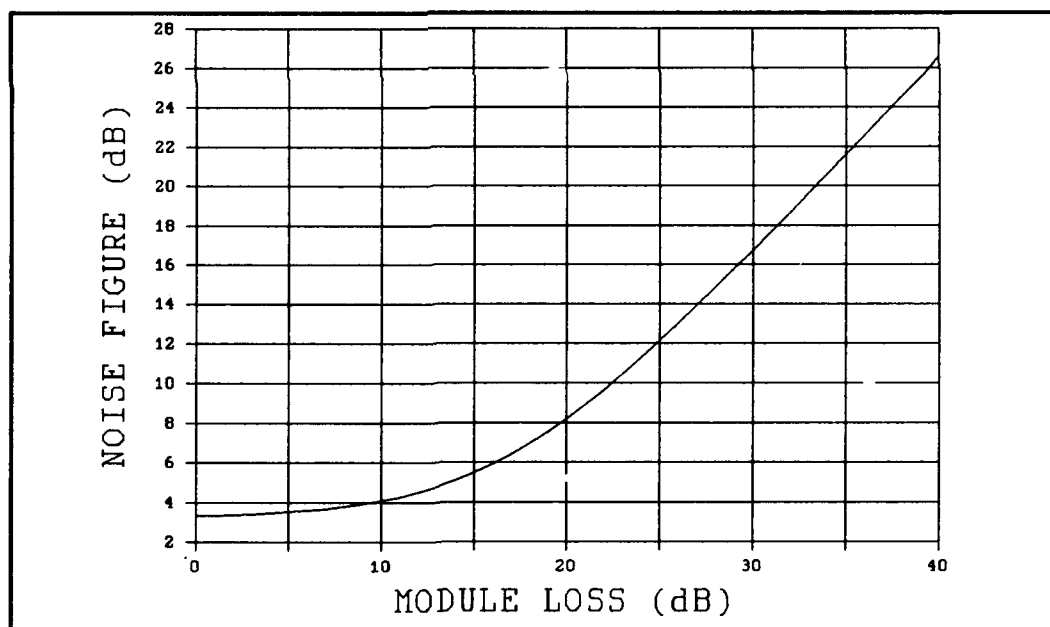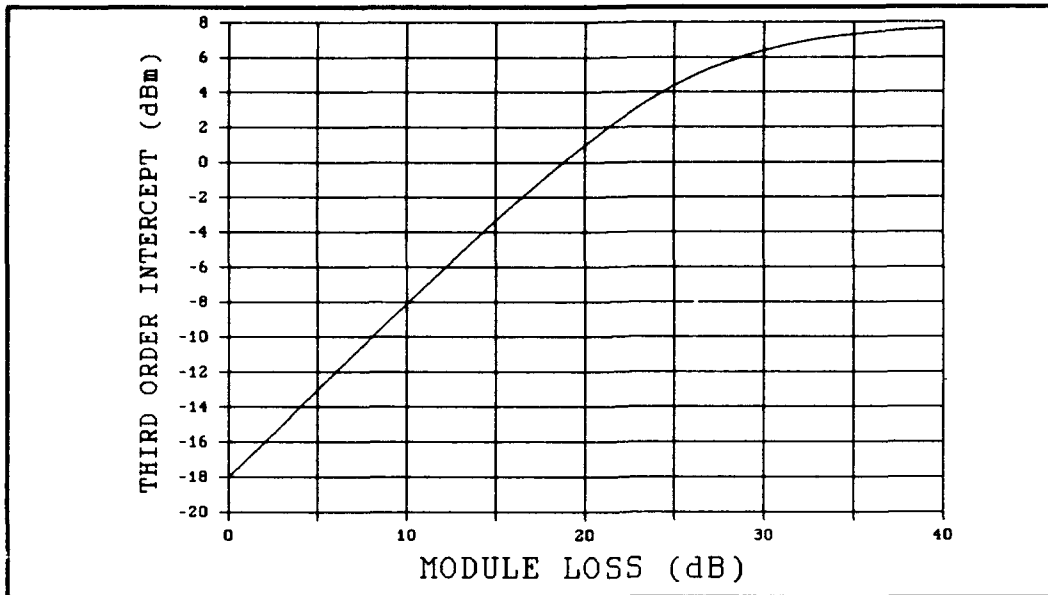

Figure C-27C. Case 27, HEMT/HBT 2-Stage Dynamic Range, Reference Page 53.

Case 28:   HEMT/HBT 2-Stage Configuration. F_1 = 0.8 dB, F_2 = 4 dB, G_1 = 15 dB, G_2 = 12 dB, TOI_1 = 28 dBm, TOI_2 = 35 dBm, L_R = 2.0 dB, L_A = 3 dB, G_B = 40 dB, F_R = 10 dB, G_R = 10 dB, TOI_R = 55 dBm, Reference Page 54.

Figure C-28A is unique among all the cases in that the beginning noise figure is significantly different than that obtained in Reference[C-1], $\approx$ 1 dB. By varying the parameters, the results were duplicated using G_1 = 5 dB vs the 15 dB specified. Possibly this was done in the original text and not caught because no review cycle was completed.

Figure C-28A. Case 28, HEMT/HBT 2-Stage Noise Figure, Reference Page 54.

Figure C-28B. Case 28, HEMT/HBT 2-Stage Third-Order Intercept, Reference Page 54.
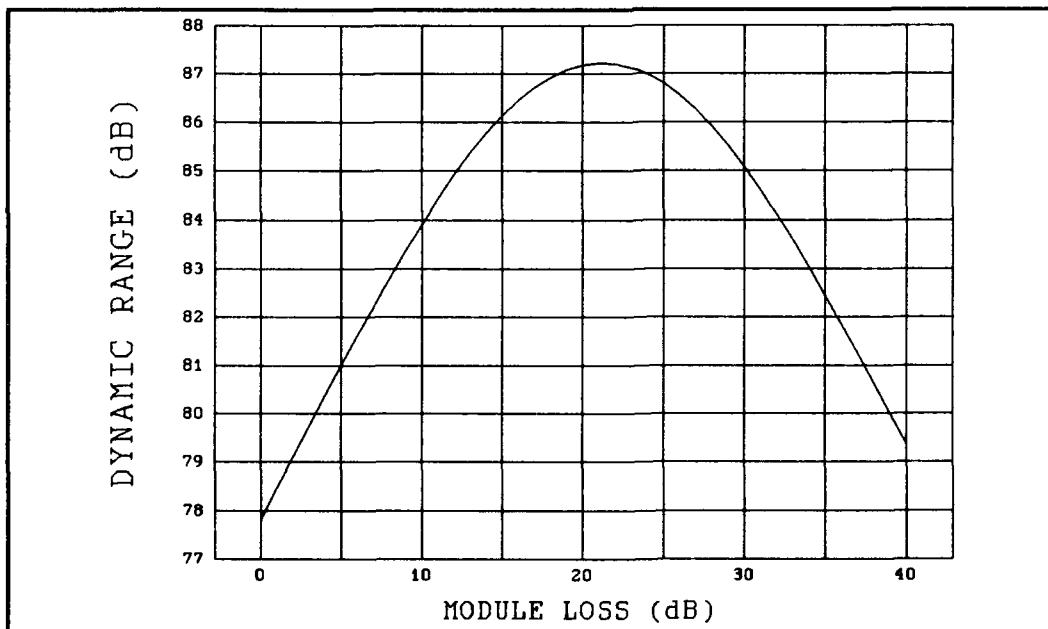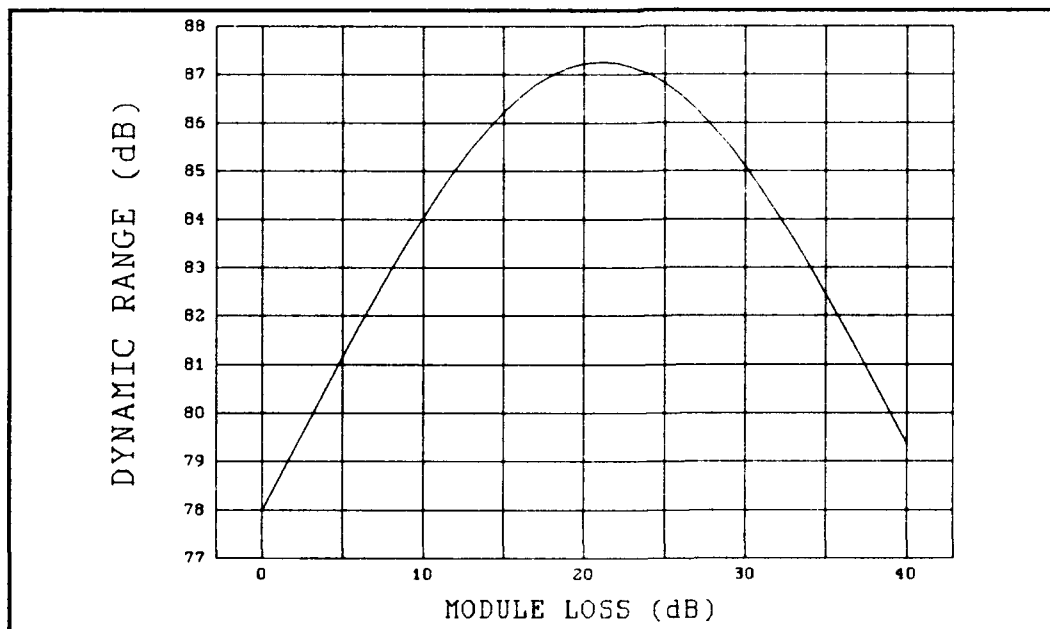

Figure C-28C. Case 28, HEMT/HBT 2-Stage Dynamic Range, Reference Page 54.

Case 29: MESFET 2-Stage Configuration. F_i = 2.0 dB, G_i = 11 dB, TOI_i = 33 dBm, L_R = 1.0 dB, L_A = 3 dB, G_B = 40 dB, F_R = 10 dB, G_R = 10 dB, TOI_R = 55 dBm, Reference Page 55.

Figure C-29A. Case 29, MESFET 2-Stage Noise Figure, Reference Page 55.

Figure C-29B. Case 29, MESFET 2-Stage Third-Order Intercept, Reference Page 55.

Figure C-29C. Case 29, MESFET 2-Stage Dynamic Range, Reference Page 55.

Case 30: MESFET 1-Stage Configuration. F_1 = 2.0 dB, G_1 = 11 dB, TOI_i = 33 dBm, L_R = 1.0 dB, L_A = 3 dB, G_B = 40 dB, F_R = 10 dB, G_R = 10 dB, TOI_R = 55 dBm, Reference Page 56.
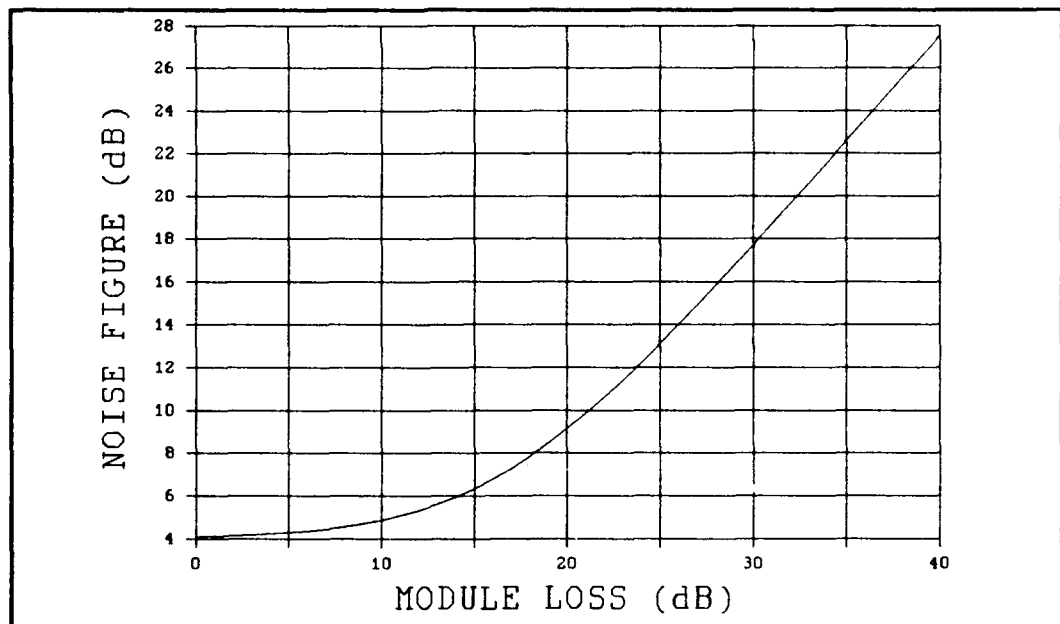

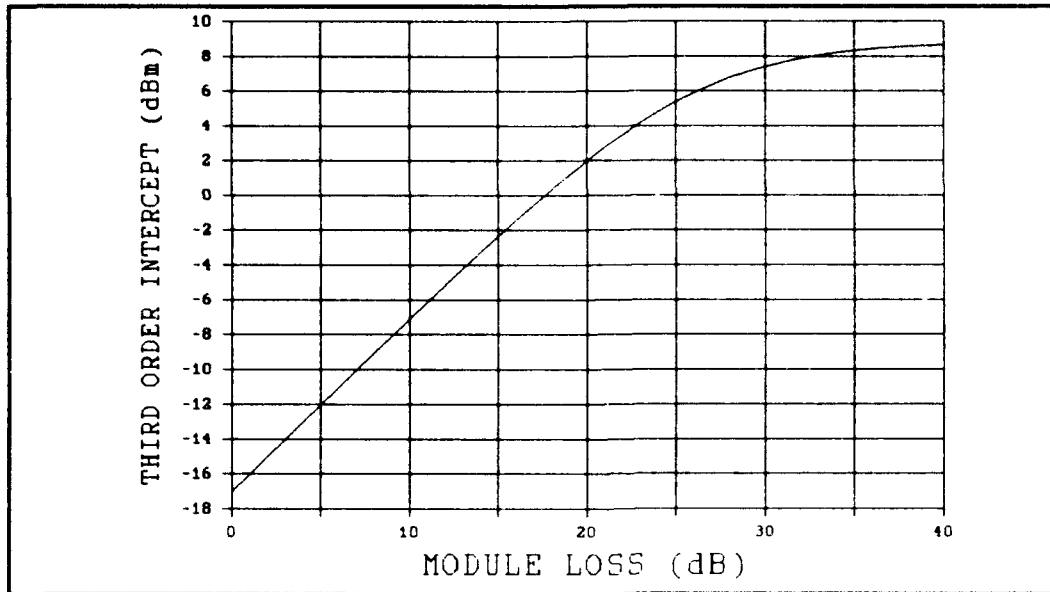Figure C-30A. Case 30, MESFET 1-Stage Noise Figure, Reference Page 56.

Figure C-30B. Case 30, MESFET 1-Stage Third-Order Intercept, Reference Page 56.

Figure C-30C. Case 30, MESFET 1-Stage Dynamic Range, Reference Page 56.

Case 31:   HEMT 3-Stage Configuration. F_i = 2.4 dB, G_i = 15 dB, TOI_i = 28 dBm, L_R = 0.5 dB, L_A = 3 dB, G_B = 40 dB, F_R = 10 dB, G_R = 10 dB, TOI_R = 55 dBm, Reference Page 57.

Figure C-31A. Case 31, HEMT 3-Stage Noise Figure, Reference Page 57.
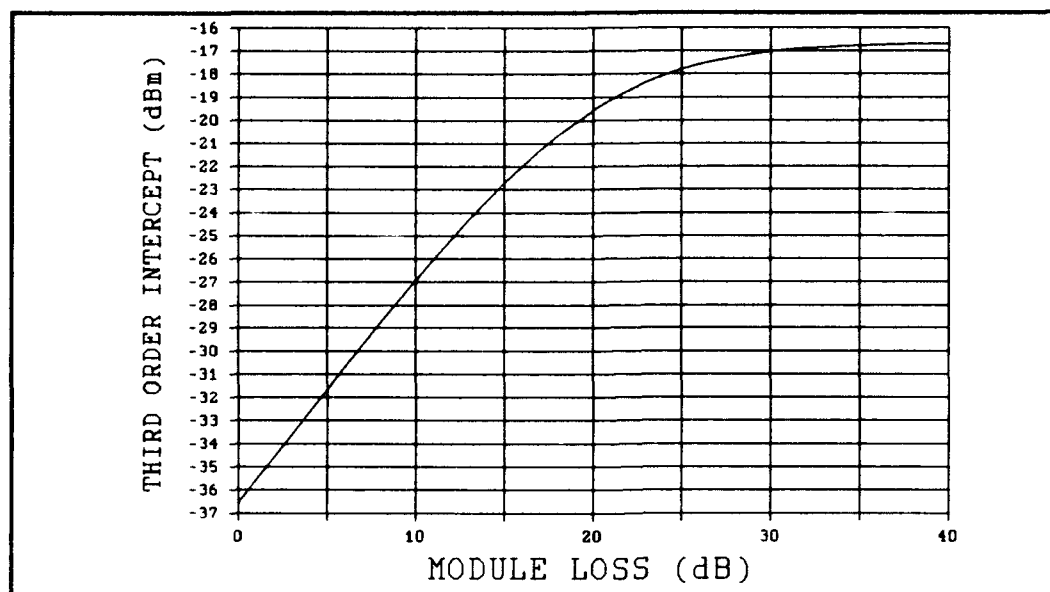
**Figure C-31B. Case 31, HEMT 3-Stage Third Order Intercept, Reference Page 57.**

Figure C-31C. Case 31, HEMT 3-Stage Dynamic Range, Reference Page 57.

Case 32: HEMT 3-Stage Configuration. F_i = 2.4 dB, G_i = 15 dB, TOI_i = 28 dBm, L_R = 1.0 dB, L_A = 3 dB, G_B = 40 dB, F_R = 10 dB, G_R = 10 dB, TOI_R = 55 dBm, Reference Page 58.
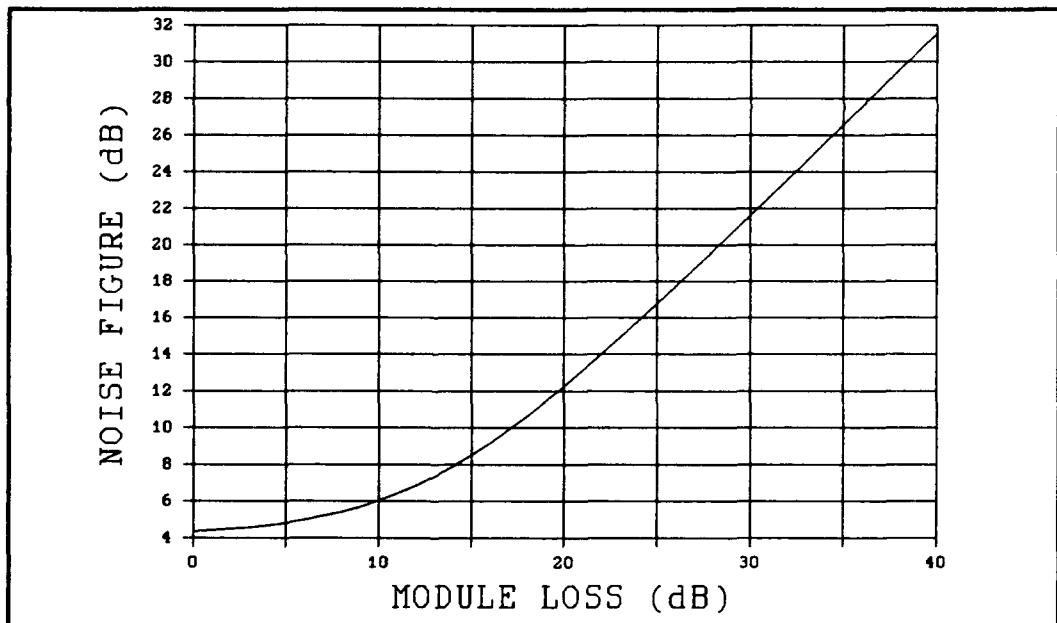

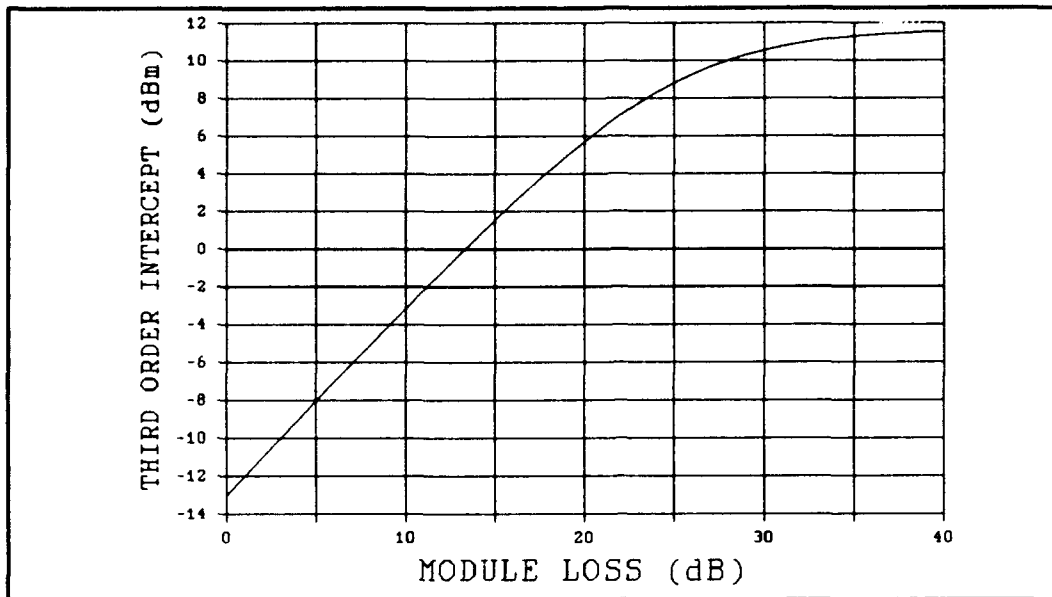Figure C-32A. Case 32, HEMT 3-Stage Noise Figure, Reference Page 58.

Figure C-32B. Case 32, HEMT 3-Stage Third–Order Intercept, Reference Page 58.
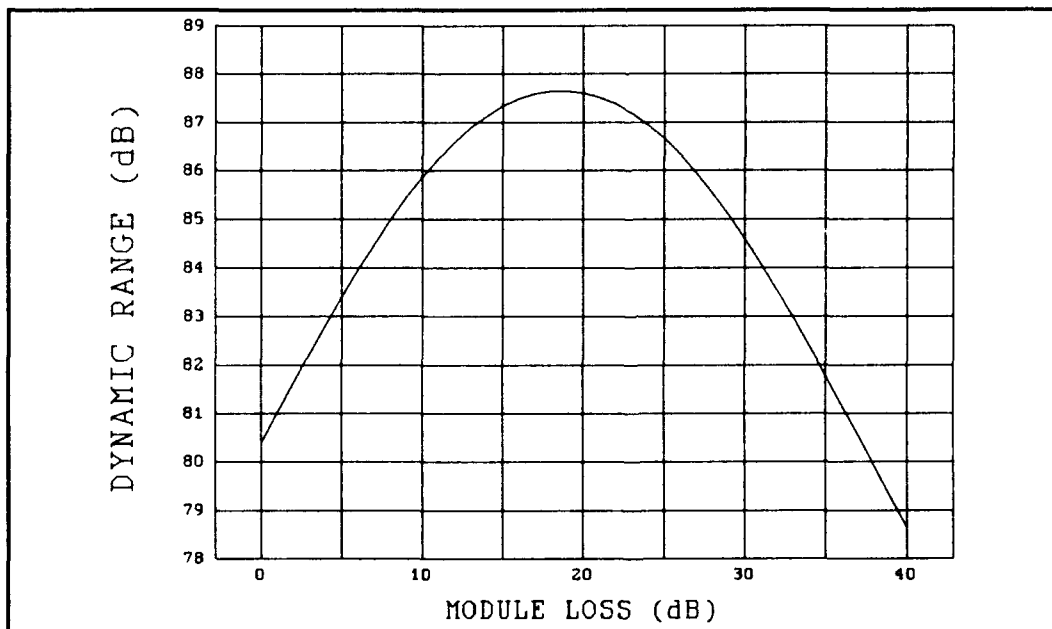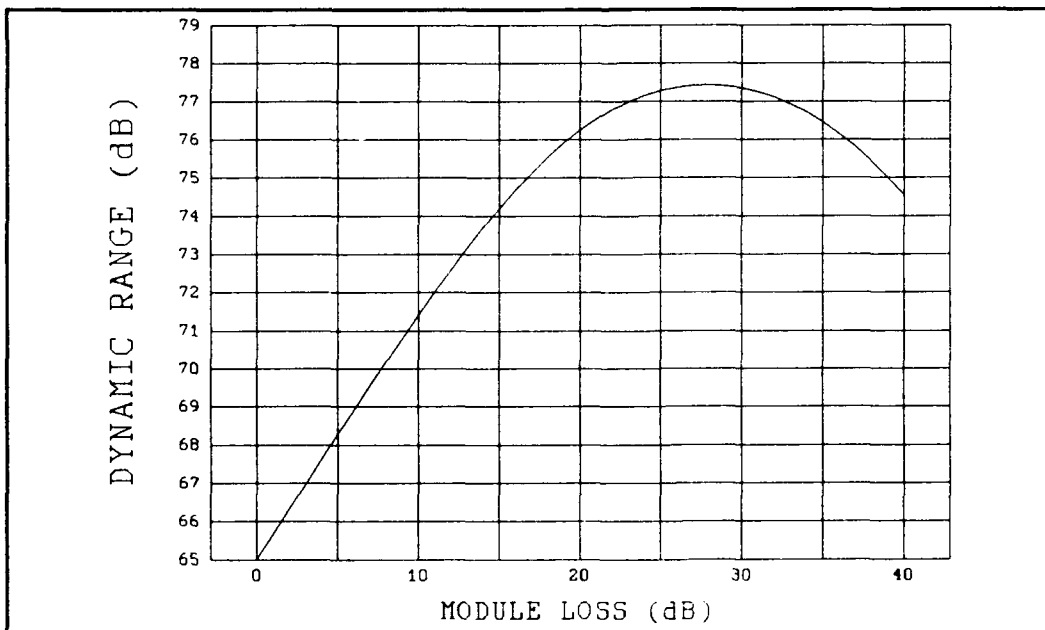

Figure C-32C. Case 32, HEMT 3-Stage Dynamic Range, Reference Page 58.

Case 33:   HEMT 3-Stage Configuration. F_i = 2.4 dB, G_i = 15 dB, TOI_i = 28 dBm, L_R = 2.0 dB, L_A = 3 dB, G_B = 40 dB, F_R = 10 dB, G_R = 10 dB, TOI_R = 55 dBm, Reference Page 59.
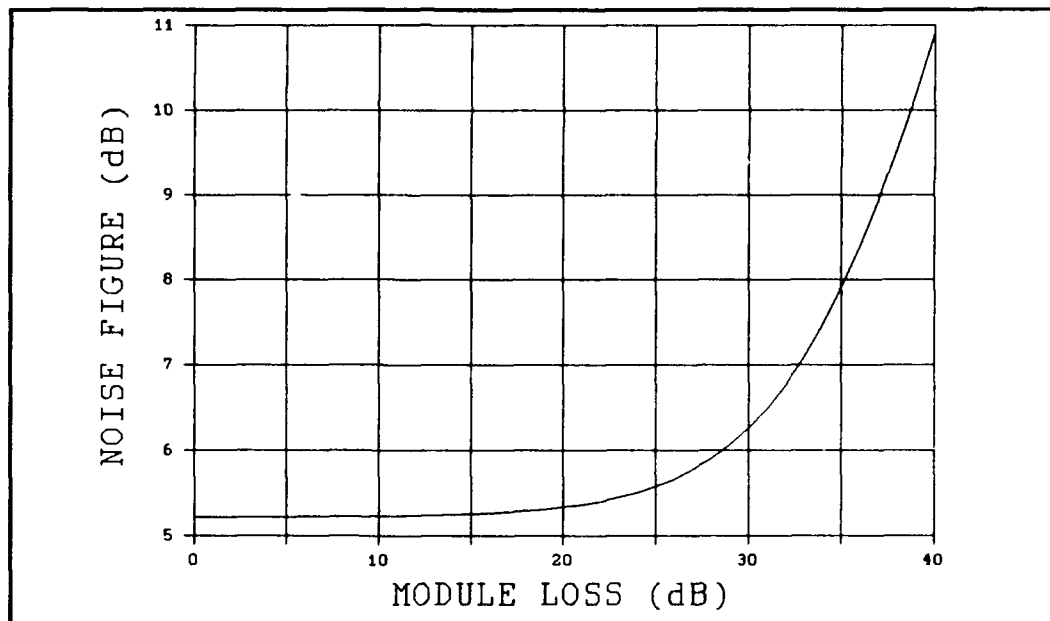
Figure C-33A. Case 33, HEMT 3-Stage Noise Figure, Reference Page 59.
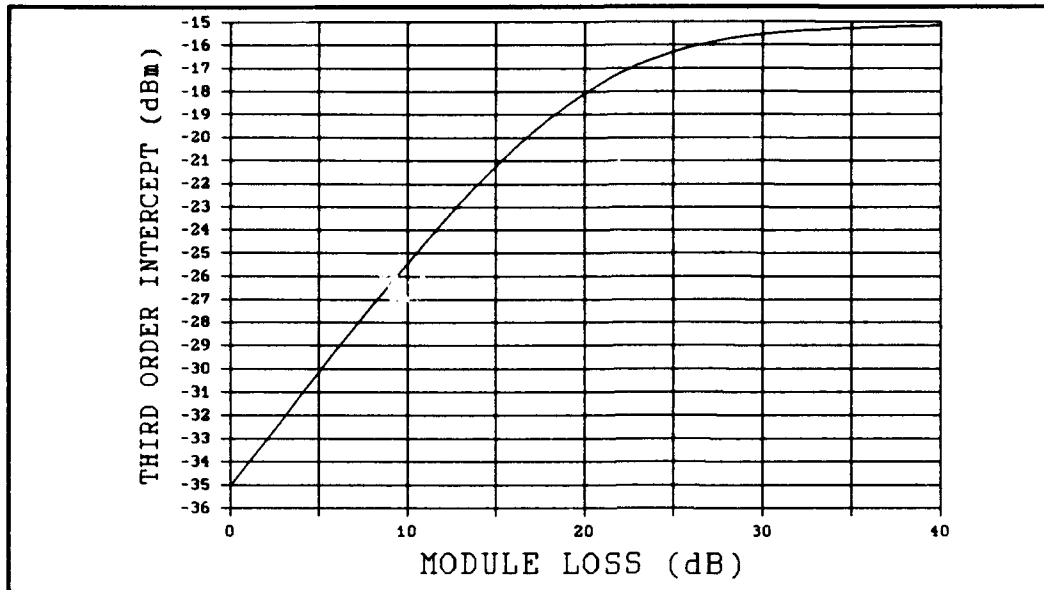
Figure C-33B. Case 33, HEMT 3-Stage Third - Order Intercept, Reference Page 59.
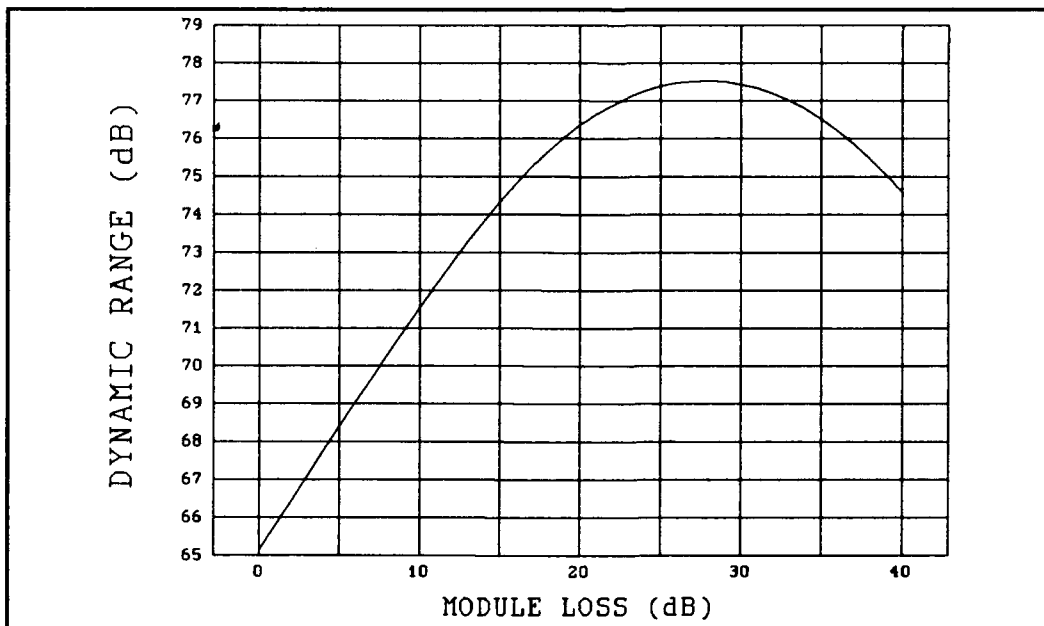
Figure C-33C. Case 33, HEMT 3-Stage Dynamic Range, Reference Page 59.

Case 34:   MESFET 3-Stage Configuration. F_i = 2.0 dB, G_i = 11 dB, TOI_i = 33 dBm, L_R = 0.5 dB, L_A = 3 dB, G_B = 40 dB, F_R = 10 dB, G_R = 10 dB, TOI_R = 55 dBm, Reference Page 60.
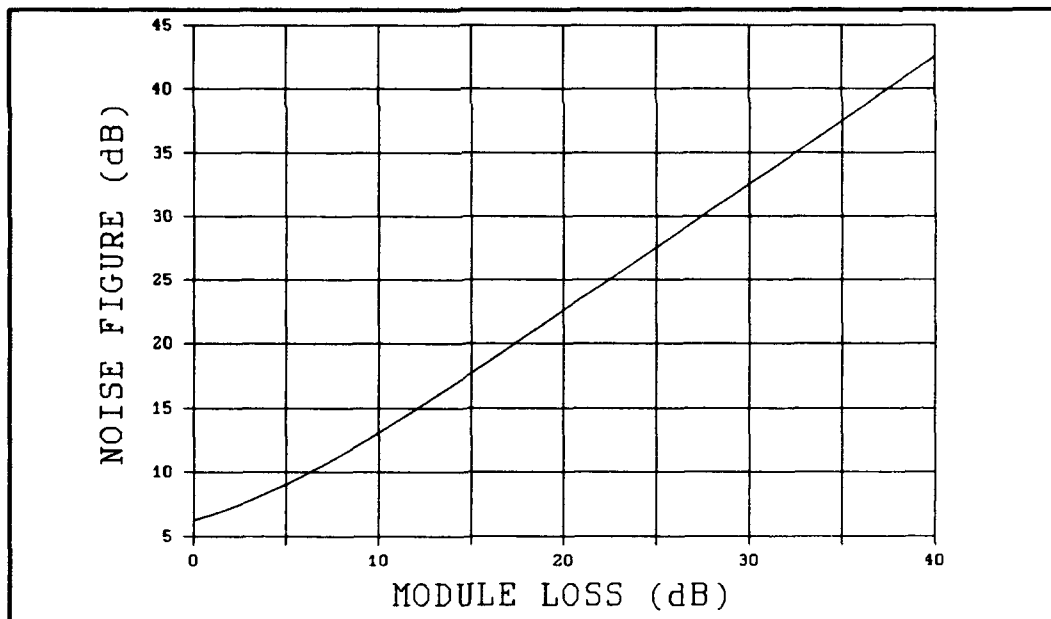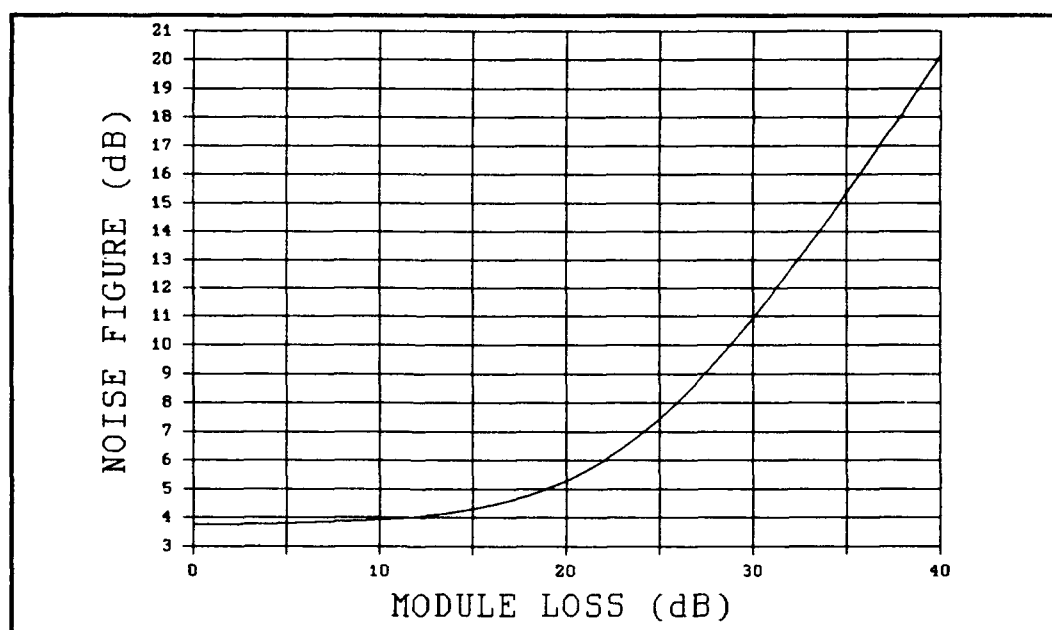

Figure C-34A.   Case 34, MESFET 3-Stage Noise Figure, Reference Page 60.
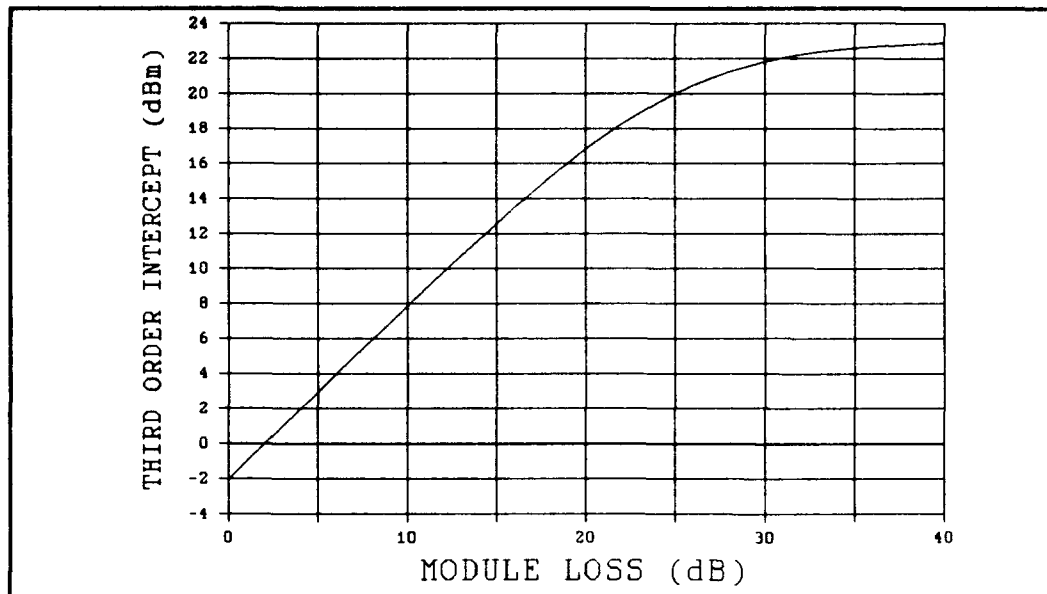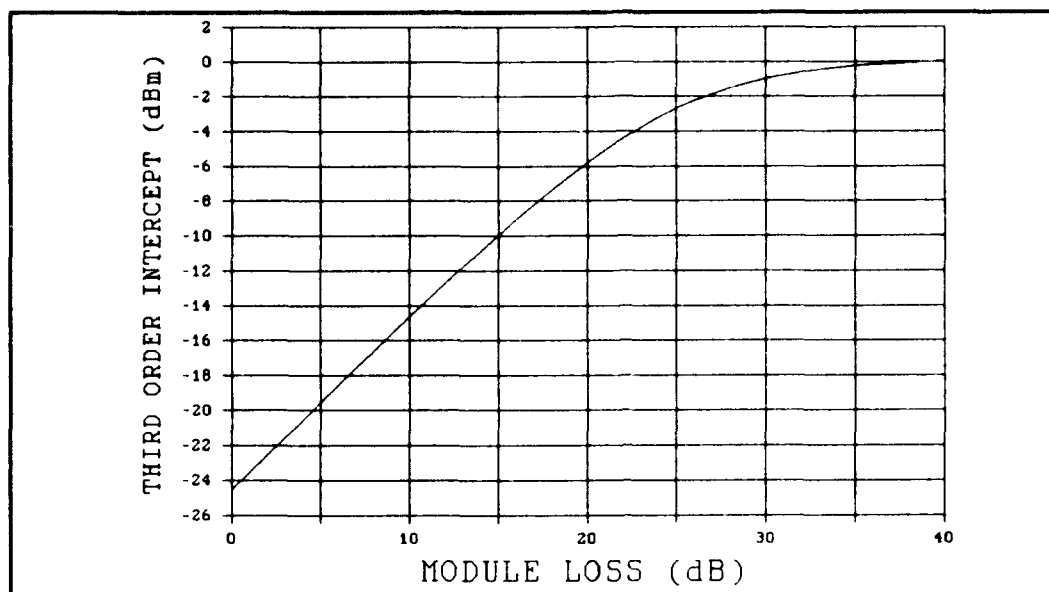
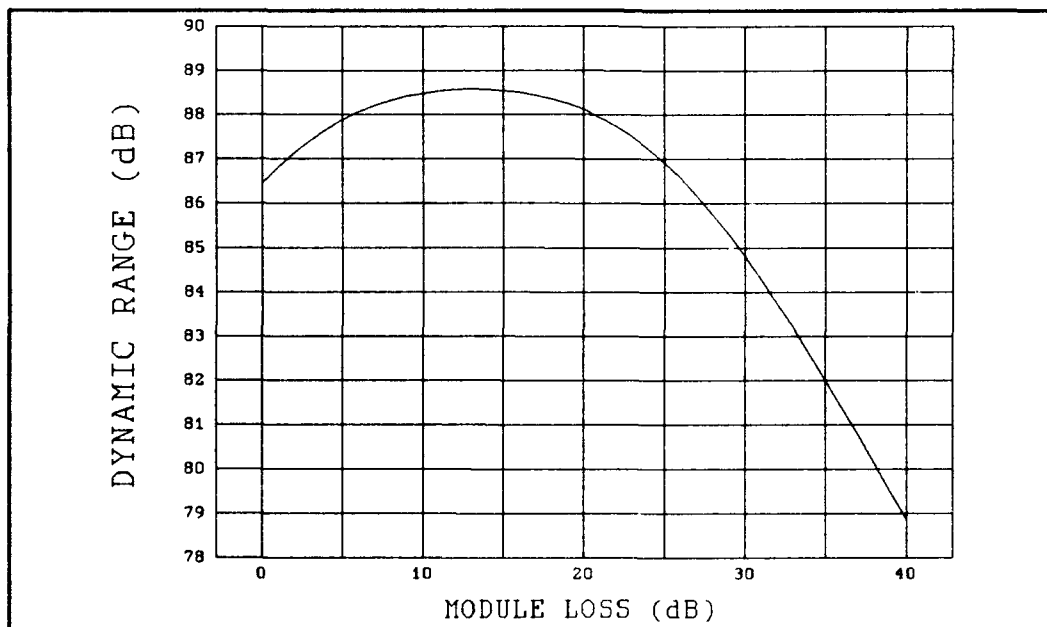**Figure C-34B. Case 34, MESFET 3-Stage Third -Order Intercept, Reference Page 60.**
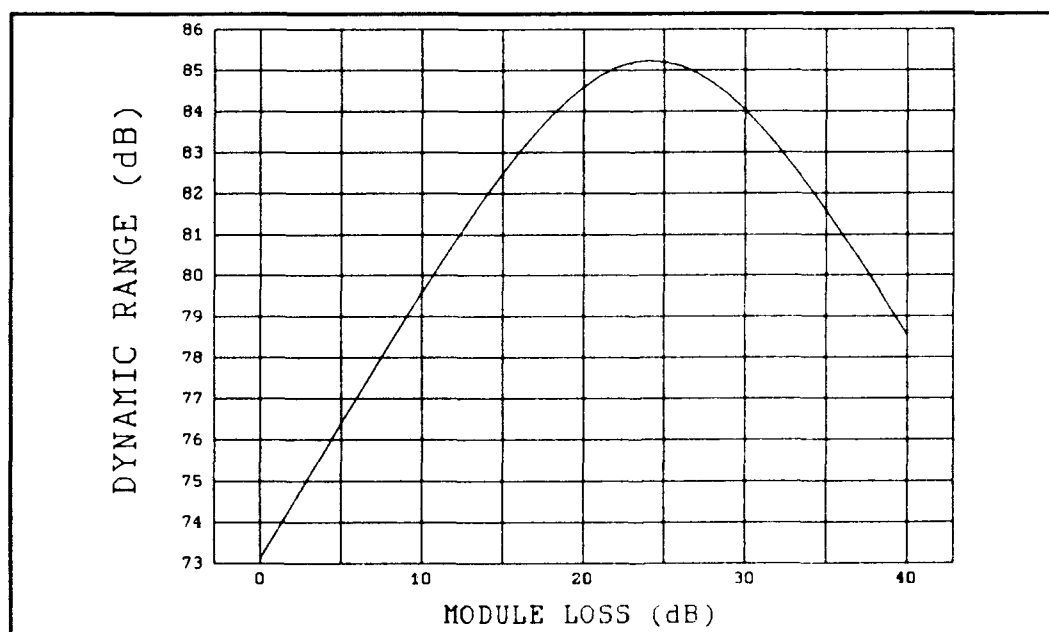
Figure C-34C. Case 34, MESFET 3-Stage Dynamic Range, Reference Page 60.

Case 35: **MESFET 3-Stage Configuration.** F_i = 2.0 dB, G_i = 11 dB, TOI_i = 33 dBm, L_R = 1.0 dB, L_A = 3 dB, G_B = 40 dB, F_R = 10 dB, G_R = 10 dB, TOI_R = 55 dBm, Reference Page 61.
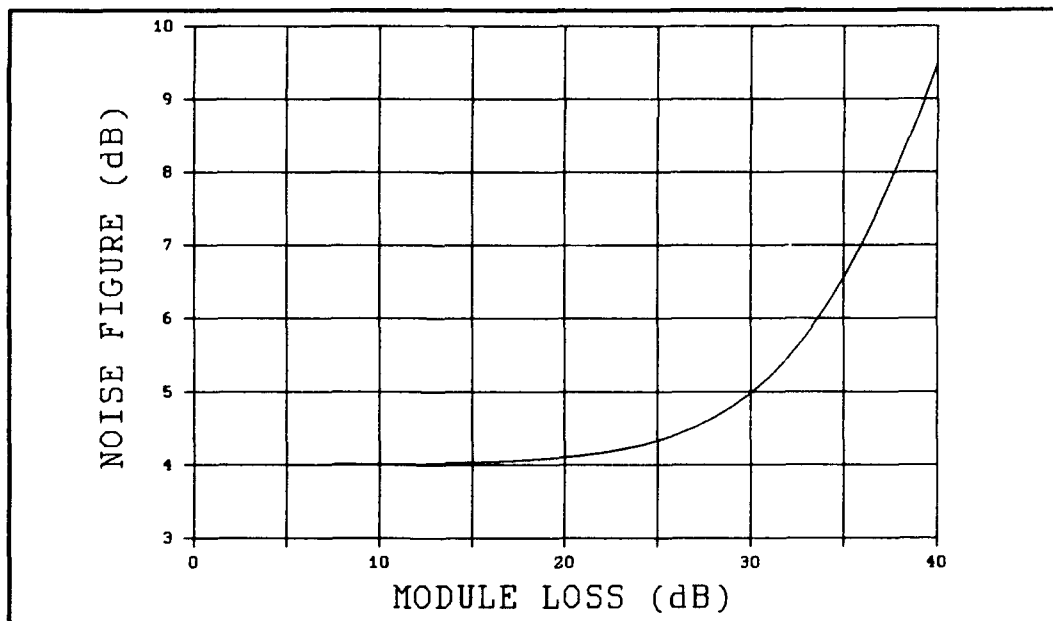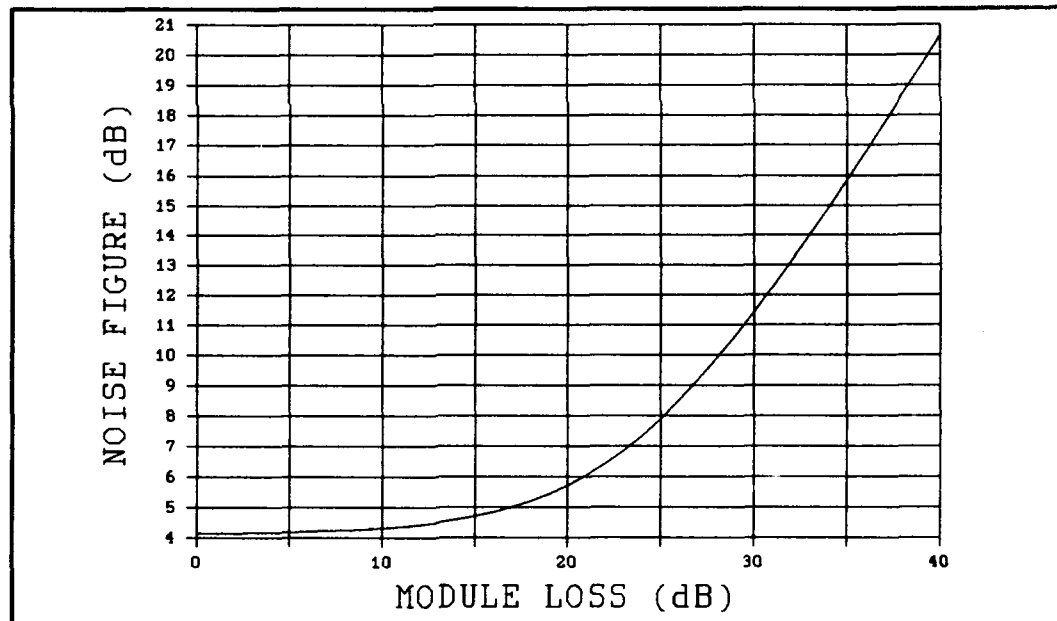

Figure C-35A. Case 35, MESFET 3-Stage Noise Figure, Reference Page 61.
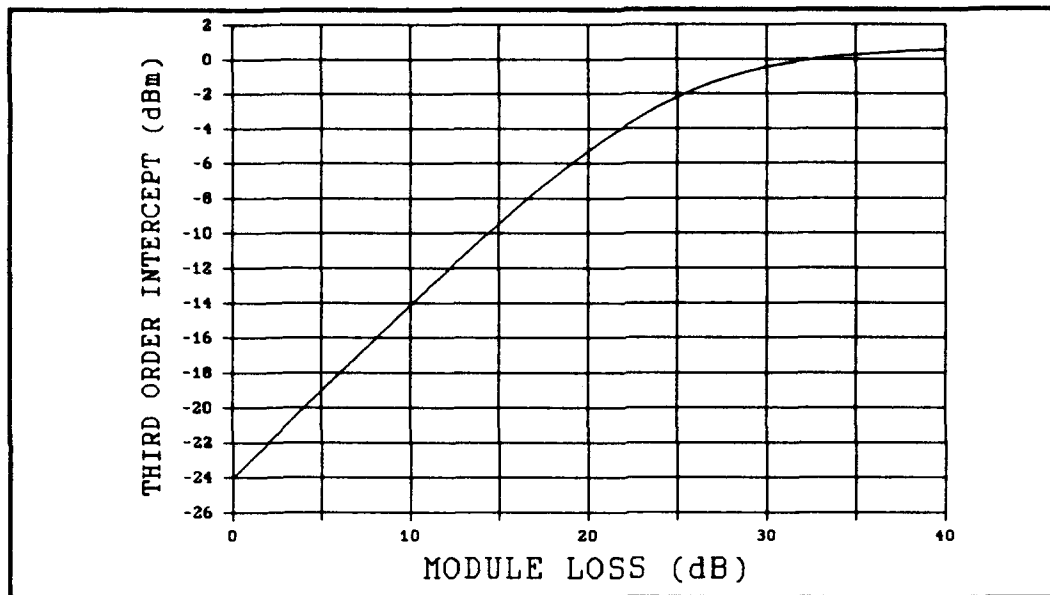
Figure C-35B. Case 35, MESFET 3-Stage Third-Order Intercept, Reference Page 61.
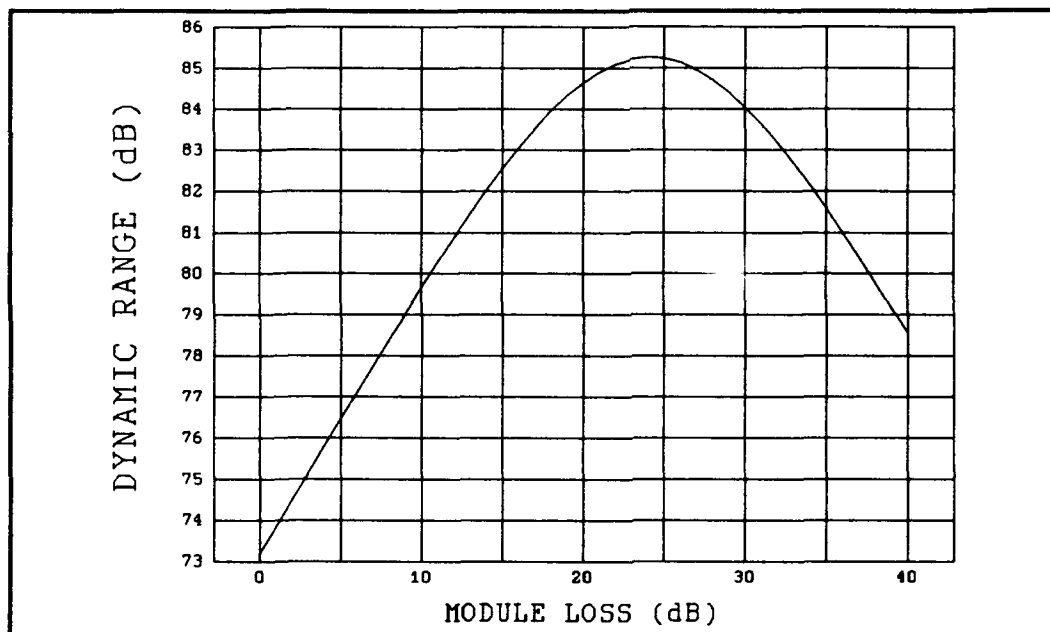
Figure C-35C. Case 35, MESFET 3-Stage Dynamic Range, Reference Page 61.

Case 36: MESFET 3-Stage Configuration. F_i = 2.0 dB, G_i = 11 dB, TOI_i = 33 dBm, L_R = 2.0 dB, L_A = 3 dB, G_s = 40 dB, F_R = 10 dB, G_R = 10 dB, TOI_R = 55 dBm, Reference Page 62.
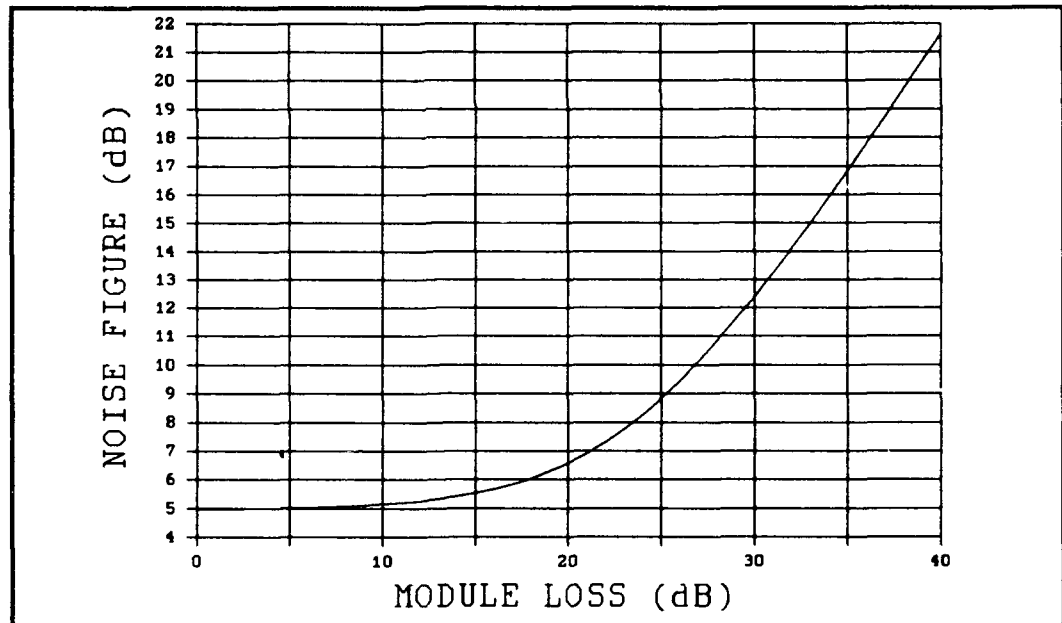
Figure C-36A. Case 36, MESFET 3-Stage Noise Figure, Reference Page 62.
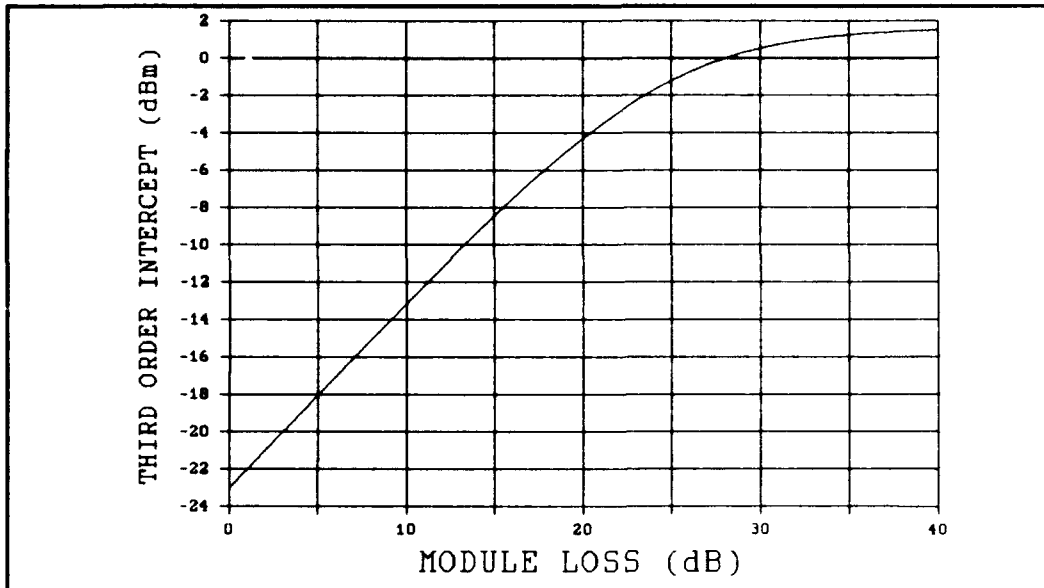
Figure C-36B. Case 36, MESFET 3-Stage Third-Order Intercept, Reference Page 62.
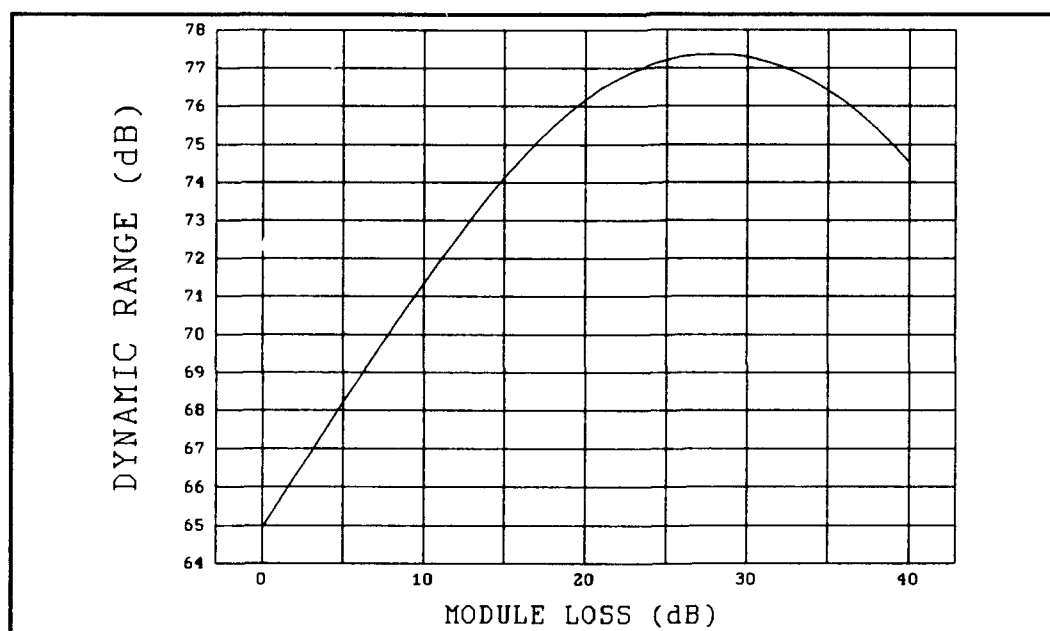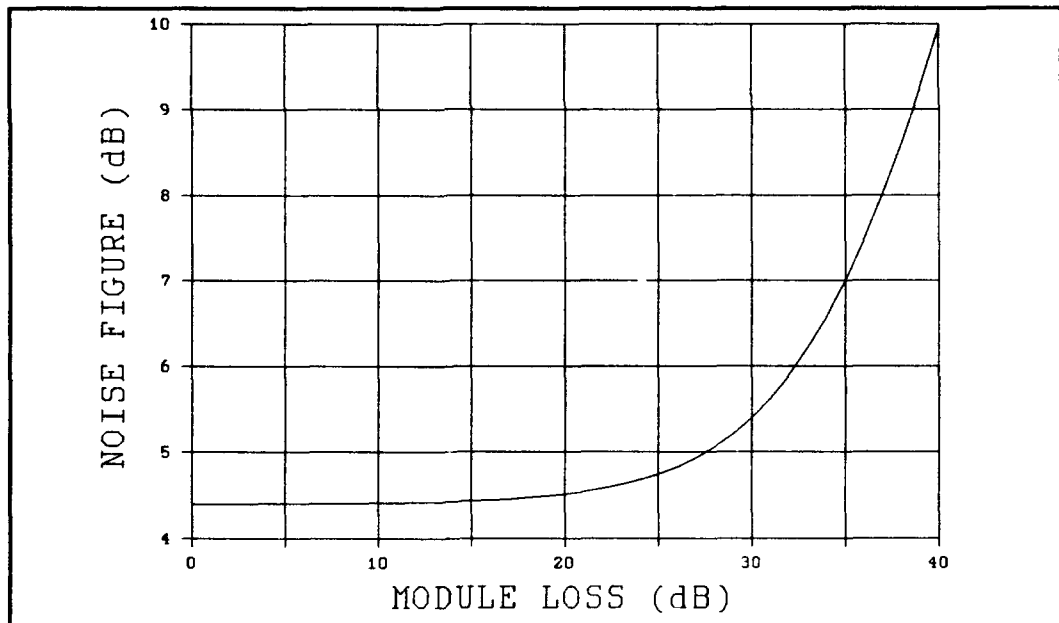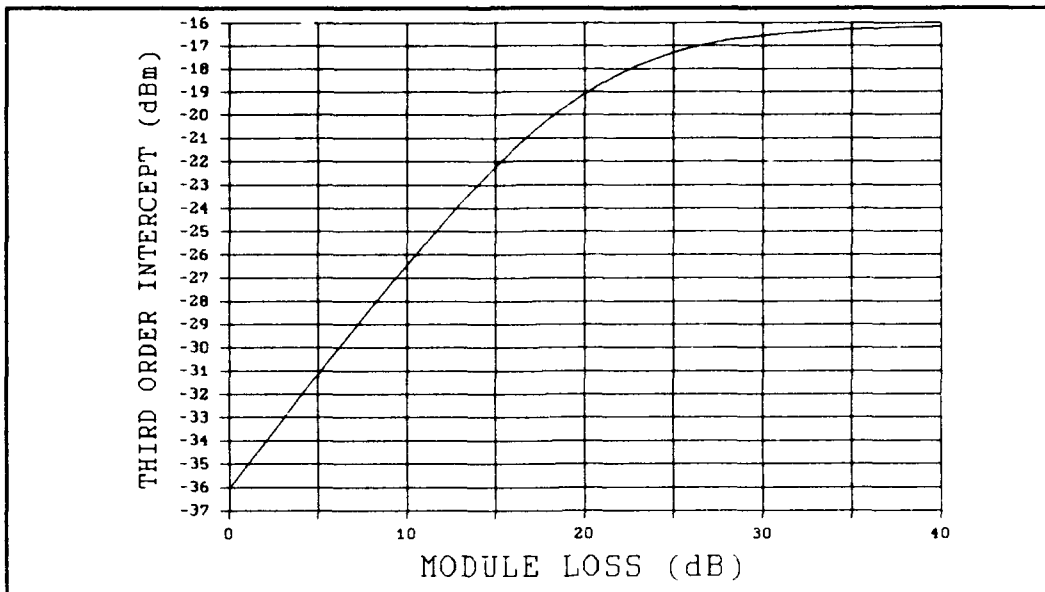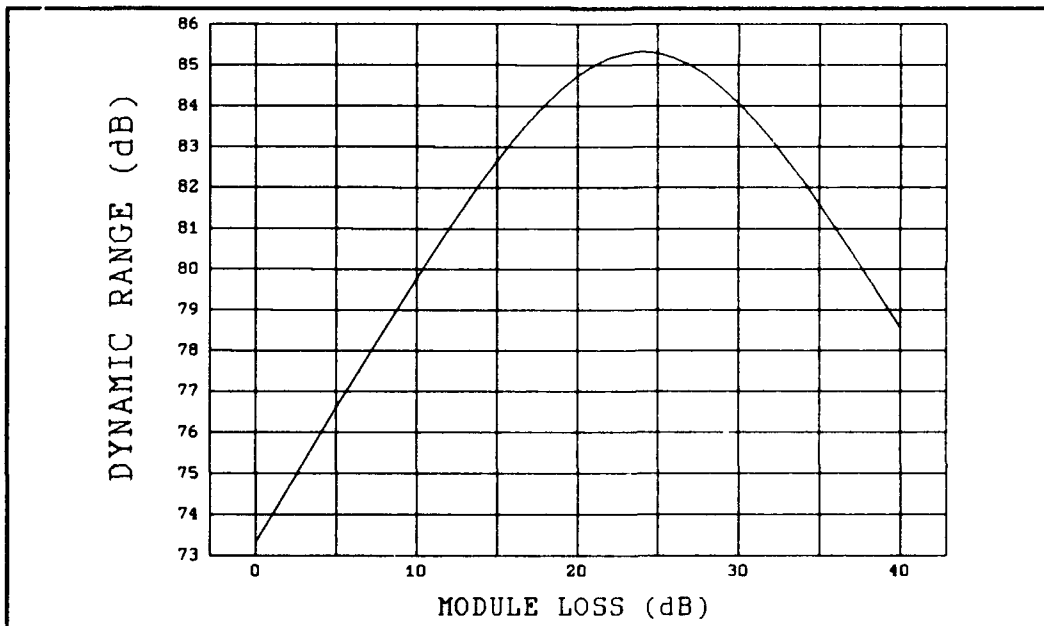

Figure C-36C. Case 36, MESFET 3-Stage Dynamic Range, Reference Page 62.

APPENDIX D

TAPER-WEIGHTING EFFECTS

APPENDIX D NOMENCLATURE

HEMT   High-electron mobility transistor

HBT   Heterojunction bipolar transistor

MSFET   Metal semiconductor field-effect transistor

This appendix computes the magnitude of the effects that array-amplitude weighting on receive has on overall array-noise figure. The weighting is accomplished by adding attenuation to the receive chain, determined by the taper function, just before the beam-former network. The results are compared to the effects of adding attenuation on all modules equal to the maximum taper weight.

The first step that must be taken is to rewrite the system-noise figure equation.

$$F_{SA} = F_A + L_R * [F_1 + \frac{(F_2-1)}{G_1} + \frac{(F_3-1)}{G_1 * G_2} + \frac{L_m * L_B * (\frac{1-G_b}{G_b}) + (L_m * L_B * F_R - 1)}{G_1 * G_2 * G_3}]$$

This, as before, can be rewritten:

$$F_{SA} = F_A + L_R * F_1' + \frac{L_R * (F_2-1)}{G_1} + \frac{L_R * (F_3-1)}{G_1 * G_2} - \frac{L_R}{G_1 * G_2 * G_3}$$

$$+ L_m * [\frac{L_R * L_B * (\frac{1-G_b}{G_b}) + L_R * L_B * F_R}{G_1 * G_2 * G_3}]$$

(D-1)

Again as before, an array with nonuniform attenuation (L_m) over the array (as for the case of taper weighting) could utilize Equation D-1 in the general form:

$$F_{SA} = F_{AA} + L_m(r, \Theta) * F_{BB}$$

(D-2)

For the cases of linear and cosine-squared-on-a-pedestal and referring to their respective Equations (14) and (18) from the body of this report, Equation (D-2) can be rewritten in the respective forms of Equations (D-3) and (-4):

$$F_{SA} = F_{AA} + F_{BB} * \left(\frac{1}{3} + \frac{2 * L_{m,max}}{3} \right)$$

(D-3)

$$= F_{AA} + F_{BB} * (.666666667 * L_{m,max} + .333333333)$$

and:

$$F_{SA} = F_{AA} + F_{BB} * \left[1 + (L_{m,max} - 1) * \left(\frac{1}{2} + \frac{2}{\pi^2} \right) \right]$$

$$= F_{AA} + F_{BB} * \left[\left(\frac{1}{2} + \frac{2}{\pi^2} \right) * L_{m,max} + \left(1 - \left(\frac{1}{2} + \frac{2}{\pi^2} \right) \right) \right]$$

(D-4)

$$= F_{AA} + F_{BB} * [.702642367 * L_{m,max} + .297357633]$$

As evidenced by Equations (D-3) and (-4), the final results for the selected taper factors are remarkably similar. It remains as an exercise for the reader to determine if a true Taylor weighting would also have a similar form. It is hoped that the cosine-squared-on-a-pedestal case is a reasonable indicator of the more complex weighting functions. The maximum weights for Taylor, etc., functions will generally be larger than the cosine function, which, in turn, would be larger than the linear case presented here. If the cosine function is reasonably similar to the more complex functions, then perhaps applying the larger weights to the cosine case will be a reasonable indicator for the magnitude of changes that would occur in noise figure with the more complex weighting functions applied to the array face.

For this example, we must return to Hoffmn's work[1-D] and extract the parameters used for one of the configurations listed there. The test case is for a three-stage HEMT module of the configuration shown in Appendix A, Figure A-1. Those parameters are:

G_i = Individual Stage Gains = 15 dB
F_i = Individual Stage Noise Figures = 0.8 dB
G_b = Beamformer Gain = 40 dB
L_B = Beamformer Loss = 3.0 dB
G_R = Off-Array Receiver Gain = 10 dB
F_R = Off-Array Receiver-Noise Figure = 4.0 dB
L_R = Premodules Receive Loss = 0.5 dB
F_A = Antenna-Noise Figure = unknown

It should be noted that the postmodule receive loss has been included in the beamformer loss. Also, note that the antenna-noise figure, related directly to antenna temperature, is unknown.

[1-D] Hoffman, J.B., *Preliminary Results of Active Array Noise Figure/Third Order Intercept Tradeoff Analysis*, Technology Services Corporation, Silver Spring, MD, 11 December 1991.

The next step that must be taken is to determine this antenna-noise figure. This will be done by using the noise-figure results in Reference D-1 (with $L_m = 0$) to compute the contribution of F_A to F_{SA}.

The curve for noise figure in Reference D-1, with $L_m = 0$, shows:

$$F_{SA} \approx 2.75 \ dB$$
$$= 1.883649089 \ factor$$

Substituting the appropriate parameters into Equation (D-1) yields:

$$F_{SA} = F_A + 1.356330959 + L_m(r, \Theta) * .000107040$$
$$= F_{AA} \qquad\qquad + L_m(r, \Theta) * F_{BB}$$

And for $L_m = 0$, $F_{SA} = 1.883649089$, so that:

$$F_A = 1.883649089 - 1.356330959 - .000107040$$
$$= .527211090$$

(D-5)

and:

$$F_{AA} = F_A + 1.356330959$$
$$= 1.883542049$$

(D-6)

and:

$$F_{BB} = .000107040$$

(D-7)

and finally:

$$F_{SA} = F_{AA} + F_{BB} * L_m(r, \Theta)$$
$$= 1.883542049 + .000107040 * L_m(r, \Theta)$$

$$(D-8)$$

At this point, it is necessary to digress somewhat and discuss the apparently ambiguous results for the antenna-noise factor, Equation (D-5). If this value were used to calculate antenna temperature, the results would be a negative noise temperature. Yet, this factor appears to be necessary for the noise-figure equation to support all the data generated in Reference 1. The explanation appears to be that the antenna temperature seems to be degraded by a rather high antenna ohmic loss not mentioned in the text of Reference D-1. The loss appears to be greater than 3 dB, which corresponds to an antenna temperature of approximately 15 deg K. A loss of 5 dB would correspond to an antenna temperature of approximately 200 deg K, which one would think is closer to reality. The results presented in Equation (D-5) are used throughout this work to compute noise figures.

Coming back to the task at hand, Equations (D-8), (-3), and (-4) can now be combined to determine the effects of attenuation (module loss) for the linear and cosine-squared-on-a-pedestal taper functions. These results were computed for several losses with the results shown in Figure D-1. It is evident that, for the case of this three-stage HEMT module, the effect is significant only for attenuations greater than approximately 30 dB. How likely is this? For Taylor weighted antenna designs of up to -55-dB sidelobe levels, the attenuation required does not reach more than approximately 25 dB. A Taylor-weighted design for -70-dB sidelobes can reach 40-dB attenuation, but this would be a very stressful design to actually produce. It does not seem likely that 40-dB attenuation would be used.
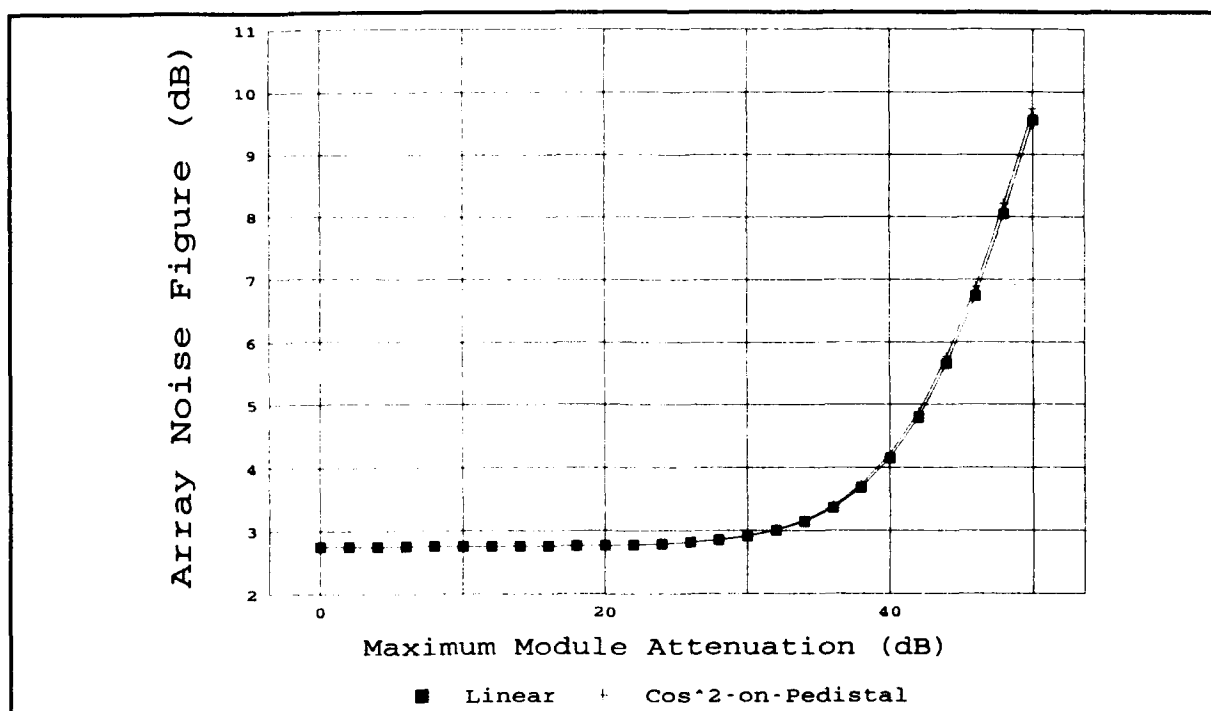
FIGURE D-1. RELATION BETWEEN MODULE-NOISE FIGURE AND TAPER-MAXIMUM
ATTENUATION FOR A THREE-STAGE HEMT-MODULE DESIGN

Look at two other cases—a two-stage HEMT/HBT design with the parameters:

G_1 = 1st stage gain = 15 dB
F_1 = 1st stage noise figure = 0.8 dB
G_2 = 2nd stage gain = 12 dB
F_2 = 2nd stage noise figure = 4 dB
G_b = beamformer gain = 40 dB
L_B = beamformer loss = 3 dB
G_R = off-array receiver gain = 10 dB
F_R = off-array receiver-noise figure = 10.0 dB
L_R = premodules receive loss = 1.0 dB
F_A = antenna-noise figure = 0.527211090

and a one-stage MESFET design with the parameters:

G_1 = 1st stage gain = 11 dB
F_1 = 1st stage noise figure = 1.1 dB
G_b = beamformer gain = 40 dB
L_B = beamformer loss = 3 dB
G_R = off-array receiver gain = 10 dB
F_R = off-array receiver-noise figure = 4.0 dB
L_R = premodules receive loss = 1.0 dB
F_A = antenna-noise figure = 0.527211090

The resulting equations for these two cases are:

$$F_{SA} = 2.098449736 + L_m(r,\Theta)*.045107352 \qquad (D\text{-}9)$$

and

$$F_{SA} = 2.049021188 + L_m(r,\Theta)*0.301680955, \qquad (D\text{-}10)$$

respectively. The resulting curves are shown in Figures D-2 and -3.
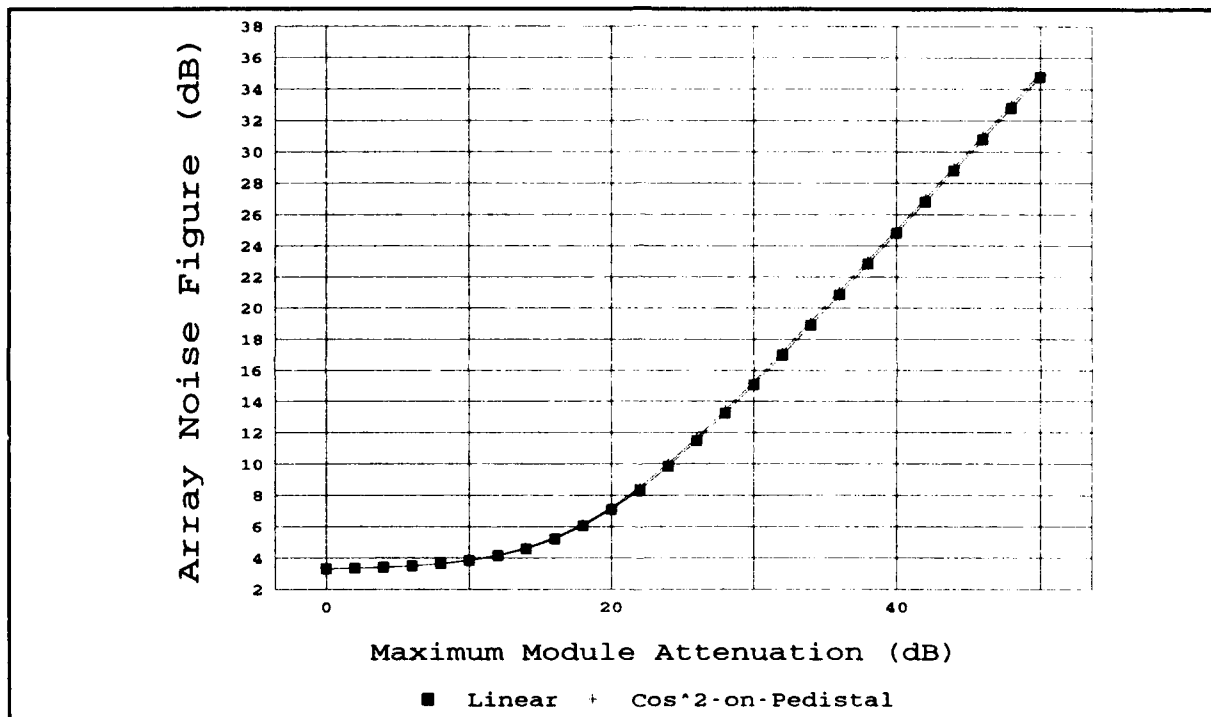
FIGURE D-2. RELATION BETWEEN MODULE-NOISE FIGURE AND TAPER-MAXIMUM ATTENUATION FOR A TWO-STAGE HEMT/HBT-MODULE DESIGN
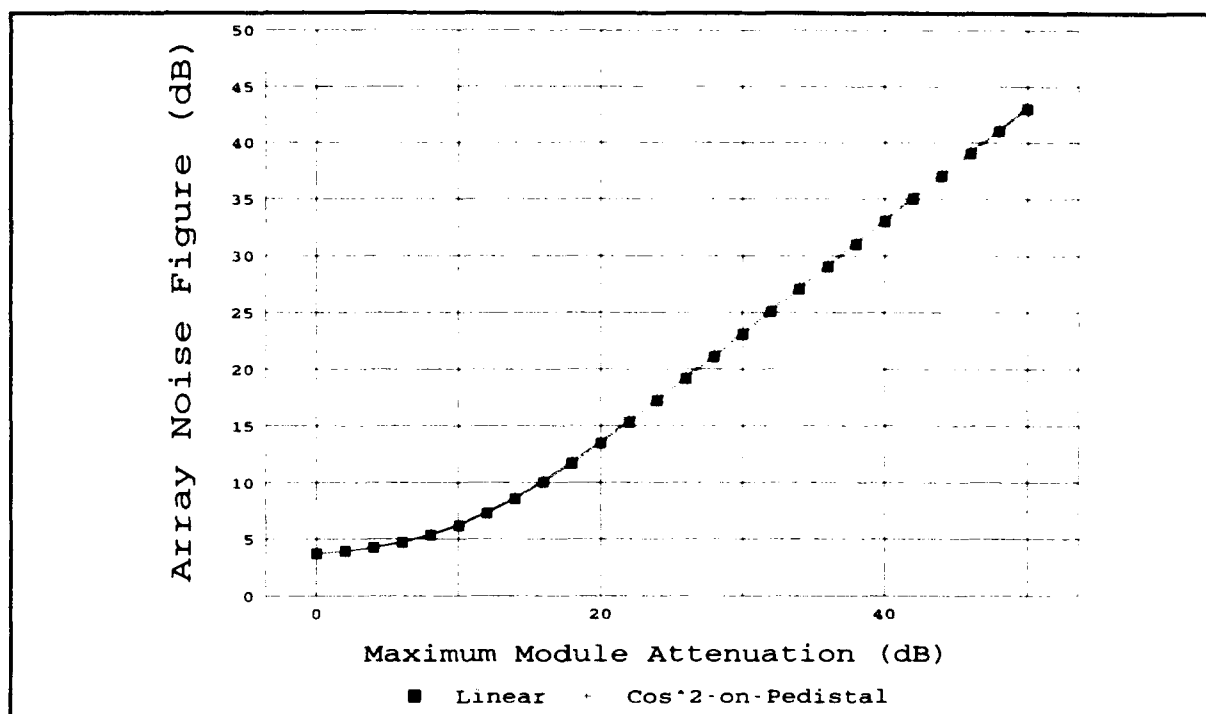
FIGURE D-3. RELATION BETWEEN MODULE-NOISE FIGURE AND TAPER-MAXIMUM
ATTENUATION FOR A ONE-STAGE MESFET-MODULE DESIGN

These figures show that there are designs with a much higher likelihood of using weights that will contribute to the overall noise figure than was evident in the first case. In fact, care must be exercised to avoid sensitivity to this effect. In both cases (considering a -55-dB sidelobe design), an attenuator requirement of 20-25 dB would have an extreme effect on overall noise figure. Clearly, this would be unacceptable in a majority of systems.

As mentioned earlier, if (as Mr. Hoffman suggested) these modules were to be operated at high-module loss to improve the third-order intercept, the combination of high, overall modulelosses and taper attenuation would cause the noise figure to become even more extreme. Care must be exercised to produce a good active-array design.

It should be reiterated that these curves are for linear and cosine-squared-on-a-pedestal tapers and not for a Taylor taper. The fact that these two tapers yield almost identical results seems to suggest that the curves for more complex tapers would be similar. This is assumed to infer noise-figure effects when the maximum weights for examples of Taylor-tapered antennas are used with these curves . This is hopefully a reasonably valid assumption even without any supporting objective analyses.

DISTRIBUTION

	Copies			Copies
DOD ACTIVITIES (CONUS)		**INTERNAL**		
DEFENSE TECHNICAL INFORMATION		E231		3
CENTER		E232		2
CAMERON STATION		E282	(ORENDORF)	1
ALEXANDRIA VA 22304-6145	12	E29		1
		F		1
CENTER FOR NAVAL ANALYSES		F40		1
4401 FORD AVE		F42		1
ALEXANDRIA VA 22302-0268	1	F42	(HARROP)	1
		F10	(GIORGIS)	1
NONDOD ACTIVITIES (CONUS)		F41	(CREECH)	1
		F41	(T. HITE)	1
LIBRARY OF CONGRESS		F41	(J. G. MORRISSETT)	1
GIFT AND EXCHANGE DIVISION		F05	(QUEEN)	1
WASHINGTON DC 20540	4	F405	(CAVANAUGH)	1
		N05	(GASTON)	1
		N74	(GIDEP)	1

REPORT DOCUMENTATION PAGE

Public reporting burden for this collection of information is estimated to average 1 hour per response, including the time for reviewing instructions, searching existing data sources, gathering and maintaining the data needed, and completing and reviewing the collection of information. Send comments regarding this burden estimate or any other aspect of this collection of information, including suggestions for reducing this burden, to Washington Headquarters Services, Directorate for Information Operations and Reports, 1215 Jefferson Davis Highway, Suite 1204, Arlington, VA 22202-4302, and to the Office of Management and Budget, Paperwork Reduction Project (0704-0188), Washington, DC 20503.

1. AGENCY USE ONLY *(Leave blank)*	2. REPORT DATE February 1994	3. REPORT TYPE AND DATES COVERED Final

4. TITLE AND SUBTITLE

Solid-State, Active-Phased Arrays–Some Aspects of Receiver Design

5. FUNDING NUMBERS

6. AUTHOR(S)

Joseph D. Harrop

7. PERFORMING ORGANIZATION NAME(S) AND ADDRESS(ES)

Naval Surface Warfare Center (Code F42)
Dahlgren Division
Dahlgren, Virginia 22448-5000

8. PERFORMING ORGANIZATION REPORT NUMBER

NSWCDD/TR-93/249

9. SPONSORING/MONITORING AGENCY NAME(S) AND

10. SPONSORING/MONITORING AGENCY REPORT NUMBER

11. SUPPLEMENTARY NOTES

12a. DISTRIBUTION/AVAILABILITY

Approved for public release; distribution is unlimited

12b. DISTRIBUTION CODE

13. ABSTRACT *(Maximum 200 words)*

The Navy's use of solid-state transmitter technology has been limited to communication equipment or other uses requiring relatively lowpower, low frequency, or both. It has now become necessary to address some of the issues and tradeoffs involved in the design of transmit/receive modules so that active phased-array characteristics can be fully understood.

The analytical work performed here determines the general relationship among the system noise figure, and third-order intercept requirements of phased-array receivers and the effect on noise figure of adding receive-attenuation to implement weighting (taper) of the array elements.

14. SUBJECT TERMS

system noise figure, signal and third-order intercept curves, phased-array receivers, linear taper, cosine-squared-on-a-pedestal taper

15. NUMBER OF PAGES
140

16. PRICE CODE

17. SECURITY CLASSIFICATION OF REPORT	18. SECURITY CLASSIFICATION OF THIS PAGE	19. SECURITY CLASSIFICATION OF ABSTRACT	20. LIMITATION OF ABSTRACT
UNCLASSIFIED	UNCLASSIFIED	UNCLASSIFIED	SAR

GENERAL INSTRUCTIONS FOR COMPLETING SF 298

The Report Documentation Page (RDP) is used in announcing and cataloging reports. It is important that this information be consistent with the rest of the report, particularly the cover and its title page. Instructions for filling in each block of the form follow. It is important to *stay within the lines* to meet *optical scanning requirements*.

Block 1. Agency Use Only *(Leave blank)*.

Block 2. Report Date. Full publication date including day, month, and year, if available (e.g. 1 Jan 88). Must cite at least the year.

Block 3. Type of Report and Dates Covered. State whether report is interim, final, etc. If applicable, enter inclusive report dates (e.g. 10 Jun 87 - 30 Jun 88).

Block 4. Title and Subtitle. A title is taken from the part of the report that provides the most meaningful and complete information. When a report is prepared in more than one volume, repeat the primary title, add volume number, and include subtitle for the specific volume. On classified documents enter the title classification in parentheses.

Block 5. Funding Numbers. To include contract and grant numbers; may include program element number(s), project number(s), task number(s), and work unit number(s). Use the following labels:

C	-	Contract	PR	- Project
G	-	Grant	TA	- Task
PE	-	Program Element	WU	- Work Unit Accession No.

BLOCK 6. Author(s). Name(s) of person(s) responsible for writing the report, performing the research, or credited with the content of the report. If editor or compiler, this should follow the name(s).

Block 7. Performing Organization Name(s) and address(es). Self-explanatory.

Block 8. Performing Organization Report Number. Enter the unique alphanumeric report number(s) assigned by the organization performing the report.

Block 9. Sponsoring/Monitoring Agency Name(s) and Address(es). Self-explanatory.

Block 10. Sponsoring/Monitoring Agency Report Number. *(If Known)*

Block 11. Supplementary Notes. Enter information not included elsewhere such as: Prepared in cooperation with...; Trans. of...; To be published in... . When a report is revised, include a statement whether the new report supersedes or supplements the older report.

Block 12a. Distribution/Availability Statement. Denotes public availability or limitations. Cite any availability to the public. Enter additional limitations or special markings in all capitals (e.g. NOFORN, REL, ITAR).

DOD	-	See DoDD 5230.24, "Distribution Statements on Technical Documents."
DOE	-	See authorities.
NASA	-	See Handbook NHB 2200.2
NTIS	-	Leave blank

Block 12b. Distribution Code.

DOD	-	Leave blank.
DOE	-	Enter DOE distribution categories from the Standard Distribution for Unclassified Scientific and Technical Reports.
NASA	-	Leave blank.
NTIS	-	Leave blank.

Block 13. Abstract. Include a brief *(Maximum 200 words)* factual summary of the most significant information contained in the report.

Block 14. Subject Terms. Keywords or phrases identifying major subjects in the report.

Block 15. Number of Pages. Enter the total number of pages.

Block 16. Price Code. Enter appropriate price code *(NTIS only)*

Block 17.-19. Security Classifications. Self-explanatory. Enter U.S. Security Classification in accordance with U.S. Security Regulations (i.e., UNCLASSIFIED). If form contains classified information, stamp classification on the top and bottom of this page.

Block 20. Limitation of Abstract. This block must be completed to assign a limitation to the abstract. Enter either UL (unlimited or SAR (same as report). An entry in this block is necessary if the abstract is to be limited. If blank, the abstract is assumed to be unlimited.